UNIVERSITÀ DEGLI STUDI DI PALERMO

Dottorato in Scienze della Terra e del Mare
Dipartimento di Scienze della Terra e del Mare.
Settore Scientifico Disciplinare

SEISMIC NOISE ANALYSIS OF BROADBAND STATIONS OF THE ITALIAN SEISMIC NETWORK, USING POWER SPECTRAL DENSITY

IL DOTTORE
MARIA CATANIA

IL COORDINATORE
PROF. MARCO MILAZZO

IL TUTOR
DOTT. SALVATORE STRAMONDO

CO TUTOR
DOTT. ANTONINO D'ALESSANDRO

CICLO XXXIII
ANNO CONSEGUIMENTO TITOLO 2022

Contents

Abstract

The characteristics of background noise in Italian Seismic Network (IV) have been investigated within the 0.025 Hz to 30 Hz frequency range. More than 230 seismic stations operating continuously in the 3-yr period 2015 - 2017, equipped with broadband sensors, have been selected. Whit the aim of investigate seismic noise power and frequency distribution on the Italian territory, PSD (Power Spectral Density) and the PDF (Probability Density Function) of each seismic station have benne estimated. Noise levels varies in the frequency domain and in space according to the predominant sources in each station. In fact, a catalog of seismic background noise spectra has been obtained from spectral analysis and some cases designated have been evaluated for characterization of the main noise sources. In addition, a new seismic noise model for the Italian territory has been obtained. A statistical and spatial approach as well have been used. Especially interpolation models and 2D spatial filters, allowed as to describe the noise distribution and to detect regional trends for each frequency band. Finally, a regression analysis was performed in order to verify a possible correlation between seismic noise and different geographical and meteorological parameters (altitude, rainfall, and distance to the coastline). The results of this work have great scientific and operational relevance as it is very useful to evaluate the performance of the IV Network, in particular in terms of detection magnitude and quality of hypocentral location, and for future upgrades of the monitoring infrastructure.

Chapter 1

Introduction: nature and origin of seismic noise

The ambient vibration seismology is based on the study of the so-called ambient vibrations. The term "noise" is taken from seismology in which it was a disturbing and obliteration element respect to the "signal" consisting in seismic events.
Seismic noise is a generic term to describe ambient vibrations of the ground caused by natural and/or anthropic sources and each corresponding to different frequency content.
Especially seismic noise depends on the characteristics of the site (geology, topography, etc.), local meteorological conditions (wind, meteorological conditions, and oceanic waves) and/or can due by anthropic vibrations (traffic, power plants, factories, industrial machinery). Especially are divided into two large categories according to their origin natural (microseisms) or anthropic (microtremors).
In addition, noise recorded can also be attribute to other external sources:

- Secondary signals resulting from wave propagation (like scattering phenomena);
- Effects of gravity (Newtonian attraction of atmosphere, horizontal accelerations due to surface tilt);
- Signals resulting from the sensitivity of seismometers to ambient conditions(temperature, air pressure, magnetic field, etc.);
- Signals due to technical issues or deterioration of the sensor (corrosion, leakagecurrents, defective semiconductors, etc.);
- Intrinsic self-noise of the sensor (Brownian noise, electronic and quantization noise);
- Artifacts from data processing.

Although seismic noise is undesired and disturbing component in a seismic record, since several years it has assumed a very important role and more studies performed.
In fact, there has been a progressive interest growth of seismologists and engineers for of its potential

applications for characterisation dynamics of the subsoil and of the building structures. Geophysical techniques, usually used to determine the ground characteristic, are not adapted for to investigate the seismic hazard in urbanized areas while noise techniques are a good and easy alternative, resulting cheaper than traditional geophysical techniques.

The aim of this chapter is to discuss about the existing scientific literature in order to gatherall the available information regarding the origin and the nature of the ambient seismic noise wavefield.

There is an overall agreement about the origin of seismic noise and its frequency dependence. It is possible to distinguish microseisms and microtremors, corresponding to natural and anthropic sources, and low and high frequency, respectively.

At lower frequenciesthan 1 Hz, the variation seismic noise is correlated to natural activities, whereas at higher frequencies it is related to human activities.

Regarding the nature of the seismic noise wavefield, many issues are still open and the scientific literature highlights scarcity and variability of data. The most of interpretations consider that seismic noiseis composed mainly by Surface waves but its nature would seem to depend on to change about the characteristics of source and ground.

Seismic signal is a transient waveform radiated from unique localized natural or anthropic seismic source and with a good defined phase and phase spectrum. On the contrary seismic noise is characterized by a stationary signal resulting by overlapping of several random signals due to a large number of independent (i.e. spatially distributed and unrelated to each other) and different sources (traffic, wind, waves in the ocean). Especially stationarity depends on the type of the source cause its temporal and spatial variability, as observed by Okada (2003).

Microseisms have been observed on seismic records since the 19th century. In 1872, Bertelli installed a pendulum and observed during many years that sometimes the pendulum movedcontinuously for hours or days. He noticed a correlation between the “microseisms” and disturbed air pressure (Gutenberg 1958). Since this date, many studies about noise have been carried out.

Gutenberg (1911) is probably the first major reviewer about the nature and the origin of microseisms. After Gutenberg (1911), some authors studied the relations between microseisms, meteorological conditions and oceanic waves. From 1950 to 1970 started development several techniques based on seismic noise like array techniques: the spatial auto-correlation analysis of signal (SPAC) (Aki,1957, 1965), and the frequency – wave number analysis (f–k) (Capon et al., 1967; Capon, 1969; Lacoss et al., 1969). Other methods were also used to investigate the seismic noise wavefield,such as particle motion analysis (Toksöz, 1964), or borehole techniques sometimes coupled with arrays analysis (Douze, 1964; Douze, 1967). Since 1970 up to now many surveys are were performed. Analysing seismic noise for seismic city microzonation is probably one of the most important purpose. Two

major techniques have been developed: the site-to-reference spectral ratio and theHVSR. Especially, the HVSR ratio technique was proposed first by Nogoshi and Igarashi (1971), and then strongly emphasized by Nakamura (1989, 1996, 2000).

1.1 Origin of seismic noise

Seismic noise describe ambient vibrations of the ground and it is caused by overlapping of several random signals due to a large number of independent (i.e. spatially distributed and unrelated to each other) and different sources (traffic, wind, sea waves). Depending on the origin, the seismic noise behaviour can be different in time and spectral domains.

Basing on the type natural or anthropic sources, in the literature two terms are distinguished, although both terms may be largely confused in some recent works.

The term "microseism" refers to natural sources (wind, ocean and sea waves, large- scale meteorological condition) and it is characterized by lower frequency (< 1 Hz). "Microtremor" is used for the higher frequencies (>1 Hz) normally carried out by man-made signals (human activity, urban traffic, industrial machinery, footsteps) and they are often referred to as "anthropic noise" or "cultural noise".

In intermediate frequencies range (from 1 to 5 Hz) both sources may occur (Gutenberg, 1911; Asten 1978; Asten and Henstridge 1984; Bonnefoy-Claudet et al. 2006; SESAME Project, report WP08, 2003). Depending on the characteristics of the subsoil, both natural sources and anthropic can affect environmental vibrations, with a level of variable stationarity from case to case.

In 1958 Gutenberg established a list of the different types of sources according to their frequency Gutenberg (1958) and some years later Asten (1978) and Asten and Henstridge (1984) supported and validate the same conclusions (Table 1). These assays confirm natural or anthropic origin of the seismic noise, having a different frequency content. This also means that low frequency vibrations have large wavelengths (hundreds or thousands of meters) and therefore must be generated by large-scale phenomena.

Furthermore the studies carry out by Haubrich (1967), Toksöz and Lacoss (1968), Horike (1985) suggested that the high level of low frequency components (<1 Hz) and the two characteristic peaks are mainly attributable to ocean, while high frequency components (>1Hz) were attributable to human activity and climatic conditions.

According to the publications of Gutenberg and Asten, the boundary frequency established between low frequency of microseisms and higher frequency of microtremors is around 1 Hz, but this range is strongly debated in the scientific community.

	Gutenberg (1958)	Asten (1978,1984)
Oceanic waves striking along the coasts	0.05 - 0.1 Hz	0.5 - 1.2 Hz
Monsoon/Large scale meteorological perturbations	0.1 - 0.25 Hz	0.16 - 0.5 Hz
Cyclones over the oceans	0.3 - 1 Hz	0.5 - 3 Hz
Local scale meteorological conditions	1.4 - 5 Hz	-
Volcanic tremor	2 - 10 Hz	-
Urban	1 -100 Hz	1.4 - 30 Hz

Table 1: summary of ambient seismic noise sources according to frequency established by Gutenberg (1958) and Asten (1978) and Asten Henstridge (1984). Bonnefoy-Claudet et al., (2006).

Others same careful surveys carried out by Frantti et al.(1962) and Frantti (1963) that attribute a natural source at lower frequencies (<1Hz) and anthropic sources at high frequencies (>1Hz) proposing a change in the noise behaviour around 1 Hz. They measured the ground particle velocity of seismic noise at 48 site in the United States and other countries. These locations display different geological stratification (rock or sediment), several geographical emplacement (close to the ocean, mountains or urban site), and daily and seasonal variations. They observed that a strong decrease in seismic noise level from 0.6 up to 1 Hz: at higher frequencies the noise levels showed relatively stationary trends over frequencies and they are similar for all sites while the absolute levels displayed wide changesin the several areas. Frantti concluded that characteristics and behaviour noise change for frequencies around 1 Hz. Peterson (1983), Stutzmann et al. (2000), Okada (2003), Berger and Davis (2004) and McNamara and Buland (2004) show similar results in the frequency band of interest for site effect studies, but their surveys based on lower frequencies (down to 1 mHz in some cases). According to Seo (1997), the limit between microseisms and microtremors can be shifted to a lower frequency.

Finally, it is possible consider that for many authors (Gutenberg, 1911; Asten,1978; Asten and Henstridge,1984; Bonnefoy-Claudet et al., 2006; Haubrich,1967; Toksöz and Lacoss,1968; Horike, 1985; Frantti et al., 1962; and Frantti, 1963; Grecu et al., 2013), ascribe a natural source at lower frequencies (< 1Hz) and anthropic sources at high frequencies (> 1Hz).

1.1.1 Microseisms

Microseisms are small- and long-continuing ambient vibration unrelated to earthquakes but induced by natural events.

They have been observed on seismic records and studied since the 19th century (Bertelli, 1872), and in the Second International Seismological Conference, Wiechert (1904) proposed that microseisms are caused by ocean waves on coasts.

Banerji (1924, 1925) has pointed out the relations between microseisms, meteorological conditions and oceanic waves and many authors approved these relations. In fact, he observed microseisms associated with Indian monsoon in south Asia, and he suggested that microseisms due to Rayleigh waves originated at the bottom of the sea by the train of waterwaves maintained by the monsoon currents.

Bernard (1941 a, b) and Longuet - Higgins (1950) showed the relation between the microseism periods and oceanic swells (the predominant period of microseismsis equal to half the natural period of swell height).

Microseisms are characterized by long-period waves with periods between 2 and 40 sec.

Many surveys have been made both on land and on the ocean bottom and microseisms are continuously recorded by seismic sensors and determine noise seismic levels in frequency band from 0.04 to 2 Hz (Essen et al., 2003; Bromirski et al., 2005). These microseisms have the same features than signals recorded onshore except for amplitude, which results strongly weakened, therefore seismic stations located near the coast record more energetic signals. They are caused by natural sources and mainly can be resulting by ocean waves, in fact they are observed worldwide with greater amplitudes in coastal sites than at sites continental (Bromirski, 2001).

Low frequency (0.01 to 0.2 Hz) seismic noise, arising from pelagic storms, is commonly observed as microseisms in seismic records from land and ocean bottom detectors (Cessaro,1994).

Several studies have shown that the ocean-bottom microseism spectrum is similar in shape to the continental microseismic spectrum, but with greater amplitude, and correlates well with known storm systems. Analysis of Ocean Bottom Seismometer (OBS) data recorded near a cyclonic source suggests that microseisms arise from nonlinear interaction of storm waves. (Ostrovsky and Rykunov, 1982).Numerous research have shown that microseisms can be detected in the pressure field of the oceans by deep-ocean acoustic measurements, employing, for instance, ocean bottom seismometers (Duennebier et al., 2012).

Ardhuin et al. (2011) presented the first comprehensive numerical modelling of microseism, valid for global ocean and based on random ocean waves generation furthermore taking into account

coastal reflections.

Regarding medium-period ocean/sea microseisms are characterized low attenuation and they can therefore propagate hundreds of km inland (Bormann and Wielandt, 2013).

As pointed out by many authors (e.g. Haubrich et al. 1963), most of microseismic energy is in the form of Rayleigh waves and its spectrum is strongly related to ocean wave energy coupling into the Earth motion.

Also Grob et al., (2011) observed that mainly the particle motion of microseisms appear to propagate mainly by Rayleigh-wave, they are caused by the coupling of ocean waves into Rayleigh waves, but may contain also body waves and / or Love waves.

Microseisms propagating as long-period surface waves were identified by Haubrich et al., (1963) in two different type of microseisms and they having two different frequency bands, 80 and 150 mHz, respectively:

- *Primary ocean microseisms* are characterized by periods between 10 and 20 s, typically around 14 ± 2 s;
- *Secondary* or *double frequency* microseisms that is related to the main noise peak around6 ± 2s.

Primary microseisms are observed between about 40 and 80 mHz on land (Oliver, 1962; Oliver and Page, 1963; Haubrich et al., 1963; Haubrich and McCamy, 1969) and on the ocean bottom (Barstow et al., 1989; Sutton and Barstow, 1990). Frequency content was later confirmed also by Cessaro 1994; Barruol et al.2006, having a range from 0.05 to 0.1 Hz. Their spectral peak reflects the frequencies of the ocean waves and appear to formin shallow water by the interaction of ocean swells with a shoaling ocean bottom (Oliver, 1962; Haubrich et al., 1963, Hasselmann, 1963). Thus, they are generated only in shallow waters in coastal regions because the amplitude of pressure fluctuations decreases exponentially from the free surface to the sea bottom, thereby the level of primary microseism may result undetectable. Therefore, the wave energy can be converted directly into seismic energy caused verticalpressure variations, which have the same period as thewater waves (Bormann and Wielandt, 2013). Haubrich et al. (1963) compared the spectra of microseisms and of swell at the beaches and could demonstrating a good relationship between the two data sets. Energy is transferred between ocean waves and seismic waves through nonlinear interaction of ocean waves and bathymetry (Hasselmann, 1963).

The peak is called the *single-frequency peak* because it mimics swell frequencies.Depending Cessaro, 1994, in the centre of the continents or an ocean basin, the single- frequency peak
is due to storm waves on near-shore locations. Amplitude seems to be relatively stable in continental sites around the earth.

Holcomb (1998) that also reports on a persistent peak of unknown origin in the seismic noise spectrum at 26 s period also supports this interpretation. The signals are largest during the southern winters and the amplitudeof the peak is correlated between sites worldwide.

The secondary ocean microseisms are dominated by a frequency that is approximately twice the ocean wave frequency (double-frequency) and they have been interpreted as generated by the overlapping of ocean waves of equal period but travelling in opposite directions producing stationary gravity waves of half the period (Longuet-Higgins, 1950 and Hasselmann, 1963). The secondary ocean microseisms observed also on land (Bernard,1941; Iyer, 1958; Hasselmann, 1963; Haubrich et al., 1963) .They are commonly observed, with dominant peak frequencies between 100 and 160 mHz or approximately double that of the peak ocean wave frequencies.

An early theoretical work by Miche (1944) suggested that low-frequency sea-bottom pressure perturbations could be generated by the nonlinear interaction of surface ocean waves. Expanding on Miche's work, Longuet-Higgins (1950) proposed that double - frequency microseisms arise from nonlinear second-order pressure perturbations on the ocean bottom caused by the interference of two ocean waves of equal wavelengths travelingin opposite directions.

These waves propagate with very low attenuation and then turn into microseismic energy. The frequency content of secondary microseism ranges from 0.1 to 0.5 Hz (Cessaro, 1994; Barruol et al.,2006). Although not checked in all areas, according to research by Stephen et al., (2003) and Bromirski et al., (2005), in turn, the secondary microseism may be further divided into long and short period microseism with 0.085 - 0.2 Hz and 0.2 - 0.5 Hz range respectively. Long period microseism it due to far away sources (such as swell from distant storms), and short period microseism linked to sources located near the coast (such as waves induce by local wind). Have been observed that the noise peak of secondary microseisms has a shorter period whengenerated in shallower inland seas or lakes ($T \approx 2$ to 4 s) instead of in deep oceans. In addition, off - shore interference patterns largely depend on coastal geometries and the latter may allow the development of internal resonance phenomena in bays, fjords or channels, which affect the fine spectrum of microseisms. The association of primary and secondary microseisms with the same atmospheric disturbance was first noted by Oliver and Page (1963), who observed that primary microseisms have twice the dominant periods of the related secondary microseisms.

These type of waves have been interpreted as short-period P waves, higher mode Surface waves, long-period Surface waves, and ultra-long-period Surface waves (Cessaro, 1994).

1.1.2 Microtremors

Microtremors are those ambient vibrations that are characterized by frequencies >1 Hz and whose sources are mainly linked to anthropogenic factors. In urban densely populated and industrialized

areas, both natural and cultural noise components may play a major role in a wide range of frequencies. Measuring and analysing urban seismic noise (USN) requires broadband recordings and data analysis. Broadband urban seismic noise must be considered as a temporally and spatially non-stationary random process (Groos and Ritter, 2009).

Groos and Ritter (2009), occurred that a high variability of USN of single measure like the standard deviation of a seismic noise time-series or the power spectral density at a given frequency, does not allow to characterize a sample (time series) of USN comprehensively. Therefore, they calculated long-term spectrograms from a broadband seismic data setrecorded in the metropolitan area of Bucharest, Romania. The aim was to identify the frequency-dependent behaviour of the time-variable processes that contribute to USN. Basedon the spectral analysis of the data in eight frequency ranges between 8 mHz and 45 Hz proposed an automated statistical classification in the time domain to quantify and characterize USN; this classification allow as to identify Gaussian distributed seismic noisetime series as well as time-series dominated by transient or periodic signals due to traffic, rotating machinery etc. They found that only 40% of the analysed time series are characterized by Gaussian distributed noise and that the most common deviations from a Gaussian distribution are due to large-amplitude transient signals.

Especially they observed that the human activity as a dominant influence on the USN above and below the frequencyband of ocean-generated microseism between 0.04 and 0.6 Hz. Peruzzetto et al., (2018) for broadband ambient noise characterization have carried out a joint analysis between cross-correlation and MUSIC algorithm: it a novel method ofdetermining the wavefiled velocity. Other important and dominant sources of high-frequency noise is anthropic noise (power plants, factories, rotating or hammering machinery, road and rail traffic, etc.) often called *cultural noise*.

The term anthropic or cultural noise is used to describe any seismic noise associated with man or man-made machinery: power plants, factories, trains, highways and even cattle. Cultural noise is in principle avoidable, although it is often impractical to site stations at sufficient distances away from cities or highways.

Some rules suggest that it may be necessary located the short-period stations far as 25 km from power plants, 15km from railways, 6km from highways, and a kilometre or more fromsmaller roads. Instead, for moving waters it is advisable to install the stations away from movingwater between some 60 km for very large waterfalls and dams to 15 km for smaller rapids (Wilmore, 1979).

Noise changes from site to site (Fig.4) and its levels may differ also by 30 dB or even morewithin a day (Fyen, 1990) or show diurnal or weekly character (Given, 1990). Fyen (1990) show noise levels are lowest in the early morning in data from the NORESS array, rising rapidly near 07:00 to levels sustained throughout the working day decrease the evening hoursand weekends but increase during

holidays cause traffic.
Cultural noise propagates mainly as high-frequency surface waves (>1–10 Hz, 1–0.1 s) thatattenuate within several kilometres in distance and depth (Khairy et al., 2012).

1.2 Nature of the seismic noise

In the last years, many researchers showed major interest for to clarify and to increase knowledge about the physical nature of seismic noise wavefield. The nature of the seismic noise depends byits wavefield.
Some research has led to the development of F-K Array Method (Capon, 1969; Capon et al., 1967; Lacoss et al 1969; Aki, 1957, 1965) for to study dispersive properties, marker of Surface waves. Especially increasing the number of processing techniques based on the assumption that the seismic noise wavefield is mainly originated by fundamental mode Rayleigh waves. For analyse one particular type of wave as representative of the ambient seismic noise the most widespread approach is to extract the surface wave (Rayleigh and/or Love) dispersion curves and to invert for a vertical shear-wave velocity profile (Peruzzetto et al., 2018). Other method used to investigate the nature of seismic noise is the MUSIC high-resolution array analysis (Schmidt, 1981; Cornou, 2002; Cornou et al., 2003a, b; Peruzzetto et al., 2018).
The spectral ratio of horizontal and vertical components (HVSR) and array methods are the two main techniques used for to investigate the nature of noise wavefield.
The first one (HVSR) to analyse the ellipticity and dispersive property of Rayleigh waves to estimate the fundamental frequency and the amplification of ground. Instead, assuming that seismic noise is constitutedby fundamental mode Rayleigh waves, array studies allow to determine the shear waves velocity profile of ground (SESAME Project, report WP08, 2003).
These methods are strongly linked with the nature of seismic noise wavefield and likely it have to be constituted by fundamental Rayleigh waves, but nobody has managed to provide clear and unanimous conclusions about this hypothesis.
In order to establish a state of art about the actual knowledge of the nature and estimating the relative proportions of each wave type, the scientific community has decided to carryout more in-depth studies based on the following three assumption in order to characterize the noise wavefield:

- Ratio of body waves to surface waves;
- Ratio of Love waves to Rayleigh waves;
- Ratio of the fundamental Rayleigh mode to higher modes.

Nowadays, few results exist; these have been obtained by analysing these ratios already mentioned above.

1.2.1 Ratio of body waves to surface waves

In the Surface waves amplitude decay with increasing depth and their attenuation property allow to study the content of the seismic noise, while it is not possible in the Body waves because no decrease of amplitude with depth. Especially many authors associate the low frequency with fundamental mode Rayleigh waves, basing on this assumption.

Depending Toksöz and Lacoss (1968) assume that at frequencies lower than 0.15 Hz the seismic waves are fundamental Rayleigh waves based on a study carried out by them usingthe F-K Method. Measurements performed from the LASA array (Large Aperture Seismic Array) in Montana (USA) composed by 546 seismometers, were allowed to compare the theoretical value for Body waves and Rayleigh waves observing the nature of low frequency seismic noise (Fig.1).

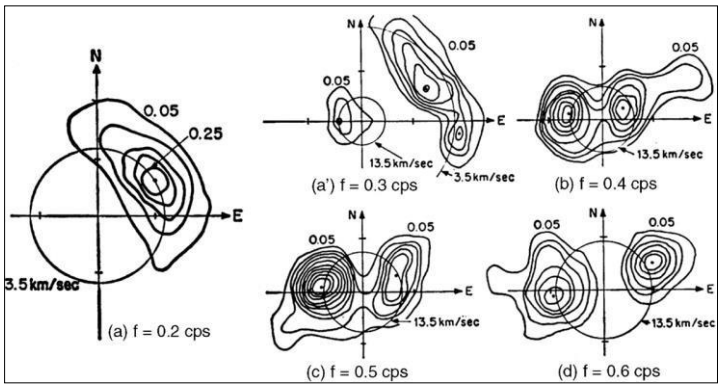

Figure 1: Seismic noise recorded at the LASA array for different periods. Depending on the frequency, Body waves (13.5 km/s) and/or Surface waves (3.5 km/s) phase velocities are observed. It has been noted that for 0.2 Hz phase velocity is about 3.5 km/s that corresponding to the theoretical phase velocity of the first or second higher Rayleigh waves mode. For 0.3 Hz two distinct velocities are identified corresponding to Rayleigh waves (3.5 km/s velocity) and P waves (around 13.5 km/s) attributed since so high velocities on the vertical component can be reached only for slightly oblique p waves. For more frequencies between 0.4 and 0.6 Hz, only the fast P waves have been received. At frequencies lower than 0.15 Hz, these authors assume that the seismic waves are fundamental Rayleigh waves. Toksöz and Lacoss (1968).

In the view Douze (1964,1967) has carried out a comparison between observed and theoretical ratio of deep seismic noise to surface noise amplitude: for periods lower than 2 seconds (F > 5 Hz) it was possible to observe a strongly decrease in the ratio (SESAME Project,report WP08, 2003). This suggests that the amplitude decrease with depth and these are Surface waves. In this range, the ratio

is close to 1 indicates that we have Body waves (because in these waves no decrease of amplitude with depth). Especially Douze(1964, 1967) observed three several periods (0.5, 1 and 2 seconds). He concludes that seismic noise is composed by P waves and the third Rayleigh waves mode, for 2 Hz (0.5 sec) and for 1 Hz (1 sec) is a mix between P waves and the first Rayleigh waves mode. Finally at 2 sec (0.5Hz) it is not easy to dive a clearly conclusion (maybe seems to be P waves and the firsts Rayleigh waves mode) (Fig.2).

In other and more recent research seems that several authors such as Li et al.(1984), Horike (1985), Yamanaka 1994, Withers et al. (1996) and Bormann (2002) according to associate to lower frequencies (below 1 Hz) at fundamental Rayleigh waves mode. About higher frequencies, there is no agreement cause more difficult to discriminate thenature of noise, but some authors considers that it may be associated to P waves and general Rayleigh waves.

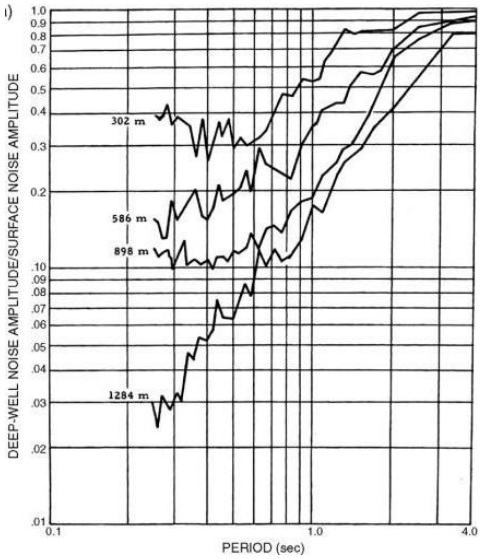

Figure 2: Deep-to-surface noise Fourier spectra amplitude ratio (vertical component) as a function of period for Eniwetok island borehole (1288 m deep, Marshall Islands). It possible to observe a decrease of the measured seismic noise depending on depth. Douze, 1964.

1.2.2 Ratio of Love waves to Rayleigh waves

A third assumption assumes that seismic noise is mainly composed by Surface waves, and Array methodsare the best way for to estimate Rayleigh and Love content in the seismic noise.

There are few resultsabout the content and there is no a conclusion to establish the proportion of Rayleigh and Love waves in seismic noise. Some authors prefer to use 3-component array analysis for to explain the nature of the seismic noise, especially SPAC Method (SPAtial auto-Correlation Method) developed byAki (1957, 1965). It seems to be the best way to determine the relative

proportion of Love waves and Rayleigh waves in seismic noise.

Although Chouet, et al., (1998) studied volcanic tremor of Stromboli volcano, they proposed SPAC Method with very interesting results (but volcanic tremor have a different origin by microtremors). In order to obtain Rayleigh and Love waves phase velocities, it was necessary to inverting the spatial auto-correlation curves. The authors have been observed that higher frequency (>2 Hz) the most of energy (77%) is attributed by Love waves while only 23% by Rayleigh waves. This interpretation is widely supported by Arai and Tokimatsu (1998, 2000) and Yamamoto (2000) that give all comparable results. In fact, Araiand Tokimatsu (1998, 2000) analyse four sites using SPAC and F-K Method (Fig.3) and the contribution of Love waves is 70% (frequencies range 1 to 12 Hz) with an energy ratio around 0.7.

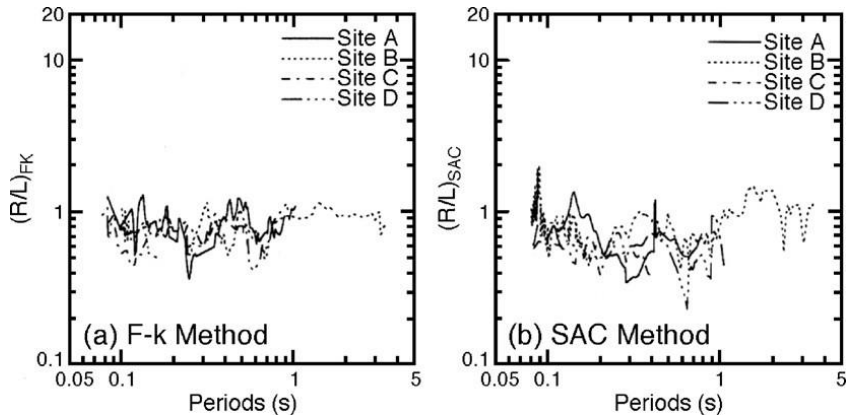

Figure 3: Energy ratio between Rayleigh and Love waves estimated at four different sites and from two array techniques: (a) F-K analysis, (b) SPAtial autoCorrelation Method. Arai and Tokimatsu, 1998.

Instead, Yamamoto (2000) using the SPAC technique to estimate the energy ratio through the dispersions of both Rayleigh- and Love waves. In three urban sites in the Morioka city (Japan), he observed that, in the frequency range 3 to 10 Hz, Love waves values are always major of 50%, especially for one site where Love waves carry from 40% to 85% (Fig.4).

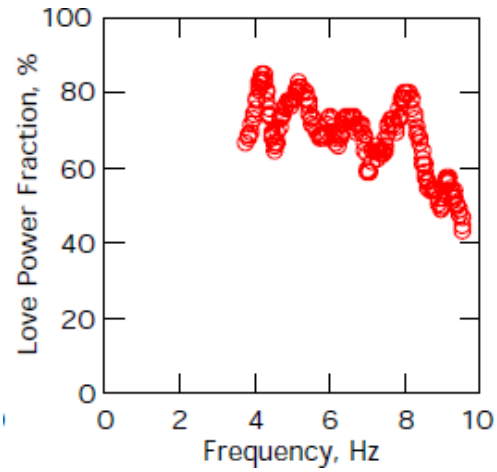

Figure 4: in the 3–10 Hz frequency range, 40% to 85% of the noise energy is carried by Love, waves at Nioh site (Morioka, Japan). Yamamoto, (2000)**.**

Köhler et al., (2007) used a modified 3-component SPAC technique and they observed a significant contribution of Love waves (65-90%) at intermediate frequencies (0.5 to 1.3 Hz)in the seismic noise wavefield recorded at the Pulheim site (Germany).

The SPAC Method can detect Rayleigh and Love waves from three-component array measurements, and allow deriving an average contribution of each wave type (Okada, 2003, chapter 3).

A large number of authors presuppose that seismic noise is mainly composed by Surface waves.

In addition to concluding, also in the various studies it is important to observe that all sites selected are located in several areas with different sediment and thickness (Table 2).

It is possible to deduce once again that geology and geometry (sediment thickness, slope, geometry of the sediment-to-bedrock interface) as well as the source properties (Ohmachi and Umezono, 1998) may strongly influence the Rayleigh and Love waves type.

	Frequency range	Rayleigh waves proportion	Love waves proportion	Sites
Chouet et al. (1998)	>2 Hz	23%	77%	Volcanoes
Yamamoto (2000)	3–8 Hz	<50%	>50%	Sedimentary (thickness< 100 m)
Arai and Tokimatsu (1998)	1–12 Hz	40%	60%	Sedimentary (thickness< 100 m)
Cornou (2002)	0.1–1 Hz	50%	50%	Sedimentary (thickness ~ 500 m)
Okada (2003)	0.4–1 Hz	<50%	>=50%	Sedimentary (thickness ~ 50 m)
Köhler et al. (2007)	0.5–1.3 Hz	10–35%	65–90%	Sedimentary (thickness ~ 200 m)

Table 2: Frequency range report, proportion of Rayleigh and Love waves in noise wavefield and geological characteristics of the investigated sites (Bonnefoy-Claudet et al., 2006, modified)

The low frequency seismic noise (lower than 1 Hz) was investigated with the MUSIC method (Multiple Signal Characterisation) high-resolution array analysis (Schmidt, 1981). Cornou (2002) and Cornou et al. (2003a,b) observed a good agreement between themeasured phase velocities and the theoretical surface wave velocities, and they estimated energy ratio between Rayleigh and Love waves through the ratio of the energy carried by radial and transverse components. While the meteorological conditions changed over the period of the study (four months), Cornou (2002) observed that the content is around 50% of Rayleigh waves contained in microseisms over the frequency range 0.2 to 1 Hz (Table 3).

Julian days	Hours (TU)	Rayleigh waves proportions (%)
076	01–02	55±6
	15–16	50±6
085	01–02	52±12
	15–16	50±8
090	01–02	52±7
	05–06	50±8
	15–16	57±10
105	01–02	51±9
	05–06	50±7
	15–16	49±6

Table 3: Rayleigh waves proportions (as percentage, ± standard deviation) contained in microtremors, for different days and hours, using MUSIC high-resolution array analysis. Cornou (2002) and Cornou et al. (2003a, b).

However, some interesting, though incomplete results could be obtained with numerical simulation using random, surface and local sources with arbitrary directions in horizontallylayered half-spaces. Bonnefoy-Claudet (2004, pp.147–172) concluded that Love waves are always present in thesynthetic seismic noise wavefield for sources having a horizontal component.

In the same way, Ohmachi and Umezono (1998) simulated seismic noise propagation in simple 1D models (one layer over a half space) with the closed form equations established by Harkrider (1964). Assuming this ground model type and considering different excitation types (number, position and direction of forces), the horizontal to vertical ratio and the coherence between radial and vertical synthetic noise components are analysed. Unfortunately, a strong variation in the Rayleigh to Love waves ratio in the synthetic noise is recorded, cause the type of excitation (vertical, transverse or radial forces the observation direction, and the impedance soil contrast. The wide variability (10% to 90%) of this ratio not allow establishing certainties about the proportions of Rayleigh waves.

Nevertheless, this approach does not provide reliable and does not give quantitative estimateof the relative proportion of Rayleigh to Love waves in real noise, because it is depends onorientation of the random sources.

1.2.3 Ratio of the fundamental Rayleigh mode to higher modes

In the literature, there are not enough studies about Rayleigh higher modes and the ratio between fundamental and higher modes of Rayleigh waves involves many difficulties. The most of few results is provided by HVSR analysis.

Stephenson (2003) analyses the relation between HVSR and ellipticity of particle orbits of Rayleigh waves, saying that if the seismic noise wavefield is constituted only by the fundamental mode of Rayleigh waves then the HVSR curves, it should have a peak/trough structure. Also Konno and Ohmachi (1998) show peak/trough structure on HVSR curves. Lermo and Chavez-Garcia (1994), Mucciarelli (1998), Ohmachi and Nakamura (1992), and Seekins et al., (1996), also support this statement.

A consistent second peak on HVSR curves have been observed, in according to Bodin et al., (2001), Asten and Dhu (2002) and Asten (2004). Bodin et al. (2001) note that there is no a clear correlation the frequency of this HVSR peak and the resonance frequency of soft soils,and they associate this second peak with the first higher harmonic of Rayleigh waves. This work show that ellipticity curves of higher modes Rayleigh waves do exhibit peaks at higherfrequencies that may be associated with the second peak observed on HVSR curves (Asten,2004).Currently exist a research that show the possible presence of higher mode of Rayleigh wavesin seismic noise (Tokimatsu,1997). Tokimatsu does not give any quantitative answer about the proportion of Rayleigh higher modes in noise, but he observe that higher modes of Rayleighexisting in seismic noise and this is dependent on geological stratification.

Microseisms appear to propagate mainly by Rayleigh wave motion but may contain Love wave components where propagation is through continuous layered structure (Rind and Donn, 1979).

1.3 Seismic noise at the seabottom and on land

The microseism mechanism controls in the sea bottom up to frequencies of a few Hertz.

The analogues of wind and air pressure generated noise on the Earth surface are on the ocean floor the ocean currents.

Very important are the ocean currents on the ocean floor. According to Webb (1998), they also set up a turbulent boundary layer with adverting pressure fluctuations. However, on theocean floor, the deformation signal decays already completely within a few meters depth below the sea floor cause much lower velocities and hence much shorter wavelengths are associated with ocean currents than with wind.

While thereis little difference in the microseism band between land and the sea floor at longer

periods, the major difference occurs at frequencies near 1 Hz. Almost always there is much more noise energy around 1 Hz on the ocean floor than on land, often by more than 140 dB.

The role which long-term ocean-floor seismic observatories have been given is very important. In fact, in recent years many ocean-bottom seismographs installed (OBS) for to acquire the microseisms (Fig.5). Generally, the seismic noise level at the ocean bottom, even in deep seas, is higher than that on land (about 10 to 30 dB) and increases with higher frequencies (Bradner and Dodds,1964; Webb, 2002). Background noise can be reduced by installing the OBS in boreholes.

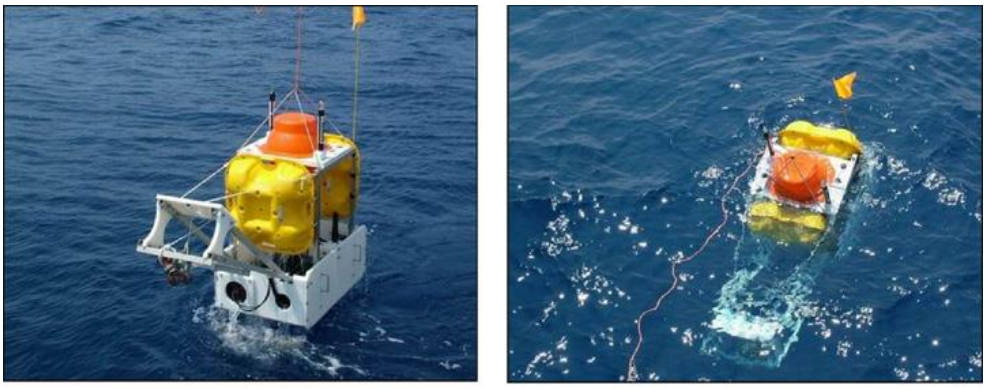

Figure 5: Example of Broadband OBS installed by INGV in the Tyrrhenian Sea (INGV website).

Webb (2002) provide a clearly explanation about the mechanisms which generate short- period noise on the sea floor the reasons why noise on the sea floor decays with depth belowthe sea floor. The sea floor in the band from 0.5 to 5Hz is noisier than the typical land site because of microseisms generated by small-amplitude, high-frequency ocean waves that can be produced already by light winds.

One expects to see winds exceeding 5 $msec^{-1}$ over most sites in the oceans most of the time,so the average sea-floor site is very noisy near I Hz most of the time. A notable exception isthe Arctic Ocean where the ice cap prevents the excitation of the ocean surface waves that ultimately couple to noise in the microseism peak. The Arctic sea floor has been observed to be very quiet near I Hz during the winter (Webb and Schultz, 1992). Parts of the North Atlantic and Indian oceans can also experience long intervals of near calm conditions duringthe summer months and may provide quiet sites for detection of short-period body waves (Webb, 1998).

Short-period natural and anthropic sources contributions of background seismic noise on land, is more complex and coming from several directions, and can be stationary and random noise field. The particle motion of short - period noise is therefore more irregular than for long-period ocean noise (Bormann and Wielandt, 2013). For very long period is usually associated with atmospheric

pressure fluctuations**.** At these very low frequencies, vertical component seismometers react to changes in gravity when the mass of the atmosphere above a site changes with atmosphericpressure (Bormann and Wielandt, 2013). Depending Murphy and Savino (1975) the ground deforms under the fluctuating pressures are associated with turbulence in the boundary layer of the atmosphere for higher frequencies.

Long-period seismometers are more susceptible to external variations such as pressure fluctuations and temperature changes seismometers at permanent stations are often installed beneath the Earth's surface in shallow boreholes. Generally, recording sites weakly coupled to the ground or on poorly consolidated ground will be noisy, both at long and short periods. Other reasons for increased long-period noise may be air circulation in the seismometer vault or underneath the sensor cover. Special carein seismometer installation and shielding is therefore required in order to reduce drifts and long-period environmental noise (Bormann and Wielandt, 2013).

Instead, seismic noise levels on land at frequencies above 0.5 Hz depend mainly on wind (wind friction; trees and other vegetation or built-up objects swinging or vibrating in the wind) on anthropic noise, but a contribution could also come from the movement of water (river, waterfalls and creeks). Each site has different characteristics depending on the windy characteristics of the site, on its distance from the ocean, cultural sources like industrial and settlement areas, major infrastructure facilities, and depth of burial of the sensor.

At some site, seasonal cycles mayaffect cause to changes in wind or river water flow.

It is well known that the meteorological conditions and, in particular, the wind velocity, have an important role in the generation of seismic noise on the seafloor (Wilcock et al., 1999).

Wind noise couples mostly into surface-wave modes, while cultural noise couples at least partly into body waves that can propagate also to greater depth (Carter et al., 1991).

Especially wind noise is broadband and the dominant source from 0.5 to about 15 to 60 Hz (Young et al., 1996). Wind noise obviously depends on the strength of the wind and the character of the site. Recorded noise power near 1 Hz in a surface vault may increase by 10-20 dB, as compared to records on calm days, when wind speed reaches about 5 m/s (Bormann and Wielandt, 2013).

High-frequency noise associated probably by the direct action of the wind on trees, bushes, and other structures, while at lower frequencies the pressure fluctuations associated with wind that can directly drive motions of the ground.

For instance, Withers et al., (1996) carried out a survey about high frequency (> 1 Hz) seismic noise characteristics. A remote site, close to the town of Datil in west central New Mexico has been chosen. This location was characterized by very low levels of anthropic noise; but appeared to be an excellent candidate to study the effects of wind noise on seismograms (cause strong winds especially winter

and spring). They deployed a three-component set of surface sensors and a vertical borehole seismometer (they used a deep borehole) at several depths (5, 43, and 85 m) to investigate signal and noise variations, whilewind speed was measured with an anemometer. For wind speed below 3 to 4 m/sec, they observed an omni-directional background noise at frequencies below 15 Hz, while this coherence is destroyed when wind speeds exceed 3 to 4 m/sec. In fact, short-period wind noise becomes detectable source in records at surface sites located far from anthropic sources at wind velocities above about 3m sec^{-1} and at 4 m sec^{-l} for subsurface sensors (Fig.6).

Usually, noise levels increase with higher wind speeds. However, there is apparently no linear relationship between wind speed and the amplitude of wind generated seismic noise.

If wind speeds greater than 3 to 4 m/s, wind noise increases dramatically and may reach down to several hundred meters depth below the surface at wind speeds > 8 m/s (Young, 1996).

Generally, wind show level and variability much higher at or near the surface while show an important decrease with depth. However, the signal-to-noise ratio for high-frequency arrivals can be optimized by choosing most repaired sites (Withers et al., 1996).

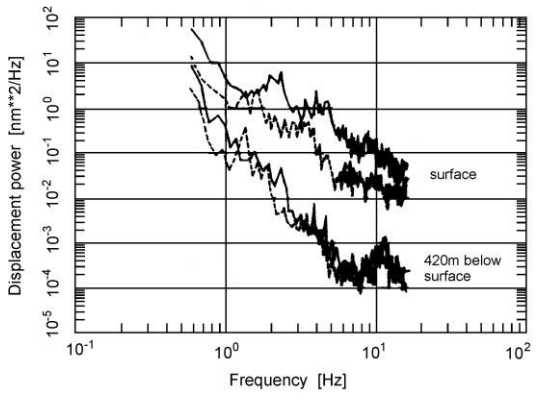

Figure 6: Displacement power noise spectra measured at the surface (upper curves) and at 420 m below the surface in a disused salt mine at Morsleben, Germany (lower curves). Hatched lines show a very quiet day and full lines show a day with light wind on the surface (wind speed about 4 m/s). Withers et al., (1996).

1.4 Daily, Weekly and Seasonal variations

Stationary seismic noise may exhibit considerable variations in noise levels as a function oftime of day, season, and location and installation type. Daily and weekly variations in spectral amplitudes of microtremors have been observed in several works. Especially at higher frequencies than 1 Hz seismic noise systematically shows daily and weekly variations linked to anthropic activities. The latter is different from site to site and ithas characteristic frequencies depending on the source of the disturbance and the distance tothe source. Usually the daily variations are also related to variations

in temperature ranges between day and night.

In addition to daily and weekly variations, seasonal variations are very evident in different research. For instance, microseismic noise is mostly caused by water waves in oceans or the lakes show a surge in the noise level in monsoonal months in comparison with autumn or winter.

In the 1961, Kanai and Tanaka had already demonstrated results on continuous seismic noise measurements achieved in Tokyo (Japan) monitoring noise amplitude variation over 24 hours for two different days and observing the maximumamplitude (between 0.4 and 0.5 micrometer) during the daytime, while value decreasing in the night hours (to 0.1-0.2 micrometer). Therefore, they show the average of spectral amplitude over time and they realize that the period depends by micro tremor according to hours (higher period during night-time than daytime). Moreover, they perform noise measurements during daytime and night-time at thirty site in Japan, taking into account various types of subsoil, and show the following relation (Equation 1):

$$[\text{Amplitude (midnight)}] = 0.3 \times [\text{Amplitude (daytime)}]^{1/5}$$

These results emphasize the different noise behaviour in spectral domain depending on the origin of the noise, with clear physical differences between low frequency and higher frequency.

These statements are also supported by many recent studies that lead to the same conclusion.

Okada 2003, (pp. 9 -16) confirm as well the temporal variation of the seismic noise Fourier spectra according to natural or anthropic sources. In 1993 Yamanaka et al., conducted an interesting research about noise spectral behaviour over time on the campus of the University of Southern California in Los Angeles. Outcomeshave a small delay for the maximum amplitude, but an agreement of the swell change with that of microseisms at long period (6.5 s) is recorded, which are related to ocean disturbancesin the Los Angeles basin. Short period microtremors are related to anthropic activities and in the spectrum amplitude noted a daily variation (maximum at midday and minimum at midnight) and in the weekends spectral amplitude decreased.

Especially these results show the different seismic noise behaviour in spectral domain depending on the origin of the seismic noise, with clear physical differences between low frequency and higher frequency. Many diurnal variations are also demonstrated by McNamara and Buland, 2004; Marzorati and Bindi, 2006; Sheen et al., 2009; Diaz et al., 2010, Grecu et al., 2012, and weekly that are related to human activities during the days-nights and in the different days. Jana et al., (2017) emphasizes also the behaviour between day and night. Day/night variation studies reveal that daytime registers more cultural noise overnight time. In fact, microseismic noise is low during the daytime. Likewise, the night time 12.00–05.00 hours data has been sampled as PSDs and the cultural noise

during night is lower than the daytime, while the microseismic noise level is unperturbed temporally. Although the microseismic noise are of the same level in all the stations temporally, seasonallythe distinction in the microseismic noise can be noted. They show also seasonal variationcomparisons too in the same station. In fact, the PSDs sampled over the months July – August, the monsoon season, exhibit a higher level of microseismic noise than those over the others seasonal plots, especially for the winter season, with an overall upward trend in the long-period noise. The case is attributable to the low temperature that could be a main reason for the less variations. However, the cultural noise level remains the same irrespective of the season.

Even at seasonal level, there are many researches. It has been observed that the levels of the peak of the noise at low frequency in the winter period are greater than the summer period probably due to a greater intensity of the meteorological.

In Grecu et al., (2012), noise level of the Romanian broadband stations operating since 2006 has been studied in order to identify the variations in background seismic noise as a function of time of day, season, and particular conditions at the stations. They showed that, in the frequency range 1–20 Hz, most of the stations exhibit important power variations during daytime and night time. Also in the microseismic band, important seasonal variations were observed. For most of the stations, the noise level is the lowest in summer and increases during winter. Especially a shift of the double-frequency peak from lower periods in summer to longer periods in winter.

Instead, Marzorati et al., (2006), shows the noise seasonal variability for a station (MAR2), which is equipped with a broadband sensor. For frequencies <1 Hz, the seasonal variability of noise is evident. In winter, the noise power is higher than summer and the peak of the mode is shifted toward lower frequencies (Fig.7). Instead, for frequencies > 1 the winter and summer noise levels are similar since the short-period background noise it is mainly dominated by man-made activities.

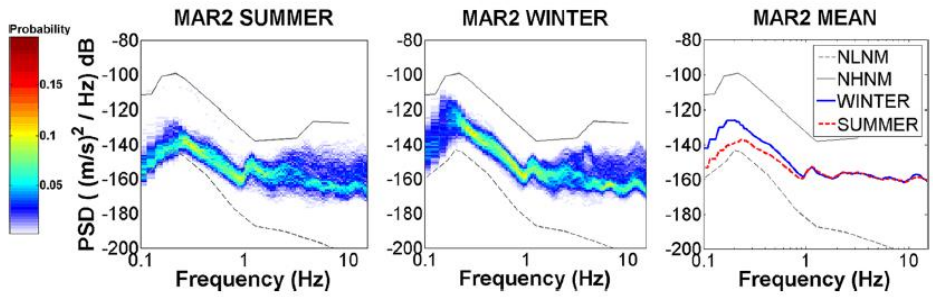

Figure 7: Seasonal variations of noise level for MAR2 station: PDF of MAR2 station for summer recording (left; PDF of winter recordings (middle).
On the right PDF mode of winter (blue solid line) and summer (red dashed line) recordings: for the frequencies >1Hz in winter the seismic noise is lower than in summer while it is similar for higher frequencies. Marzorati et al., (2006).

1.5 Effect geological site

The geological condition of the site is fundamental and influences the background seismic noise.
According to Seo (1997), in deep soft Mexico basin, daily variation can be observed at frequencies lower than 1 Hz. In the time domain, diurnal variations are recorded at the sediment site, but not at the rock site. Indeed, in the spectral domain, diurnal variations in noise spectral amplitude are obvious in the frequency range at the sedimentary site, while atthe rock site daily variations appear only for frequencies higher than 1 Hz. This confirm the role played by the geology that influencing the power of seismic noise and therefore accordinglydaily variations of seismic noise could be observed also at low frequency (below the 1 Hz limit) in case of deep soft basin.
Grecu et al., (2012), by the analysis of the probability density functions, for stations located in different Romanian geologic conditions, demonstrated that stations sited on softer geologic formations are characterized by higher noise levels than those sitedon hard rocks. Especially, to better illustrate the difference, they compared the PDFs of two stations: Station GZR, located in the Southern Carpathians on very hard rocks (granites), shows lower noise levels than station PETR, that is located in the Focsani Depression on very thick Neogene (~ 8 km) sediments.
Instead, Marzorati et al., (2006), analysed the seismic noise variation in three stations in different geological contexts in the north central Italy. They observed that two large-scale geologic features characterize the analysed region: the Po Plain and the Alps. Impedance contrast between these two units causes a noise reduction of about 10 dB in the frequency range 0.2 - 0.6 Hz (Fig.8).
Therefore compared to hard rock sites, both noise and signals may be amplified on soft soil cover. This signal amplification may partly or even fully outweigh the higher noise observed on such sites. This confirm that the Signal Noise Ratio variations are due to the local site conditions. In addition, for "free-surface effect", peculiarities of the local noise field and geological conditions, the SNR does not necessarily increase steadily with depth. It may depend also on local geological and installation conditions. Nevertheless, we can generally expect a significant SNR improvement within the first few hundred meters depth. In mines or boreholes a depth of 100 m is generally sufficient to achieve most of the practicable reduction by -20 to -30 dB of long-period noise with periods between 30 s and 1000 s).

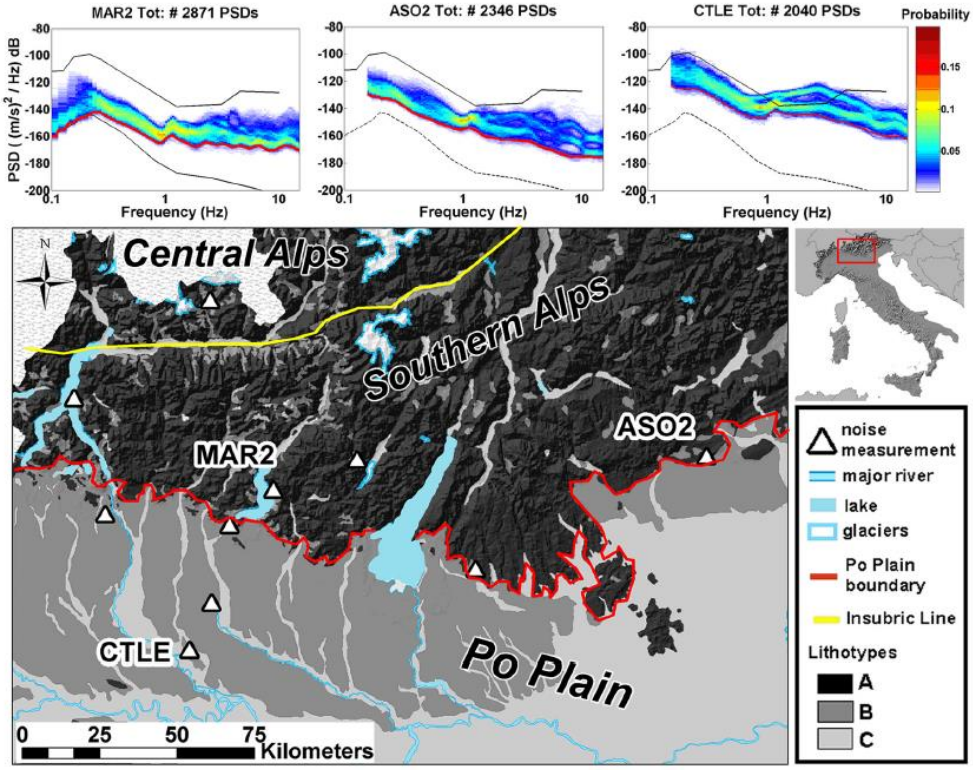

Figure 8: The three stations analysed are in different geological contexts: the MAR2 station is installed on rocks; CTLE site is installed further south on over a thick sedimentary cover in the Po plain and ASO2 station is located on a Pliocene hill at the margin of the Po Plain, partially covered by Po Plain sediments. For each station, the relevant PSD is shown below. Red lines in top panels are the 5th percentiles of PDFs. Marzorati et al., (2006).

Chapter 2

Italian Seismic Network and data

2.1 Introduction to IV Italian Seismic Network

A properly organized seismic network is a valuable tool for monitoring seismic events and seismic risk assessment and it can be a valid tool for study the seismic noise.

The Italian Seismic Network was developed immediately after the Irpinia seismic crisis in 1980. Initially, the National Seismic Network consisted of only a few stations. In fact, in the early 1990s, the Network was exclusively analogic and included about 70 stations spread throughout Italy, with only vertical sensor, except a few sites, constituted also two horizontal sensors to achieve complete ground motion.

In the time, the ING (National Institute of Geophysics), later known as the INGV (Istituto Nazionale di Geofisica e Vulcanologia), progressively upgraded the network and in fact, towards the middle of the 90s the advances of technology bring radical changes in both the acquisition and transmission and recording of data, thanks to the implementation of the digitization of seismic tracks.

At the beginning of the 2000s, the first satellite connections start and later also UMTS and Wi-Fi. In addition to the seismic sensor velocimetric are progressively approached accelerometric sensors and geodetic GPS, what will the current National Seismic Network multiparametric.

After approximately 30 years, these upgrades led to the present-day configuration, which consists of approximately 500 seismic stations (Michelini et al., 2016).

All the collected data are managed in real time by the INGV seismology centre located in Rome. Over the years, the Network grew in terms of its spatial coverage and sensor quality, but it is important to clarify that the development of the Network does not cover the Italian territory homogeneously. The cause of the expansion and uniform coverage of the Network is controlled mainly by logistic needs and the availability of financial resources. Although the Network is currently remains lacking in some areas, in the last years, the important technological upgrades have

allowed significant improvements.
The seismic network consists mainly of the Italian National Seismic Network, characterized by 598 stations.
In addition, other local, regional and national networks belong to other Italian or foreign institutions. These have been implemented for different monitoring and research purposes and the most numerous are:

- NGV Experiments Network (TV NETWORK code, 67 stations);
- Seismic Microzonation Network, 2016 Central Italy (3A code, 50 stations);
- IEMERSITO Seismic Network, 2016 Central Italy (XO code, 40 stations);
- Italian Strong Motion Network (IT code, 40 stations);
- Regional Seismic Network of North Western Italy (GU code, 36 stations).

The Figure 9 shows an image of the National Seismic Network and in addition other local and regional networks.
The actual composition of the network and the description of the stations is available at thewebsite http://webservices.ingv.it/ as a FDSN web service.

2.1.1 IV Italian Seismic Network

The IV Italian National Seismic Network is the nationwide permanent seismological Network, operated by the Istituto Nazionale di Geofisica e Vulcanologia with contributions from collaborating institutions and observatories.
Initially, it was deployed mainly for seismic monitoring. Over the years, the IV Network has grown in both quality and quantity and more instruments have been installed, gaining importance as a valuable research infrastructure too. Several types of seismic sensors characterize the network such as shortperiod, broadband and accelorometric instruments and they are collocated at many sites.
All stations are connected to the datacentre and transmitting sensor data in real time.
Data is distributed through the Orfeus European Integrated Data Archive (EIDA) federation and International Federation of Digital Seismograph Networks (FDSN) standard protocols under an open definition compliant license (INGV Seismological Data Centre (2006)).
Increasing the seismic station number has produced a huge quantity of low-magnitude recordings. In fact, a properly structured seismic network consisting of a sufficient number of seismic stationswith

low seismic noise and with a well distribution on the territory, it is very important for a good detection of seismic events even of small magnitude that are often obliterated by very noisy stations. For this reasons, it is very important to study the performance of theseismic Network.

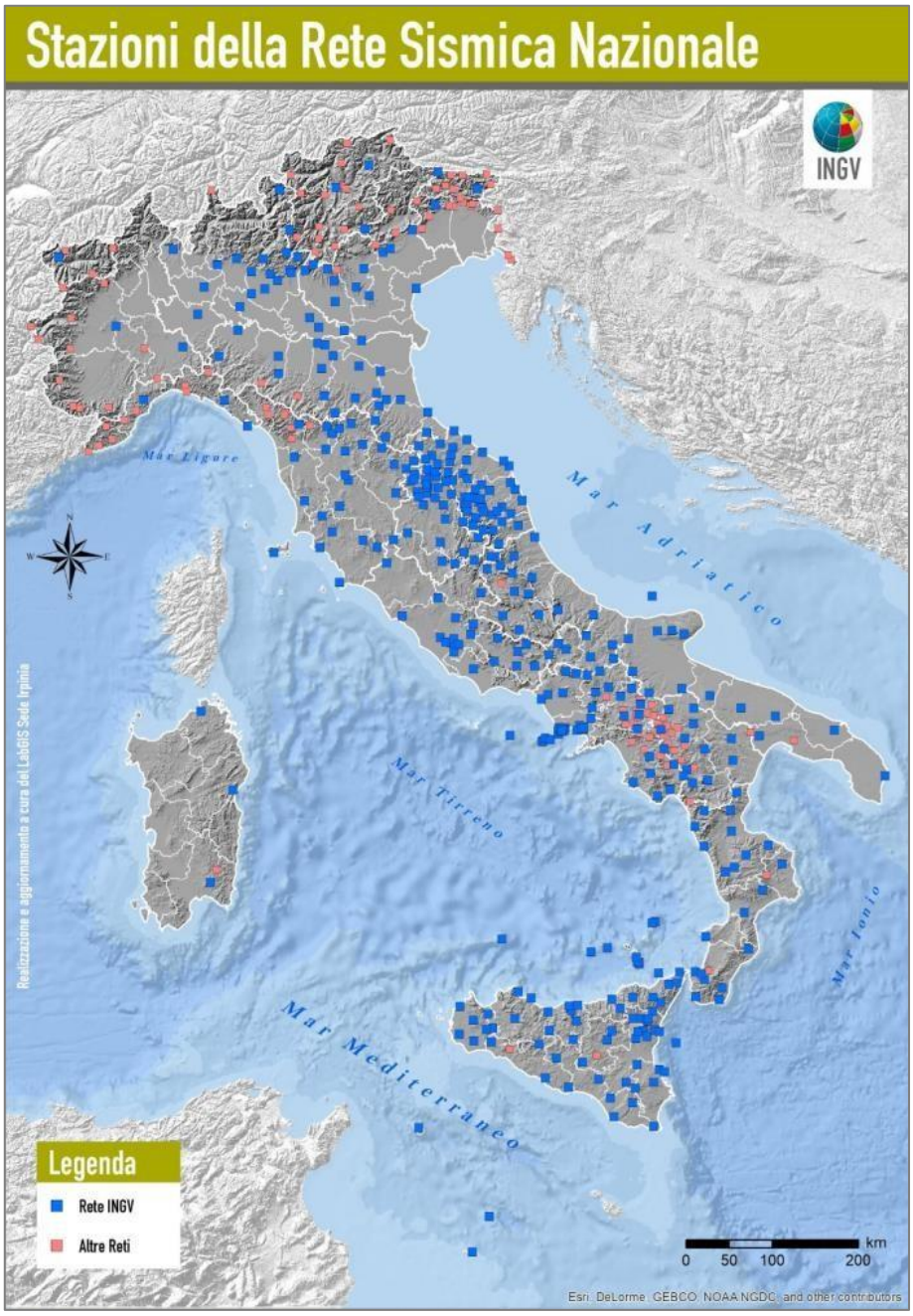

Figure 9: Spatial distribution of the INGV seismic station. INGV network is indicated with blue squares; others network are indicated with red ones. (INGV website).

2.2 Instrument description and data collection

The IV Italian network consists in 598 stations. The seismic networks of the INGV each station is characterized by a code name or acronym chosen in a unique way. In addition, the installation site can be of different types: the choice is made by discriminating the sites suitable for the characterization of seismic signals and most of the sites are located away from urban centres and possibly protected from external agents. Often in fact, if not already available, they are installed inside specially created wells. The ideal sites should be those on bedrock surfacing but unfortunately this is not always possible and many stations are also placed on sedimentary roofs.

The instrumentation is always accompanied by GPS antenna that allow sending signals in real time to the centralized network of INGV in Rome that operates continuously.

As in Figure 10, a station is usually consists of a sensor, usually stored in a box, a digitizer that allows the transformation from seismic signal to electrical impulse, a GPS antenna for the transfer of the signal to the INGV.

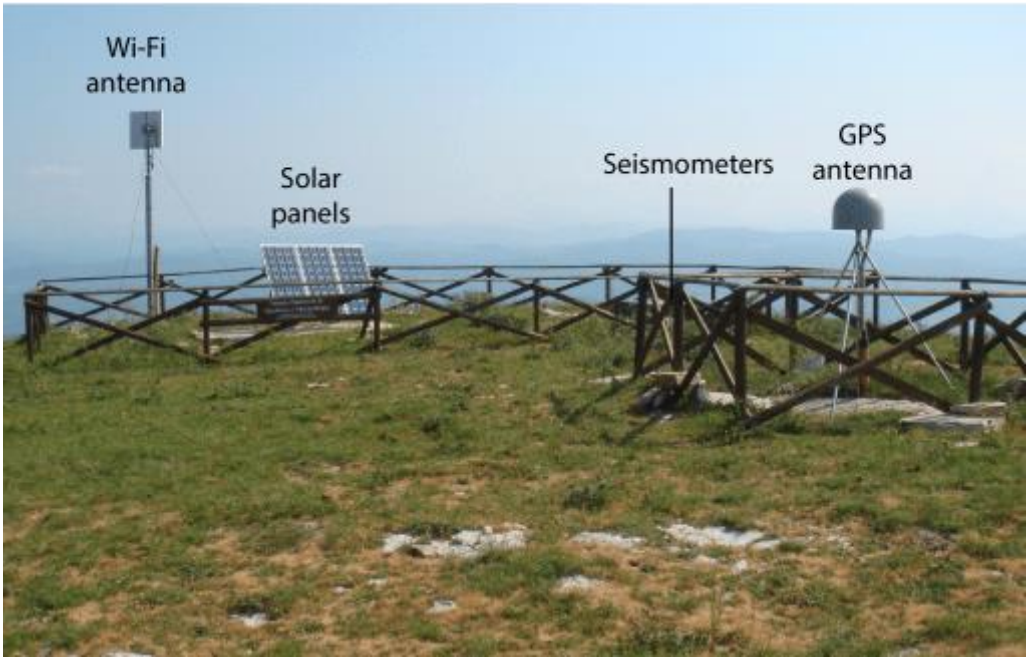

Figure 10: Example of seismic station. In the photo: Monte Tezio seismic station (ATTE). All instruments (GPS and broadband seismometer) send data in real time through a Wi-Fi system based on dedicated radio links. (Source: INGV terremoti, website).

Although the National Seismic Network consists of 589 stations, for this research, only 233 stations were selected (Fig.8), whose main characteristics are given in the table at the end of the chapter.

Only broadband sensors with minimum period of 40 seconds and at least three consecutive years of available data (2015-2017) characterize the stations subset selected.

These two criteria allowed discriminating the 233 stations.

The time window is period of three years 2015 - 2017: it has been decided and with stations working continuously without long periods of malfunction in order to have a more robust estimate. Stations with a gap of about 1 year were discarded: it was necessary to have some continuity of the data for a good evaluation. In addition, those with significant instrumental noise that obliterated the ambient noise needed for the analysis were also discarded too. This allowed eliminating all the stations that could cause disturbances and not continuity of the data in order to have a good spectral analysis of the seismic noise.

Even more selective was the choice of bandwidth and type of sensors. Having a greater interest mainly in low frequencies, only broadband velocimetric stations were chosen. This was necessary for our purpose to know the energy and capacity of seismic noise at different stations but especially understand the real performance of the National Seismic Network in terms of localization even of small magnitude events that often are obliterated by noise in the seismic records.

The selected stations are characterized by a high sensitivity from 40 to 120 seconds. Among the many broadband only six different continuously broadband sensors are returned between the selected stations. Especially, the most of stations (166 sensors) are equipped with Trillium 40S (three-component, force-balance broadbandseismometers) are the most widespread sensors. Trillium 40 seismometers are three-component, force-balance broadband seismometers that operate over a wide temperature range without manual recentring. Suitable for both portable and fixed applications, the extended response of Trillium 40 seismometers at higher frequencies makes these seismometers ideal for local and regional networks as well as volcano hazard monitoring and aftershock studies. The Figure 12 shows a Trillium 40 seismometer, while the main features of all sensors are provided in the following Table 4.

Figure 11: Spatial distribution of the 233 seismic stations selected.

Productor	Device name	Period	Number
Guralp	CMG - 3EX	120s	3
Guralp	CMG - 40T	60s	18
Nanometrics	Trillium - 120C	120s	6
Nanometrics	Trillium - 120S	120s	29
Nanometrics	Trillium - 240S	240s	11
Nanometrics	Trillium - 40S	40s	166

Table 4: Technical information of the six different models of broadband sensors.

Figure 12: Trillium 40S seismometer is reported. This is the most used sensor in the selected stations. Source: website.

A specially created software carries out the information management interface of the centralized National Seismic Network. Seisface software is a software where all the stations are registered and where you can consult the characteristics of site and sensor, the status of activity, any malfunctions and failures. In fact, it was possible to select the stations according to the characteristics sought for this work.

Each site is characterized by specific characteristics that determine a different level of seismic noise. Most station are located in the countryside while some are within buildings or near urban centres.

Showing a wide diversity of sites exploring noise levels from different sources, a wide frequency band from 0.0025 to 30 Hz has been analysed, in accordance with the seismic sensors bandwidth and the literature. Since the low frequencies are the most interesting range, a minimum period of 40 seconds has been decided (0.025 Hz). In the other hand, the highest member has been limited to 30 Hz, both because the high frequencies were of less interest and then also for reasons related to the digitizer and the sampling frequency (not exceeding 100 Hz, in turn limited to no more than 50 Hz considering Nyquist theorem). The aim was to create frequency bands in agreement with the literature but also representing homogeneous subsets. The completely period band analysed is divided into four main intervals:

- Very Low Frequency (0.025-0.12 Hz);
- Low Frequency (0.12-1.2 Hz);
- Middle Frequency (1.2-10 Hz);
- High Frequency (10-30 Hz).

They have been established roughly consistent with bibliographic data and the main type source is associated (Table 5). Especially the lower frequency seems to be generated by natural sources while

anthropogenic sources are evident at high frequencies. A common agreement with several authors was found (Banerji, 1924, 1925, Gutenberg 1958, Asten 1978 and 1984, Peterson, 1993, Okada, 2003, McNamara and Buland, 2004, and others) about the origin of seismic noise and its frequency features bands. Instead, several authors (Groos and Ritter, 2009 Bormann and Wielandt, 2013 and others) associate anthropic sources to the highest frequencies bands (10-30 Hz) as assumed.

Class	Frequency range	Main sources
Very Low Frequency	0.025 - 0.012 Hz	Large meteorological perturbations
Low Frequency	0.012 - 1.2 Hz	Oceanic waves striking along the coasts
Middle Frequency	1.2 - 10 Hz	Local scale meteorological conditions and urban sources
High Frequency	10 - 30 Hz	Urban and antropogenic sources

Table 5: The four different frequency bands and the main associated type sources.

Finally, the data extracted come from the three components of each sensor. The vertical component is indicated with Z, while E and N corresponding to East and North components. Instead, with H component the average of the two horizontal components shall be indicated. In order to build our dataset it was necessary to evaluate the average PSDs over the three-year period for each station for the four frequency bands for Z and H components.

The name of the station (code) is shown below, their geographical coordinates and their altitude. The characteristics of the 233 stations examined have been listed in the following Table 6.

Station	Latitude	Longitude	Altitude (m)
ACER	40.7867	15.9427	690
AGLI	41.1269	9.1733	180
AIO	37.9712	15.233	751
ALJA	37.749	13.7537	700
AMUR	40.9071	16.6041	443
AOI	43.5502	13.602	530
APEC	43.5585	12.4199	488
APRC	41.7574	15.5431	672
ARCI	42.8519	11.4754	1080
ARVD	43.4981	12.9415	461
ASQU	43.7967	11.7893	860
ASSB	43.0426	12.6587	734
ATFO	43.3666	12.5715	960
ATMI	43.3342	12.268	581
ATPC	43.4807	12.457	810
ATTE	43.1979	12.3536	929
ATVO	43.3821	12.4066	638
BDI	44.0624	10.597	830
BIOG	41.1999	15.1326	623
BOB	44.7679	9.4478	910
BRIS	44.2245	11.7666	260
BRMO	46.4762	10.3722	1380
BSSO	41.5461	14.5938	1010
BULG	40.0783	15.3776	815
CAAM	40.82	14.1407	130
CAFE	41.028	15.2366	1070
CAFI	43.3292	11.9663	547
CAFL	40.8439	14.0935	75
CAGR	37.622	14.4999	548
CAMP	42.5358	13.409	1283
CAR1	39.2534	16.2114	680
CASP	42.7908	10.8652	390
CAVE	44.8658	11.0031	18
CAVT	37.6788	12.7556	158
CDRU	40.4896	15.3046	1057

CELB	42.7466	10.2107	742
CELI	39.4027	16.5088	1290
CERA	41.5978	14.0183	800
CERT	41.949	12.9818	773
CESI	43.0049	12.9046	840
CESX	42.6085	12.5868	458
CET2	39.5288	15.9546	675
CFMN	40.8329	14.0935	59
CIGN	41.6542	14.905	350
CING	43.3756	13.1954	626
CLTA	37.158	13.962	246
CMDO	37.4639	13.8229	571
CMPR	40.3181	15.303	732
CMSN	40.8382	14.1818	20
COLB	40.8187	14.1473	22
CORL	37.8943	13.3038	660
CPIS	40.8292	14.147	77
CPOZ	40.8211	14.1187	2
CRE	43.6189	11.9517	1215
CRMI	43.7956	10.9795	490
CRTO	40.8212	14.4223	1122
CSFT	40.8291	14.1397	107
CSLB	37.9374	14.0579	583
CSNT	43.4731	11.2902	636
CSOB	40.8275	14.1443	175
CTI	46.0482	11.6497	1180
DGI	40.318	9.6067	354
ECNV	37.5956	14.7125	484
EMSG	37.8208	14.9498	1435
EPOZ	37.6719	15.1885	124
EPZF	37.824	14.857	1140
ESLN	37.6934	14.9744	1787
ESML	37.6181	14.8794	417
FAGN	42.2657	13.5838	761
FAVR	37.2671	13.667	289
FDMO	43.0365	13.0873	550
FIAM	42.268	13.1172	1070

FIR	43.7744	11.2551	40
FNVD	44.1678	11.1229	950
FRES	41.9735	14.6693	414
FROS	43.2097	11.1562	432
FSSB	43.6931	12.7771	523
FVI	46.5966	12.7804	1024
GALF	37.7107	14.5665	740
GATE	41.5131	14.9102	487
GIB	37.9901	14.026	1020
GIGS	42.4532	13.5728	960
GIUL	41.5583	13.2546	566
GROG	43.4262	9.892	118
GUAR	41.7945	13.3123	741
GUMA	43.0627	13.3352	574
HAGA	37.285	15.155	126
HAVL	36.9596	15.122	502
HCRL	37.2831	15.0325	240
HLNI	37.3485	14.872	146
HMDC	36.959	14.7831	595
HPAC	36.7085	15.0372	70
HVZN	37.1783	14.7155	787
IACL	38.533	14.355	145
IFIL	38.5642	14.5753	277
IFOR	40.7115	13.8551	170
ILLI	38.4457	14.9483	283
IMI	43.9105	7.8932	840
IMTC	40.7209	13.8758	59
INTR	42.0115	13.9046	924
IOCA	40.7458	13.9008	123
IST3	38.7992	15.2304	255
ISTR	38.7866	15.1918	103
IVGP	38.3968	14.9608	150
IVPL	38.3763	14.9801	486
JOPP	38.6068	15.8856	500
LATE	42.6137	11.804	610
LAV9	41.6778	12.6989	300
LINA	35.8613	12.8643	70

LMD	44.0775	11.7073	450
LNSS	42.6029	13.0403	1155
LPDG	35.5183	12.6302	50
LPEL	42.0468	14.1832	760
LRP	41.6471	13.5866	372
MA9	41.7698	12.6591	340
MABI	46.0549	10.514	1853
MAGA	45.7753	10.6286	1265
MAGO	43.2732	10.6579	280
MAON	42.4283	11.1309	237
MCEL	40.3249	15.8019	960
MCIV	42.7786	11.6765	790
MCRV	40.7826	15.1684	1191
MCSR	38.0646	15.2301	1064
MDI	45.7697	9.716	954
MELA	41.7059	15.127	115
MESG	40.5894	17.8504	78
MFNL	37.7908	12.9224	677
MGAB	42.9126	12.1121	547
MGR	40.1376	15.5535	288
MIDA	41.6419	14.254	950
MIGL	40.6044	16.441	440
MILN	45.4803	9.2321	125
MILZ	38.2713	15.2313	0
MMGO	37.6619	12.9767	397
MMN	39.891	15.9904	921
MOCO	41.37	15.158	1049
MODR	41.1459	13.8779	345
MOMA	42.8039	12.5701	1040
MONC	45.0739	7.9271	480
MPNC	38.1465	15.3528	479
MRB1	41.1227	14.9682	688
MRGE	45.7698	7.061	1660
MRLC	40.7564	15.4889	605
MRVN	41.0609	16.1958	610
MSAG	41.712	15.9096	890
MSFR	38.0339	14.5916	723

MSRU	38.2639	15.5083	408
MSSA	44.3162	9.5174	930
MTCE	42.0228	12.7422	388
MTRZ	44.3128	11.4248	570
MTSN	40.2663	15.7515	1056
MTTG	38.0031	15.6999	484
MUCR	38.043	14.8739	1042
MURB	43.263	12.5246	845
NARO	43.6108	12.5806	272
NDIM	44.8873	10.8987	19
NOCI	40.7888	17.0644	420
NRCA	42.8336	13.1143	927
OFFI	42.935	13.6857	320
OPPE	45.3082	11.1724	20
ORI	40.051	16.4504	375
ORZI	45.4056	9.9307	83
OSSC	43.5236	11.2458	452
OVO	40.8275	14.3967	584
PALZ	40.9441	15.9602	450
PAOL	41.0312	14.5675	715
PARC	43.6486	12.2386	580
PESA	43.941	12.8402	221
PETRA	37.8335	14.1148	1547
PIEI	43.5357	12.535	665
PIGN	41.2	14.1799	398
PII	43.7219	10.525	66
PIPA	39.4851	16.8158	479
PLAC	38.4494	16.4383	602
PLMA	44.0498	9.8537	22
POFI	41.7174	13.712	878
PRMA	44.7637	10.3131	78
PSB1	41.2235	14.8108	551
PTCC	46.4075	13.354	700
PTQR	42.0219	13.4006	957
PTRJ	41.3641	14.529	1027
PTRP	40.5215	16.0612	1077
QLNO	44.3242	8.3459	547

RAFF	37.2225	14.3624	310
RDP	41.7604	12.7103	760
RESU	37.6468	14.0568	785
RMP	41.8111	12.7022	380
RNI2	41.7033	14.1524	950
ROM9	41.8284	12.5155	110
ROVR	45.6468	11.0721	1316
RSM2	43.9377	12.4451	645
SACR	41.3974	14.7057	859
SACS	42.8491	11.9097	845
SALB	39.8772	16.3459	1200
SALO	45.6183	10.5243	600
SAMA	41.7805	12.5923	119
SARZ	44.8673	8.9136	266
SCTE	40.0724	18.4675	150
SEI	44.0543	11.3585	610
SERS	39.0359	16.6886	1221
SGG	41.3867	14.3792	880
SGRT	41.7546	15.7437	960
SGTA	41.135	15.365	890
SIRI	40.1821	15.8675	1063
SLCN	40.39	15.6328	986
SNAL	40.9254	15.2091	874
SNTG	43.255	12.9406	650
SOLUN	38.0919	13.5326	190
SRES	42.237	12.5099	410
SSFR	43.4363	12.7822	750
SSY	37.1577	15.0737	600
STAL	46.2601	12.7104	625
TDS	39.6601	16.3376	244
TEOL	45.3617	11.6739	370
TERO	42.6228	13.6039	673
TOLF	42.0641	12.0002	371
TREM	42.123	15.51	120
TRIF	43.1148	10.9027	596
TRIV	41.7666	14.5502	598
TRTR	42.8081	13.9138	160

USI	38.7079	13.1791	285
VAGA	41.4154	14.2342	795
VARE	45.8677	8.77	1219
VARP	40.8165	14.4101	629
VBKN	40.83	14.4299	951
VCRE	40.819	14.4314	1113
VITU	41.1833	14.6302	848
VTIR	40.8059	14.4242	612
VULT	40.9549	15.6163	1101
VVDG	40.8356	14.4238	855
VVLD	41.8697	13.6232	1051
ZCCA	44.3509	10.9765	700
ZONE	45.7636	10.1171	691

Table 6: Basic information of the 233 selected stations.

Chapter 3

Methods: data and seismic noise computation

Ambient vibrations has an essentially stochastic character and its analysis must have place with statistical/probabilistic methods.
The scientific objectives of this research are based on the spectral and statistical characterization of the environmental vibrations recorded by the stations of the National Seismic Network operating in three-year period 2015-2017.
Several spectral and statistic methodologies has been used to this research.
The study of background seismic noise is usually conducted through spectral analysis showing the different frequency contribution of the numerous signals that compose it.
A spectral analysis of all stations has been performed using the classic methods used in literature. In order to analyse the seismic noise, Power Spectral Density is used, whose reference models have been taken in the literature using those of Peterson (1993). In addition, Mcnamara and Buland (2004) method was adopted to define the probability density of seismic noise of each station.
A wider section is devoted to the statistical aspect.
Several parameters have been calculated in order to statistically describe the frequency distribution of seismic noise and a robust Kernel method has better defined the statistical approach.
Interpolations methods such filtering have also been applied in order to return interpolated maps.
Finally, linear and multiple regressions have been created between the noise power and geographical, meteorological and geological parameters.

3.1 PSD, PDF and data spectral processing

3.1.1Power Spectral Density

As observed by Okada 2003, seismic noise has both temporal and spatial variability. Especially, the time variability is due to the type of sources that generate noise: for frequencies >1 the

variability is linked to meteorological phenomena while at higher frequencies the variability is greater and is linked to human activities. Spatial variability is observed by site. A valid spatial stationarity can only occur in the case of homogeneous horizontal layer geological structures but is not discounted at either low or other frequencies.

Since seismic noise does not have a finite, duration and its characteristics depend on a wide variety of spatially distributedsources, and unrelated to each other, are assimilated to a stochastic stationary process (Bormann, 2002).

Cause of its stochastic nature, spectral analysis cannot be conducted through Fourier's ordinary transformation whose integral maynot converge (Aki e Richards, 1980).

The Fourier integral transformation can only be applied to transient signals (signals that disappear or decay in the time and having a finite energy like seismic signals) while the integral may diverge for other signals.

According to the Fourier theorem, any arbitrary transient f (t) function (1.1) in the time domain can be represented by an equivalent F (ω) function (1.2) in the frequency domain.

Bormann and Wielandt, 2013). The following relation hold:

(1.1)

$$f(t) = (2\pi)^{-1} \int_{-\infty}^{\infty} F(\omega)\ \exp(i\omega t)\, d\omega$$

(1.2)

$$F(\omega) = \int_{-\infty}^{\infty} f(t) \exp(-i\omega t) dt = \left|F(\omega)\right| \exp(i\phi(\omega))$$

The 1.2 equation represents the f(t) Fourier transform.

Where:

F (ω) is the complex Fourier transform of the continuous signal f (t), usually written as a function of the angular frequency ω which is 2π times the common frequency.

The absolute value of the Fourier transform, |F (ω)|, is called the amplitude spectrum, and itsphase φ (ω) the phase spectrum. |F (ω)|= A (ω) is the amplitude spectral density with the unit m/Hz, ω = 2 πf the angular frequency (with f - frequency in unit Hz) and φ (ω) the phase spectrum which can be expressed in degrees, rad or 2πrad.

A Fourier transformation in the strict sense does not exist for stationary signals.

Stationary signals are signals whose statistical properties and amplitude (mean) do not change with the time.

For these reasons, having no finite duration and its characteristics, determined by sources often continuous, randomly distributed in space and independent of each other, seismic noise is a stationary stochastic process.

These stationary signals need a different mathematical treatment: the 1.2 equation does not converge due to stochastic nature, and the spectral amplitude density A(ω) and the phase spectrum φ (ω) cannot be calculated consequently.

The standard method for quantifying seismic background noise is to calculate the noise Power Spectral Density P(ω). It is defined as the Fourier transform of the signal autocorrelation function (Peterson, 1993; Stutzmann el al., 2000; McNamara e Buland, 2004). In others words, Power Spectral Density is a mathematical quantitythat defines the spectral content of a signal (i.e. it describes how a signal's power is distributed in frequency) (Youngworth et al., 2005).

The most common method for estimating the PSD for stationary random seismic data is called the direct Fourier transform or Cooley–Tukey method (Cooley and Tukey, 1965).

If f(t) is expressed as displacement, velocity or acceleration, P(ω) shall be expressed as in $(m)^2/Hz$, $(m/s)^2/Hz$ or $(m/s^2)^2/Hz$ respectively.

By approximating the movement of the ground x (t) of the seismic noise by means of a sine wave x(t)= to sin(ωt), where ad is the displacement amplitude, it is possible to convert it to speed deriving according to dx/dt, or in acceleration according to dx^2/dt^2; the respective amplitudes result $a_v = a_d\omega$ and $a_a = a_d\omega^2$.

So knowing the PSD $P_d(\omega)$ relative to the displacement, you get P(ω) for speeds and accelerations:

(1.3) $$P_v(\omega) = P_d\,\omega^2 = 4\pi^2 f^2 P_d$$

(1.4) $$P_a(\omega) = P_d\,\omega^4 = 16\pi^4 f^4 P_d = 4\pi^2 f^2 P_v$$

As in acoustics, Power Spectral Density unit is dB (deciBel). Decibels is not an absolute unit of measurement, but is the ratio between the measured and the established reference level. ThedB scale is logarithmic and power ratio between two signals of amplitude is often expressedin dB. This logarithmic measure expresses a ratio as a difference of logarithms.

$$10 \log_{10}[(a2/a1)^2] = 20 \log_{10}[(a2/a1)]$$

As in the field of acoustics, the seismic signal relative to the power of noise $(a2/a1)^2$ expressed in dB (decibels); for example PSD in dB units referenced to 1 $(m/s)^2$ / Hz, is

represented as (1.5):

(1.5) $$P_v\ (dB) = 10 \log (P_v / 1\ (m/s)^2 / Hz)$$

Considering the stationary environmental noise in time and space is thus possible a spectral representation.

Transient signals have a finite energy and zero power (in the average over all times) while stationary signals have an infinite energy but a finite power.

The same holds for the spectral densities, in fact Power Spectral Density (PSD) is most appropriate for the quantification of stationary noise, while their Energy Spectral Density (ESD) more adequately describes transient signals. This difference between the two densities is not so different and it is necessary to consider from case to case as such as the comparison of earthquake signals: in some conditions neither the PSD nor the ESD are suitable measures (Bormann and Wielandt, 2013).

The concept of power is mainly applied to stationary signals such as sinewaves or seismic noise whose average power is constant or varies slowly. PSD is a very useful tool for to know frequencies and amplitudes of oscillatory signals in time series data.

Power spectral density (PSD) estimates the distribution of power with the frequency. It is a standard method for quantification of the seismic background noise (Jana et al., 2017).

The seismic noise model most commonly referenced today is Peterson (1993) model and it was based on data recorded at a variety of stations during periods of apparent low seismic noise.

Peterson (1993) marked and characterized the first comprehensive global study of noise levels of seismic stations distributed worldwide.

Based on the power spectral density (PSD) of background seismic noise, he defined a New Low Noise Model (NLNM) and New High Noise Model (NHNM), which became standards when comparing noise levels.

The spectral study of seismic noise recorded both in days of quiet that of high noise, allowed Peterson (1993) to characterize seismic noise on the earth's surface through two curves, in a frequency band of seismological interest, limit all spectra calculated with two limit.

They have been considered as a currently reference of the upper and lower limits noise respectively noise and they are shown in Figure 13, together the original noise models.

Especially they represent the upper and lower-bound envelopes of a cumulative compilation of representative ground acceleration power spectral densities determined for noisy and quietperiods at 75 digital stations worldwide.

Peterson also built a new world noise model following the same procedure used to develop the original earth noise models created by Brune and Oliver (1959). In figure 14, reported the new noise

models and network overlay spectra.

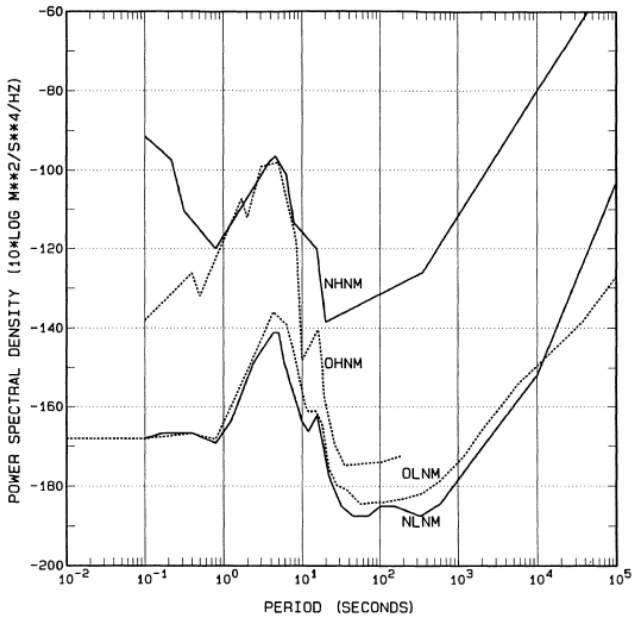

Figure 13: Comparison of original noise models (OHNM and OLNM) and new global noise model (NHNM and NLNM). Peterson, (1993).

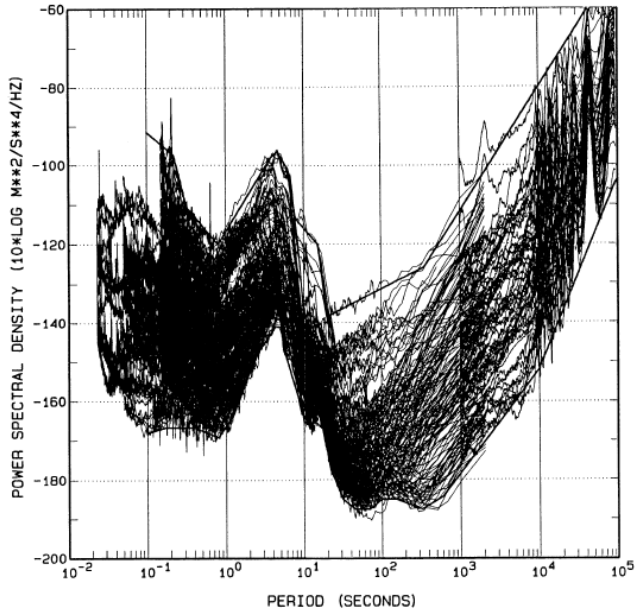

Figure 14: An overlay of network spectra (Peterson, 1993).

In the following years, several authors have tried to propose new models. For example Berger e Davis (2004) have analysed data from the118 Global Seismographic Network (GSN) stations operating during the year July 2001 through June 2002 and analysing the absolute quietest conditions for stations within the GSN. From estimate computed, they have developed a robust noise model that exhibits significant differences from previous Peterson models (1993) in both the normal mode and body wave bands (Fig. 15).

Unfortunately, both the Peterson model and the updated models did not include any deployed station in North Africa and Middle East, which reflects the noise levels within the desert environment of those regions. In fact, for 1year Soliman, 2013, conducted a survey to create a new seismic noise model from very broadband stations, which deployed in North Africa. New noise models obtained from this study: ELNM and EHNM curves can now be compared directly with the Peterson noise models (Fig. 16).

Although in the literature the limits have been redefined based on more recent observations (Berger e Davis, 2004) in any case, the Peterson model remain the most commonly referenced today: Peterson references are still a good approximation of the values in which the variability of the seismic noise is contained.

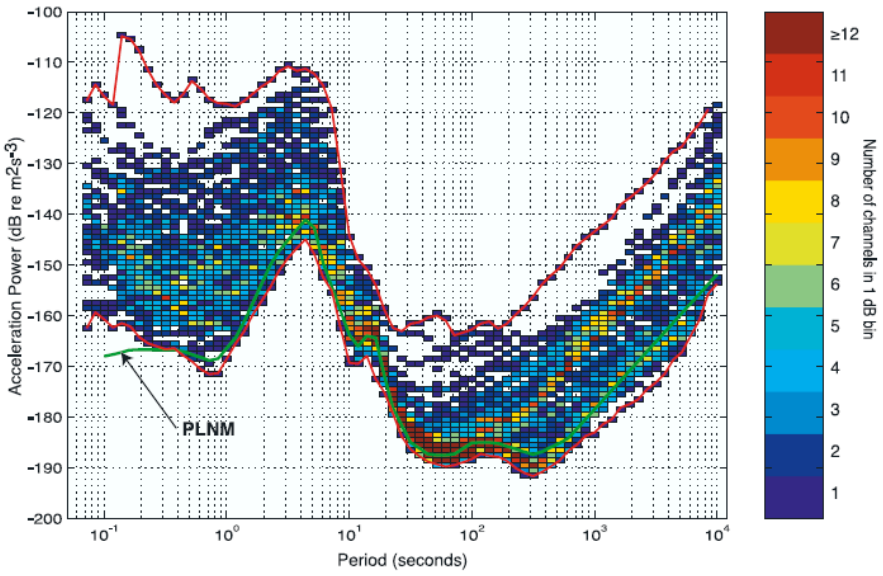

Figure 15: Results found by computing density of observations, one per component per station, for all 118 stations considered in this study. The colours indicate how many stations' spectral estimates lie in each 1 dB by 1/14th decade rectangle. This plot includes contributions from both horizontal and vertical channels. PLNM is Low Peterson Model and here the minimum spectral values are higher than those for PLNM. Berger e Davis (2004).

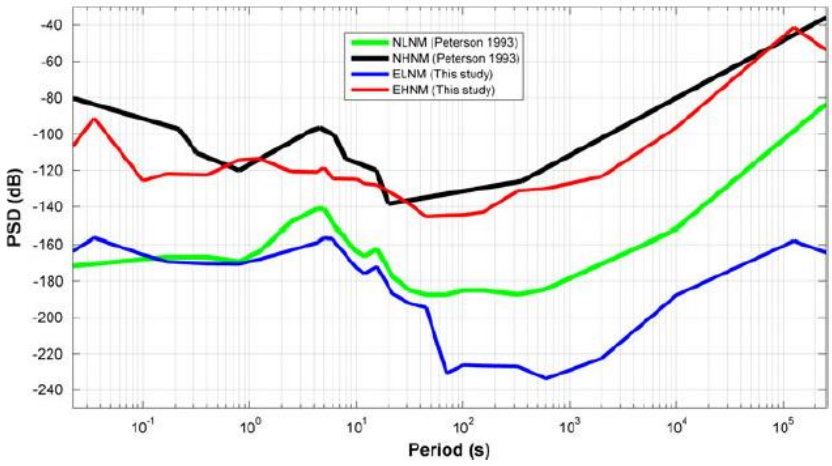

Figure 16: Comparison of the constructed new noise models (EHNM and EHNM) for Soliman (2013) and the Peterson (1993) noise models (NHNM and NHNM). Here the minimum spectral values of the ELNM noise model are significantly lower than those for the NLNM of Peterson (1993). Both the ELNM and EHNM were based on well equipment and good vaulted stations data. The difference between the obtained new noise models and the Peterson (1993) noise models are most likely due to the nature and the sources of background noise at desert areas, seismometer type, advanced technology and methods used to select and process the data. Soliman (2013).

3.1.2 Probability Density Functions

Probability Density Function (PDF), describes the frequency content in statistical terms.

A statistical approach of the PSDs provides the respective PDFs that prove to be a useful tool for monitoring the network performance and to evaluate the seismic noise level at a given station.

Youngworth et al. (2005) state that Probability Density Functions describes howa signal power is distributed in frequency.

To plot many PSDs curves into one graph (e.g. PSDs from all stations of a large network at the same time, or from many hourly or daily records of a single station) may be impossible to distinguish and label individual curves. In fact applying the Probability Density Function is the better way to represent all PSDs curves, measuring the relative density of PSDs values.

McNamara and Buland (2004) provided and documented a standard method to calculate ambient seismic background noise, starting to the standard low and high noise Peterson models (NLNM and NHNM). This new method, it is relatively easy to compare seismic noise characteristics between different networks in different regions. In fact, many authors (Marzorati and Bindi, 2006; Bonnefoy-

Claudet, 2006; Vassallo et al. 2010; Dimitrova and Nikolova, 2010; Grecu et al., 2012; Abd al-all, 2013; Custódio et al., 2014; Anthony et al., 2015; Gui and Aydin, 2015; Demuth and Ottemöller, 2016; Jana et al., 2017; and others) are based on this approach and it has since been adopted around the world.

They presented a new statistical algorithm where they compute probability density functions (PDFs) to evaluate and to estimate noise levels over a broad range of noise at a given seismic station.

Especially, their approach calculates PDF to estimate distribution of PSD of the noise in a wide frequency range from 0.01 to 16 Hz (100 - to 0.0625-sec period) across the continental United States, using broadband stations for 3-yr period (from 2001 to 2003).

The dominant noise resulting from the instrumentation itself or from ambient Earth vibrations and self-noise is well below the seismic noise and recognizable. In fact, the minimum noise levels (are generally very low probability (1%–2%), suggesting that the minimum does not represent common station noise levels. They showed that the PDF mode corresponds to the highestprobability noise level for a given station. In fact, they computed a new noise model based on the mode levels (MLNM). The MLNM was constructed from the minimum PDF mode noise values observed per octave and is generally higher than the NLNM of Peterson (1993). Most stations show that the MLNM about 10–15 dB higher than the NLNM from 0.01 to 20 sec (10–0.05 Hz) for continental United States. About higher powers, noise power estimates are spread over a wide range of powers at all periods. This region of the PDF is dominated by high power occurrences of earthquakes, cultural noise, and recording system transients. Especially, these curves are often affected by system transients or, at higher frequencies, displays jumps that are related to the diurnal variations in cultural noise. In Figure 17, is shown the PDF of HLID BHZ station: it possible to observe like several sources of seismic noise observed in the PDFs.

Stations exhibit considerable variations in noise levels as a function of time of day, season, location, and installation type. Traffic and industries are responsible for an important noise level and induce very strong diurnal variations.

The advantage of the method is that there is no need to filter data from earthquakes, gaps, spikes, calibrations pulses etc. In fact, “disturbing” signals in the seismic data has low-level probability of occurrence while ambient noise reveals itself as a signal with high probability occurrence.

The most common main results of the studies listed above include:

- cultural/anthropogenic sources significantly affect seismic noise at short-period, which often displays strong diurnal variations;
- microseismic noise (3–20 s) is strongly affected by seasonal variations and in general is well correlated with oceanic conditions;
- long-period seismic noise is often affected by the type of installation and insulation from

environmental conditions.

For instance, another interesting study based on methodology of Mcnamara and Buland (2004) regards a survey of broadband seismic background noise for Antarctica; it was characterize in the 2007 by Anthony et al., (2015). They provide a comprehensive geographical characterization of Antarctica seismic noise environment, which cannot include anthropogenic noise contamination. In Figure 18 is shown how the source of noise levels in Antarctica can be read from the PDF.

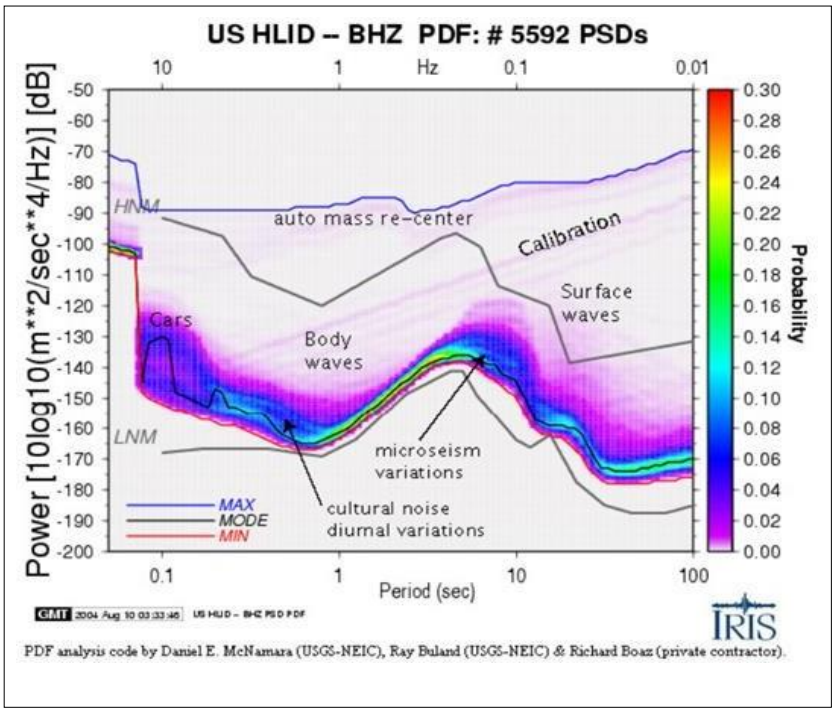

Figure 17: An example of PDF for station HLID BHZ constructed using 18,636 PSDs during the period from September 2000 to September 2003. Recording system transients, earthquakes, microseisms, anthropic noise, diurnal variation and self-noise are observable in the PDF. McNamara and Buland (2004).

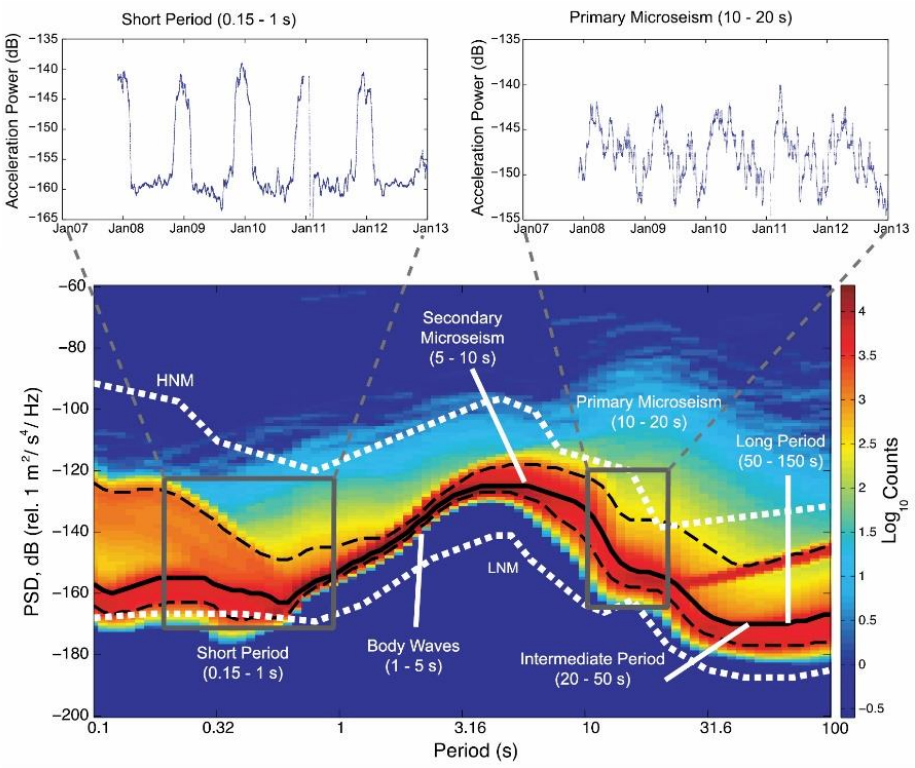

Figure 18: Characteristic seismic signals and noise observed at a broadband seismic station in Antarctica calculated from 1-hour data intervals from December 2007 to December 2012.

(a) Probability density function (PDF) of vertical-component seismic acceleration power spectral density (PSD) for QSPA station. White curves (HNM and LNM) show characteristic worldwide high- and low-noise spectral levels, respectively (Peterson 1993).

Six period bands of seismological interest are indicated: Short Period (local earthquake/icequake signals); Body Waves (dominant P and S body wave global earthquake signals); Primary and Secondary microseism bands (ocean wave), and Intermediate and Long Period Bands (seismic energy generated by longer period [infragravity] ocean waves, and seismic surface waves from large global earthquakes).

Seasonally varying annual average power levels in two period bands are shown above (b, c): in short period is shown anthropogenic austral summer activities at nearby Amundsen-Scott station, while Primary microseism signal reflect microseism signal due to the annual growth and decay of Antarctic sea ice and storminess of the Southern Ocean. Anthony et al., (2015).

3.2 Data Processing

In the present analysis, we use the McNamara and Buland (2004) approach, which uses the Probability Density Function (PDF) to generate the plot to display the distribution all of the PSDs curves.

Especially, using the data acquired, has been computed the Power Spectral Density (PSD) to characterize the background seismic noise, and consequently, to evaluate the true noise variation, all the 233 PDFs stations of the IV network have been generated from the computed PSD curves in the chosen three-year period. PSDs are computed from continuous for every channel, frequency distributions.

For the proper analysis of the seismic stations, we have used a new version of USGS-developed PQLX. In fact, the processing through the SQLX software package returning the PDFs. Like its predecessor PQLX software, uses the waveform and the instrument response files to generate the PSDs and PDFs (McNamara et al. 2009).

SQLX software, like PQLX, analyses the continuous seismic signal returning the Power Spectral Densities (PSD) on one-hour mobile signal windows with 50% overlap, following the algorithm described in McNamara and Buland (2004). For each period of the analysed spectral interval, the PSD values distribution construct the Probability Density Function of the seismic channel analysed, providing the probability that the seismic signal is located at a certain level of the spectral domain in the range analysed temporal. To estimate the true variation of noise at a given station has been generated seismic noise PDFs from thousands of PSDs processed using the methods discussed above. An example of PSD processed with SQLX in shown (Fig.19).

The probability of occurrence of a given power at a particular period is plotted for direct comparison to the Peterson high and low noise models (HNM and LNM respectively).

In this studies, body and surface waves from earthquakes or system transients and instrumental glitches such as data gaps, clipping, spikes, mass recenters, or calibration pulses, are not removed. These signals are included in our processing because they are generally low-probability occurrences that do not contaminate high-probability ambient seismic noise observed in the PDFs. In addition, transient signals are often useful for evaluating station performance. In the case of our research all, these elements are not clearly visible in detail, as every PSD and every pdf of each station represents the average over the three years and therefore what is obtained is a global result of the power of noise at a given station.

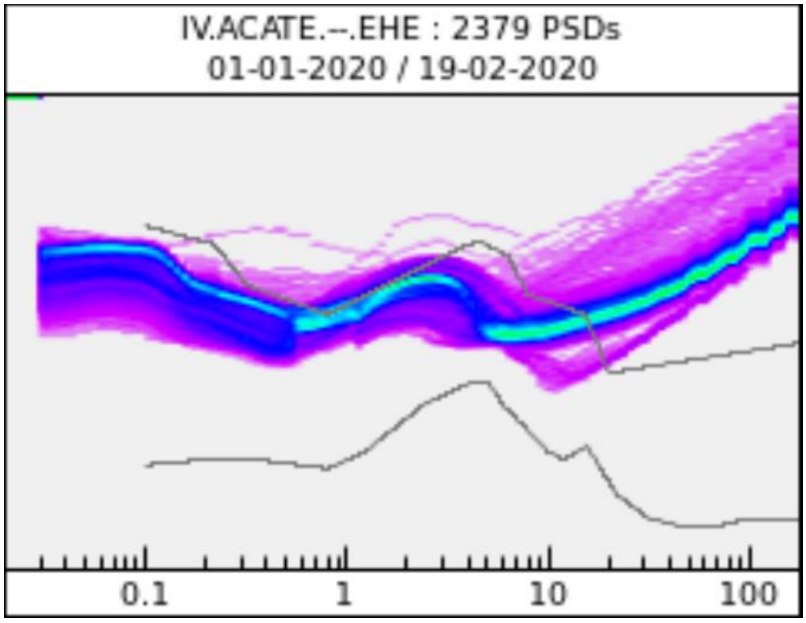

Figure 19: An example of PSD of Acate station processed with SQLX Software. They have been elaborated for this track 2379 PSDs.

3.3 Statistical properties

The field of ambient vibrations has a character essentially stochastic; therefore, its analysis must have place with statistical and probabilistic methods.

For this reason, an elaborate analysis has been carried out to describe the statistical properties of the Italian seismic noise such as mean, standard deviation, minimum, maximum, skewness and kurtosis. From the spectra analysis have been obtained the triennium PSDs means values for all 233 stations, both for frequency band and component. Analogous procedure for the relative standard deviation was done. This statistical dispersion index is useful to summarize the reliability of the means values.

Some calculations allowed verifying that the values of the two horizontal components were very similar; it was decided to treat the two components as a single horizontal component: a new component H has been calculated. This value was calculated from the difference of average of the two horizontal components N and E. The mean and the standard deviation have been calculated as for the others components.

In addition to the statistical parameters of mean and standard deviation, other parameters have been calculated. Maximum and minimum values was found for every component and each frequency band.

These values allowed us to establish the noise level for each frequency band; especially they are the noisiest and the least noisy station for each frequency band. These values were also useful for defining ranges in the data analysis. The average of the means values per frequency band and component also has been defined.

Finally, skewness and kurtosis parameters have been taken into consideration for the study of the data distribution. Skewness and kurtosis are the two important parameters statistical (shape indices) of distribution and in the descriptive statistics are studied. The skewness parameter is referring of the degree of symmetry, whereas the kurtosis defines the degree of peakedness, in the frequency distribution.

Especially in statistics with Skewness value one can identify the shape of the data distribution. Data can be distributed in different ways, like spread out more on left or on theright or in a uniform manner (Fig. 20). In this latter case, the data are scattered uniformly at the central point, and we have a normal distribution with perfectly symmetric and bell- shaped curve (i.e. both the sides are equal, and so it is not skewed). Mean, median and modelie at one point and the value is = 0. In other cases, an asymmetric distribution occurs: if it be tilted to the right, the value is >0, if to the left the value will be <0, and they will be respectively positive or negative skewness.

Kurtosis, on the other hand, refers to the pointedness of a peak in the distribution curve.

It is used to indicate the flatness or peakedness of the frequency distribution curve.

A positive kurtosis shows that the distribution is more peaked than the normal distribution, whereas a negative kurtosis represents a less peaked distribution than the normal distribution.

In fact, as shown in Fig. 21, it is possible to distinguish three types ofdistribution:

- Leptokurtic distribution: sharply peaked (> 0);
- Mesokurtic distribution: medium peaked (= 0);
- Platykurtic distribution: flattest peak and highly dispersed (< 0).

These two parameters were useful for the statistical description of histograms and curves derived from Kernel estimation.

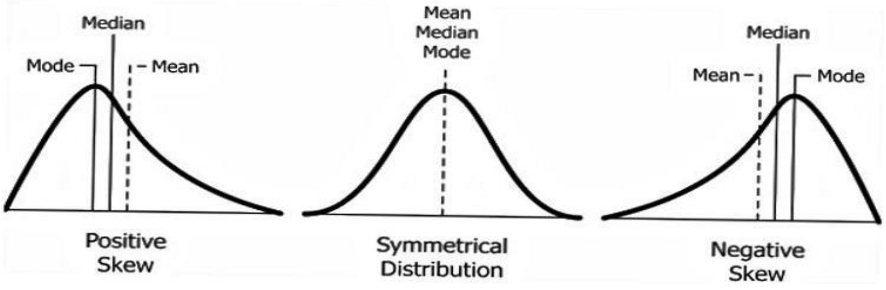

Figure 20: Asymmetric and symmetric distribution: the central curve represents a normal symmetric distribution showing bell-shaped curve; on the left and the right asymmetric curves with a skewness positive and negative, respectively. A positive skewness shows a values distribution more on left and conversely a negative skewness shows a values distribution on the right. Source: web.

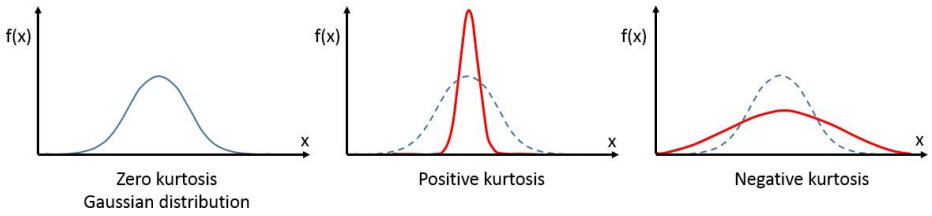

Figure 21: Types of kurtosis distribution Source: web.

In addition to the basic statistical parameters for noise characterisation, other parameters have been obtained.

For instance, computation of the horizontal to vertical spectral ratio was done. The ratio between the means of the H and Z components has been applied. Similarly, the ratio between their standard deviations has been calculated. This ratio is very important for noise and allows us to estimate the characteristics of the site on which the stations are located.

Finally, other parameters external to noise values have been calculated or downloaded: precipitation values and geographical parameters was take in account.

Among the geographical parameters the geographical location of the stations, that is, its altitude: all the elevations to which the stations are placed have been download from the INGV website (http://terremoti.ingv.it/instruments/network/IV).

The minimum distance of each station from the coastline has been computed between the geographical parameters. This procedure was carried out through a spreadsheet, which led to distance values.

Above all, the precipitation data were extracted from the ISPRA site. For a robust data that well showed the general rainfall in the Italian territory, it was chosen to consider the precipitation data in a rather long range. In fact, the data are related to the distribution by the annual height of annual precipitation in the period 1961-2017.

These three parameters will be used for linear regressions where will be discussed in details later.

Therefore, a large database for data analysis has been created.

3.4 Nonparametric Density Estimation: histograms and kernel method

It is essential to apply a density estimate to represent statistically the seismic noise distribution all over the Italian territory.

There exists a number of methods for nonparametric density estimation, and the well-known histogram is the simplest form and widely used nonparametric density estimation. A histogram is a diagram that provides a graphical representation of statistical data of a univariate distribution by a bars graph.

A histogram is a plot that lets you discover, and show, the underlying frequency distribution (shape) of a set of continuous data. This allows the inspection of the data for its underlying distribution (such as normal distribution), outliers, skewness, etc.

To construct a histogram from a continuous variable you first need to split the data into interval. In fact, the sample space is divided into disjoint categories, or bins, (the number of bins is expressed by a natural number) and the density is approximated by counting how many data points fall into each bin. As demonstrated, the bin origin has a significant influence on the final histogram shape. Histograms are based on area, not height of bars: in a histogram, it is the area of the bar that indicates the frequency of occurrences for each bin. This means that the height of the bar does not necessarily indicate how many occurrences of scores there were within each individual bin. It is the product of height multiplied by the width of the bin (that indicates the frequency of occurrences within that bin). One of the reasons that the height of the bars is often incorrectly assessed as indicating frequency and not the area of the bar is due to the fact that a lot of histograms often have equally spaced bars (bins), and under these circumstances, the height of the bin does reflect the frequency (Gramacki,2018).

In first approximation, histograms allowed us to observe the frequency distribution of power ranges of the data available. Means and standard deviations also have been represented by histogram for every frequency band and component.

Using MATLAB software for the processing data, the histograms have been realized. This was possible through a specially developed Matlab programming language plotting functions and data and representing data in frequency distribution. In MATLAB, data are loaded into the software and functions or scripts are written and saved with m-files. An m-file, or script file, is a simple text file created and all m-file names must end with the extension '.m' (Brown, 2009).

All necessary data were implemented in order to extract histograms useful for data analysis.

The histogram requires two parameters to be defined: the bin width h and the bin origin x_0. Specifically the bins must have the same base and a suitable calculation to derive the each bin size

has been performed.

As stated by Gramacki, 2018, while the histogram is a very simple form of the nonparametric density estimator, some serious drawbacks are noticeable:

First, the final shape of the density estimate strongly depends on the starting position of the first bin. Second, the natural feature of the histogram is the presence of discontinuities of density. However, these are not related to the underlying density and, instead, are only an artifact of the chosen bin locations. Third drawback is the so-called curse of dimensionality, which constitutes a much more serious problem, since the number of bins grows exponentially with the number of dimensions. In higher dimensions one would require a very large number of examples or else most of the bins would be empty (incidentally, the curse of dimensionality phenomena is a common problem for all the nonparametric techniques for density estimation).

All these drawbacks make the histogram unsuitable for most practical applications except for rapid visualization of results in one or two dimensions.

As mentioned above, histograms also produce discontinuities: fortunately, this drawback can be switched using a proper smooth kernel function. In fact, in order to exceed the limits of the histograms representation and for a more refined and statistically robust representation, among all the estimation methods, it has been decided touse a Kernel based one, because it is more flexible than other estimation methods.

Kernel Density Estimation is one of the most well-known smoothing techniques, and generally Kernel methods are a class of techniques that play a major role in machine learning and nonparametric statistics.

Similar to a histogram, the kernel distribution builds a function to represent the probability distribution using the sample data. However, unlike a histogram, which places the values into discrete bins, a kernel distribution sums the component smoothing functions for each data value to produce a smooth, continuous probability curve (Fig.22).

As evidenced in the relevant literature, Kernel algorithms were developed to model strong nonlinear relationships between independent and dependent variables. In practical applications, kernelmethods lead to flexible predictive models that often outperform competing approaches in terms of performance.

The kernel distribution is a nonparametric representation of the probability densityfunction (PDF) of a random variable. It possible to use a kernel distribution when a parametric distribution cannot properly describe the data, or when you want to avoid makingassumptions about the distribution of the data. Kernel turns out to be a non-parametric approach, no assumption is made on the distribution of data, and the number and nature of the parameters are not set.

A Kernel distribution function is defined by a smoothing function and a bandwidth value, which

control the smoothness of the resulting density curve.

The kernel smoothing function defines the shape of the curve used to generate the PDF: in fact, has been estimated the shape of the PDF function, namely *f*. For any real values of x, the Kernel density estimator's formula is given by:

(1.6)

$$\widehat{f}_h(x) = \frac{1}{nh}\sum_{i=1}^{n} K\left(\frac{x - x_i}{h}\right)$$

Where

x_1, x_2... x_n are random samples from an unknown distribution; *n* is the sample size, i.e. it is the bandwidth, which is a positive real number ; *K* is the Kernel smoothing function, a non-negative function, and $h > 0$ is a smoothing parameter called bandwidth, that is a free parameter, which exhibits a strong influence on theresulting estimate.

The function [f, x_i] = ksdensity (x) returns a probability density estimate, f, for the sample data in the vector or two-column matrix x. Ksdensity function is the kernel smoothing function estimate for univariate and bivariate data.

Several type of kernel functions are commonly used: uniform, triangular, biweight, triweight, Epanechnikov, normal, and others, but for its convenient mathematical properties, the normal kernel is often used. Among all the different curve shape mentioned above, in our case it is just a normal kernel.

For a more robust statistical representation, the kernel method was used for the available dataset, implementing the ksdensity function on Matlab software.

The mean and the standard deviation of PSDs values have been submitted to the kernel smoothing function estimate. The estimate is based on a normal kernel function,and is evaluated at equally spaced points, x_i, that cover the range of the data in x. Ksdensity estimates the density at 100 equispaced points in the x axes.

In Matlab software, the default bandwidth in 'ksdensity' function is calculated using the following formula:

(1.7) `(BandWidth = sig * (4/(3*N)) ^ (1/5)`

Where *'sig'* is an estimated value of the standard deviation of the samples.

To extract the curves a script was built with the function [f, x_i] = ksdensity (x). This has been done for the vertical component, for the horizontal components, and for the four frequency bands. This

was done also for the standard deviation. An example of string is reported below:

```
[f_MeanZ00250012Hz, xi_MeanZ00250012Hz] =
      ksdensity (MeanZ00250012Hz)
```

The previous histograms create a discontinuity of the estimated density, producing a discretedensity probability function and its realization turns out to be less performing. Instead, the kernel distribution builds the PDF by creating a single probability density curve for each data value; summing the smooth curves, (continuous and smoothed distribution). This approach creates a continuous probability density function for the dataset, offering a more robust data representation method.

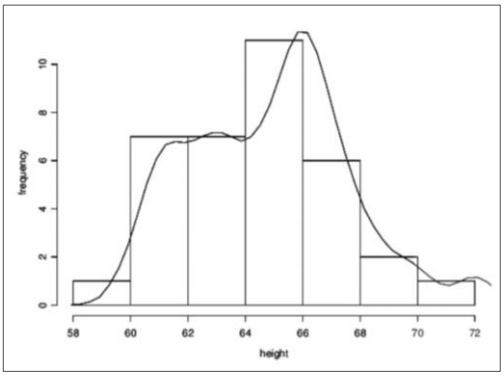

Figure 22: Comparison between a histogram and its Gaussian kernel density estimate constructed using the same data.

3.5 Spatial interpolation method: IDW interpolation method

Spatial analysis is the process of manipulating spatial information to extract new information and meaning from original information.

The available data points represent a complete enumeration of discrete events or observations, i.e. the entity of interest only occur discrete locations within a study area and therefore can only be measured at those locations. However, point data represents sampled observations of an entity that can be measured anywhere within our study area.

A class of techniques used with points that represent samples of a continuous field are interpolation methods.

Given the distribution of seismic stations showing point seismic noise values, an interpolation method should be used to estimate seismic noise values also where data have not been observed.

A frequently asked question is what the best interpolation method for any data set is. The answer to this question is none. There are many interpolation methods available and selection of a particular method should depend upon characteristics of data set as well as study objectives, but there is still no interpolation method, which will guarantee the best results for all data sets.

Geostatistics studies the natural phenomena that develop on a spatial basis starting from the information resulting from their sampling. Especially, it studies the spatial variability of the parameters that describe the phenomena extracting models and using them for to solve several problem concerning characterization and estimation of the phenomena themselves, passing from a punctual data to a continuous data. Geostatistics are based on both statistical and mathematical methods, which can be used to create surfaces and assess the uncertainty of forecasts. The models can be applied to a wide variety of scenarios and are typically used to generate predictions.

As mentioned above, geostatistics is characterized of several methods that allow you to estimate values for locations where no samples have been taken and to assess the uncertainty of these, the process of estimating parameter values at unknown locations using estimates.

Spatial interpolation, or spatial prediction known values (Reddy et al., 2017; Wu et al., 2016) create surface data based on a set of sampled points. The input data is a network of points, while the output is a surface that divides the study area into small cells with a data value for each cell (Wu et al., 2016). Two basic assumptions are very important for spatial interpolations: the first is spatial autocorrelation and the second is that values have to be smooth and continuous over space.

Currently, there are several commercial Geographic Information System (GIS) or statistics software offering spatial interpolation functions.

Usually spatial analysis is carried out with a GIS that provides spatial analysis tools for calculating feature statistics and carrying out geoprocessing activities as data interpolation. The results of the interpolation analysis can then be used for analyses that cover the whole area and for modelling. It can be used to predict unknown values for any

geographic point data, such as elevation, rainfall, chemical concentrations, noise levels, and so on.

There are more spatial interpolation algorithms provided in the literature. Some are quite flexible and can accommodate different aspects of the sample data. Others are more restrictive and require that the data meet specific conditions.

There is no general method that is suitable for all cases: it depends on the nature of the variable and on the timescale on which the variable is represented (Reddy et al., 2017). Apply an interpolation method, which is most suitable to both the sample data and the goal is very important and usually is better try several methods, if available, in order to compare the results and find the best result and the most suitable method. In fact, selection of a particular interpolation method should depend upon the sample data, the type of surfaces to be generated and tolerance of estimation errors. In addition, very important is evaluate always the sample data: this is significant for to know how data are distributed in the area and to know what the better interpolation method to use is.

An old classification of interpolation methods given by Lam, 1983 that distinguish two forms of spatial interpolation: interpolation of points and areal data. Point interpolation concern data detected at a point, such as temperature readings or elevation, whereas areal interpolation are related to data that are aggregated over a whole area, such as population counts. (Fig.23).

Former type (point or isometric methods) are further subdivided into "exact" and "approximate" methods according to whether they preserve the original sample point values, whereas areal or isopleth methods are subdivided according to whether they preserve volume. Especially in the point interpolation form, many methods exist and depending from the characteristic of preserving or not preserving the original sample point values on the inferred surface seems fundamental in analysing accuracy and in examining the nature of interpolation methods (Wren, 1975).

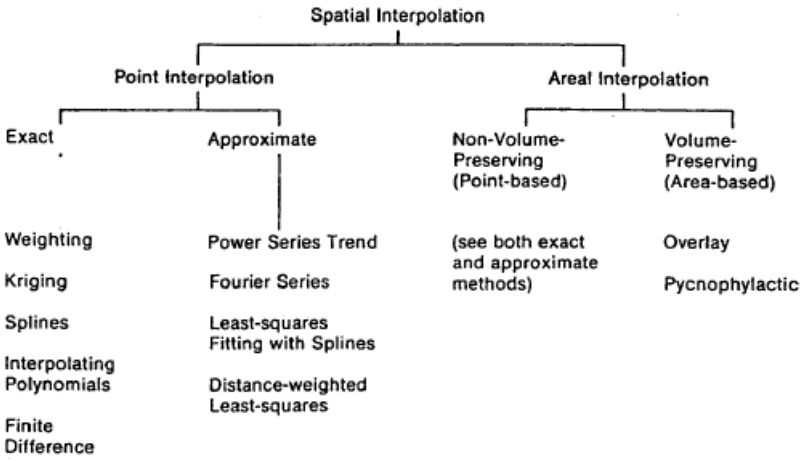

Figure 23: types of spatial interpolation methods. Lam, (1983).

Especially "exact" methods include interpolating polynomials, most distance-weighting methods, Kriging, spline interpolation, and finite difference methods. "Approximate" methods includes power-series trend models, Fourier models, distance-weighted least - squares, and least - squares fitting with splines.

A new classification of interpolation techniques are divided into two main types: deterministic and geostatistical (Johnston et al., 2001, Wu et al., 2016, Reddy et al., 2017).

Deterministic interpolation use mathematical functions for interpolation methods. They are directly based on the surrounding measured values or on specified mathematical formulas that determine the smoothness of the resulting surface. These techniques do not use a model of random spatial processes (Johnston et al., 2001).

Instead, geostatistical interpolation relies on both statistical and mathematical methods, which can be used to create surfaces and assess the uncertainty of the predictions. Especially, geostatistical methods are based on statistical models that include autocorrelation (statistical relationships among the measured points). Not only do these techniques have the capability of producing a prediction surface, but they can also provide some measure of the certainty or accuracy of the predictions (Johnston et al., 2001).

Already, Li & Heap 2008 make a good description between non-geostatistical interpolation and geostatistical interpolation methods. Among the first are the following methods: Nearest Neighbours, Triangulated Irregular Network, Natural neighbour, Inverse Distance Weighted

(IDW), Spline, and Regression Model. Each of them has its advantages and disadvantages. In 2014, with a review, the two authors, had provided a new classification of Spatial Interpolation Methods (SIMs) comparing the features of the commonly applied methods. Forty-two spatial interpolation methods are briefly described and which fall into three categories, namely: non-geostatistical interpolation methods, geostatistical interpolation methods and combined methods. (Table 7).

Non-geostatistical	Geostatistical (kriging)		Combined methods
	Univariate	Multivariate	
Nearest neighbours (NN)	Simple kriging (SK)	Universal kriging (UK)	Classification combined with other interpolation methods
Triangular irregular network related interpolations (TIN)	Ordinary kriging (OK)	SK with varying local means (SKlm)	Trend surface analysis combined with kriging
Natural neighbours (NaN)	Factorial kriging (FK)	Kriging with an external drift (KED)	Lapse rate combined with kriging
Inverse distance weighting (IDW)	Dual kriging (DuK)	Simple cokriging (SCK)	Linear mixed model (LMM)
Regression models (LM)	Indicator kriging (IK)	Ordinary cokriging (OCK)	Regression trees combined with kriging
Trend surface analysis (TSA)	Disjunctive kriging (DK)	Standardised OCK (SOCK)	Residual maximum likelihood-empirical best linear unbiased predictor (REML-EBLUP)
Splines and local trend surfaces (LTS)	Model-based kriging (MBK)	Principal component kriging (PCK)	Regression kriging (RK)
Thin plate splines (TPS)		Colocated cokriging (CCK)	Gradient plus inverse distance squared (GIDS)
Classification (Cl)		Kriging within strata (KWS)	
Regression tree (RT)		Multivariate factorial kriging (MFK)	
		IK with an external drift (IKED)	
		Indicator cokriging (ICK)	
		Probability kriging (PK)	

Table 7: The SIMs considered in the review. Li & Heap, (2014).

Instead Reddy et al., (2017), classify spatial interpolation techniques as global and local interpolation, exact and inexact interpolation, and deterministic and stochastic interpolation. Global interpolation is the method which uses whole sampled values for prediction, whereas local interpolation uses the sampled values at their local range. The Classification of Spatial Interpolation Techniques as shown in Figure 24. Exact point interpolation are here classified as deterministic techniques, except Kriging method that is a statistical method.

Another wide classification was instead implemented in Matlab software (Fig.25).

As you can see, many authors have made a wide study of the different interpolation methodologies.

Among all methods, the kriging method remains the best known geostatistical interpolation method. Kriging is a generic name for a family of generalised least-squares regression algorithms, used in recognition of work of Daniel Krige, who developed the method for geological mining applications.

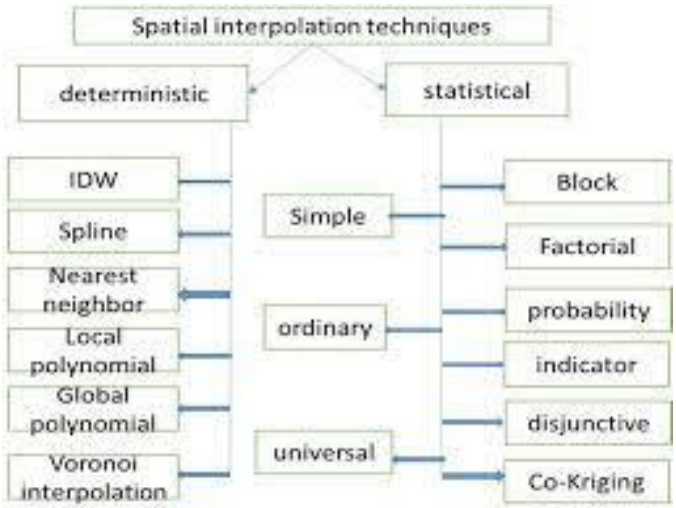

Figure 24: Classification of Spatial Interpolation Techniques. Reddy et al., (2017).

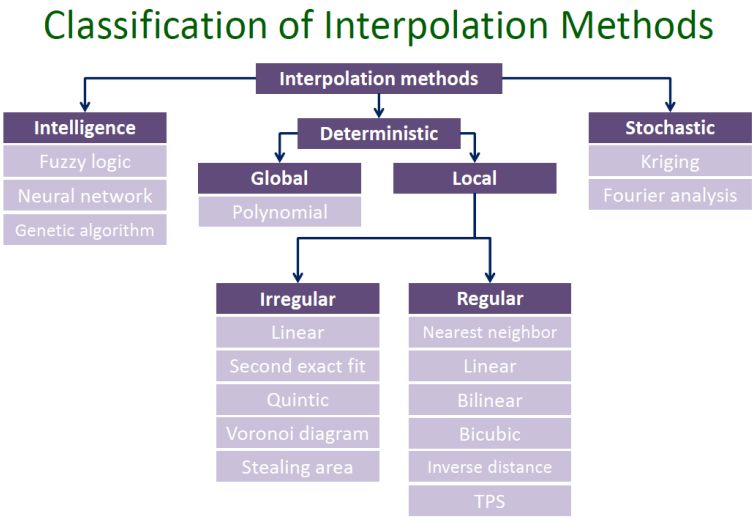

Figure 25: Deterministic and Stochastic interpolation methods implemented in Matlab.

The principles of geostatistics and interpolation by Kriging are widely described in literature (Krige, 1951; Matheron, 1971; Delfiner, 1976; Lam, 1983; Johnston et al., (2001); Wu et al., (2016) and others). Some authors classify Kriging as a statistical technique and identify the remainder as analytical methods (Delfiner, 1976).

Kriging is perhaps the most distinctive of interpolation methods (Lam, 1983) and one of the most complex methods.

Kriging regards the statistical surface to be interpolated as a regionalized variable that has a certain degree of continuity (Lam, 1983). In addition assumes that the distance or direction between sample points reflects a spatial correlation that can be used to explain variation in the surface. Rather than considering distances to control points independently of one another, kriging considers the spatial autocorrelation in the data. The Kriging estimate is based on the structural characteristics of the samples, which are summarized in the covariogram or variogram function and thus result in an optimal unbiased estimate. Kriging also provides an estimate of the error and confidence interval for each of the unknown points, an asset not provided by other interpolation procedures (Lam, 1983).

Geostatistics includes several methods that use kriging algorithms for estimating continuous attributes. Kriging methods are quite flexible, but between the Kriging methods there are varying degrees of conditions that must be met. Ordinary Kriging is one of the most basic between Kriging methods.

The others most important known Kriging methods are Simple Kriging, Kriging Universal Kriging, Block Kriging Cokriging, Disjunctive Kriging, Factorial Kriging, Probability Kriging, Dual Kriging (Reddy et al., 2017; Li & Heap 2008) but many others exist.

Although the kriging method is one of the most complete interpolation methods, the Inverse Distance Weighted (IDW) method is better suited to returning the expected result.

However, the two methods have many similarities. In fact, kriging is a stochastic method similar to IDW method and uses a linear combination of weights at known locations to estimate the data value of an unknown location. Like IDW interpolation, kriging forms weights from surrounding measured values to predict values at unmeasured locations. As with IDW interpolation, the closest measured values have the most influence. However, the kriging weights for the surrounding measured points are more sophisticated than those of IDW (Johnston et al.2001).

Kriging is similar to IDW in that it weights the surrounding measured values to derive a prediction for an unmeasured location, but while IDW is a simple analytical interpolation technique based on the distance between the estimated point and the measured points, kriging weights come from a semivariogram that was developed by looking at the spatial structure of the data.
Schloeder et al., (2001), compared IDW, kriging, and spline spatial interpolation methods. They concluded that IDW and kriging performed similarly and that both are more accurate than the spline interpolation method. Mueller et al., (2001), Kravchenko (2003), compared IDW and kriging and they concluded that there is a little difference between two methods. Instead, Lu and Wong, 2008, developed a new form of IDW that may perform better that kriging without variograms.
Given the considerable similarities, the IDW method is a good method for interpolating noise data on the Italian territory.

3.5.1 Inverse Distance Weighted (IDW)

Among all the methods listed above, despite also the great advantages that offers a statistical method such as kriging method, Inverse Distance Weighted was chosen. The IDW method is a deterministic estimation method where values at unmeasured points are determined by a linear combination of values at nearby measured points (Wu et al., 2016). In the IDW interpolation, the sample points are weighted during interpolation such that the influence of one point relative to another decline with distance from the unknown point you want to create. It gives greater weights to points closest to the prediction location, and the weights diminish as a function of distance, hence the name inverse distance weighted.
Weighting is assigned to sample points using a weighting coefficient that controls how the weighting influence will drop off as the distance from new point increases. The greater the weighting coefficient, the less the effect points will have if they are far from the unknown point during the interpolation process. As the coefficient increases, the value of the unknown point approaches the value of the nearest observational point.
The advantages of IDW are that it is simple, easy to understand, and efficient but this method has some disadvantages: it is sensitive to outliers and there is no indication of error (Longley et al., 2005; Wu et al., 2016), and the interpolation quality result can decrease, if the distribution of sample data points is uneven. Furthermore, maximum and minimum values

in the interpolated surface can only occur at sample data points. Other problem is that the IDW works well with regularly spaced data, but it is unable to account for clustering (Isaaks and Srivastava, 1989).

IDW takes the concept of spatial autocorrelation literally. It assumes that the nearer a sample point is to the cell whose value is to be estimated, the more closely the cell's value will resemble the sample point's value.

Substantially, in IDW method, assumed that the rate of correlations and similarities between neighbors is proportional to the distance between them that can be defined as a distance reverse function of every point from neighboring points.

Finally, it is possible to summarize that this technique gives weights to sample points, such that the influence of one point on another declines with distance from the new point being estimated.

In the QGIS software, this technique is implemented. Thus, the interpolations of the seismic noise data available to extract interpolation maps were performed. Especially maps with different levels of seismic noise have been extracted.

3.6 Spatial Filtering

In addition to the interpolations, filtering techniques have been applied to discriminate seismic noise by discarding some frequency bands and identifying regional trends. Out of all the available filters for signal, we applied spatial high pass and low pass filters.

The low pass filters are generally applied to highlight slow variations of the analysed parameter or those that are used to say the regional trend. In this work, we applied a 2D moving average spatial filter with zero phase shift. For this purpose we computes a zero phase moving average by reversing the input series, computing an N point moving average, reversing the result and computing another N point moving average. The reversal steps help ensure that the peak locations of the original data are preserved. The data is so effectively smoothed with an 2N point average. The high frequency filtering was done indirectly. In practice, we proceeded by subtracting the low-pass filtered data from the raw data. This allows to isolate the high frequency contributions, without any phase distortion, caused by local anomalies. Several spatial smoothing windows were tested. Reasonably, we have chosen to use a 2D spatial window with a number of points equivalent to a radius of 50 km.

3.7 Regression techniques

A regression analysis can be adopted to build mathematical models for prediction study: regression analysis has been applied also to Italian seismic noise data in the three years 2015-2017 for the data prediction.

Regression analysis is a technique used to analyse a set of data consisting of one dependent variable and one or more independent variables. The aim is to estimate a possible functional relationship between the dependent variable and the independent variables.

Especially, linear regression is a statistical modelling technique used to predict the value of one variable based on the value of another variable. The variable you want to predict is called the dependent variable (called response variable or predicted variable). The variable that is used to predict the value of the other variable is called independent variable (or sometimes, the predictor, explanatory or regressor variables).

Other the prediction, when constructing a linear regression model, it is also important to understand how strong its predictive capacity, that is, how well the independent variables (x) can predict the values dthe dependent variable (y). In fact, regression is the process of fitting models to data and its analysis provide with an equationfor a graph about the data predictions. Essentially, regression is the "best guess"at using a set of data to make some prediction.

In order to construct a prediction model of noise levels when some parameters vary, it was decided to apply a regression analysis to the available seismic noise data.

Linear regression technique was performed for three parameters. Geographical and meteorological parameters were involved: altitude, minimum distance station-coastline and rain.

The altitude is the height of every single station studied. These stations are located from zero to 1853 meters above sea level. The stations altitudes were downloaded directly from the INGV site. This regression allows observe if and how the altitude of each station could to influence the seismic noise.

In order to observe the impact of the noise signal from the most central areas to the Italian coast, instead it was decided to connect the power value with the minimum distance that each station has from the nearest coastline. For this reason, distances are computed.

Another parameter is the rain: wanting to observe how precipitation can affect the noise parameters has been taken into account. In order to make a comparison rain data were extracted from an ISPRA Institute map that collects rain data in the time window 1961-2017 on Italian territory. Averages of ranges calculated by ISPRA are considerate.

Therefore, an analysis correlated to the seasonality has not been treated but on mediated data on the entire Italian territory in order to obtain total robust data.

3.7.1 Linear regression

Initially, linear regressions first degree were performed for the three parameters. Later, second-degree polynomial regressions was obtained for a better data correspondence. This was done for each frequency band and component.

Especially, polynomials are algebraic expressions consisting of variables and coefficients and a polynomial regression is a regression model.

In fact, polynomial regression is considerate a special case of linear regression in which we adapt a polynomial equation to data with a curvilinear relationship between the independent variable x and the dependent variable y, modelling it as a polynomial of n degree.

Several mathematical software packages provide commands to determine to the regression equation, but in this research using MATLAB software.

Through the Matlab language, starting from the regression syntax, it was possible to create specific scripts for the graphic restitution of the regressions.

Especially *polyfit function* (polynomial curve fitting) has been used, whose syntax is as follows:

```
p = polyfit(x, y, n)
[p, S] = polyfit(x,y,n)
[p,S,mu] = polyfit(x,y,n)
```

Where:

p = polyfit(x, y, n) returns the coefficients for a polynomial p(x) of degree n that is a best fit (in a least-squares sense) for the data in y. The coefficients in p are in descending powers, and the length of p is n+1

(1.8)

$$p(x)=p_1x^n+p_2x^{n-1}+...+p_nx+p_{n+1}$$

[p,S] = polyfit(x, y, n) also returns a structure S that can be used as an input to polyval to obtain error estimates.

[p,S,mu] = polyfit(x,y,n) also returns mu, which is a two-element vector with centering and scaling values (MathWorks site).

Small discrepancies between the expected and observed values indicate that the modelfits well with the data. On the contrary, large discrepancies between expected and observedvalues indicate that the model does not explain well the variability present in the data. The polyfit function determines the best n-order polynomial but in addition to the polyfit, the *polyval function* (polynomial evaluation) was also used: the polyval command determines the result of applying the polynomial to an x-point vector. Syntax used is as follows:

```
[y,delta] = polyval(p,x,S)
```

This function uses the optional output structure S generated by polyfit to generate error estimates delta. Delta is an estimate of the standard deviation of the error in predicting a future observation at x by p(x). If the coefficients in p are least squares estimates computed by polyfit, and the errors in the data input to polyfit are independent, normal, and have constant variance, then y±delta contains at least 50% of the predictions of future observations at x.

In addition in the linear fit model was considered an estimate of 95% of the Prediction Interval. This is interval of values within which is estimated that the true value of the population falls, with a probability level of 0.95 obtaining a prediction interval of 95%.

Once a regression model has been built, it is important to confirm the adequacy of the model and the statistical significance of the estimated parameters.

In fact, the aim of regression analysis is to estimate a possible functional relationship between the dependent variable and the independent variables and this case, to establish the relationship between the seismic noise power and geographical and meteorological parameters.

For a good data prediction estimation, different statistic methods exist. Among these accuracy measurements are current: Mean Square Error (MSE), its Rooted variant (RMSE), the Mean Absolute Error (MAE), its percentage variant (MAPE), and Symmetric Mean Absolute Percentage Error (SMAPE).

Measuring the accuracy (or error) of predictions is not an easy task as there is no indicator valid for all cases.

Initially, the Mean Absolute Percentage Error (MAPE) also was calculated for noise data predictions. MAPE is the mean of the absolute percentage errors of forecasts, i.e. it is a measure of how accurate is a forecast system. Error is defined as actual or observed value minus the forecasted value. This measure is easy to understand because it provides the error in terms of percentages. The smaller the MAPE the better the forecast. MAPE is the most common measure used to forecast error.

Although many studies employ MAPE or the others parameters, according to recent studies, these rates share a common disadvantage. Since their values may vary between zero and +infinity, a single value of them does not say much about the performance of regression with respect to the distribution of truth elements. Indeed, Chicco et al., 2021 demonstrate that the coefficient of determination R-squared is more informative and truthful than SMAPE, and does not have the interpretability limitations of MSE, RMSE, MAE and MAPE. Especially MAPE focuses on the percentage error and relative variations have a higher impact on the regression task rather than the absolute values. However, MAPE is heavily biased towards low forecasts, making it unsuitable for evaluating tasks where large errors are expected (Armstrong & Collopy, 1992; Ren &Glasure, 2009; De Myttenaere

et al., 2015). Finally, Chicco at al., (2021) therefore suggest the usage of R-squared as standard metric to evaluate regression analyses in any scientific domain.

For these reasons, as standard metric to evaluate regression analyses, it was decided not to use the MAPE but the coefficient of determination R-squared (R^2).

The coefficient of determination or R^2, is well-defined in linear regression models, and measures the proportion of variation in the dependent variable explained by the predictors included in the model (Zhang, 2017).

In the scientific literature, it is called also goodness of fit and is only used in linear regression models. Introduced by Wright (1921) and generally indicated by R^2, its original formulation quantifies how much the dependent variable is determined by the independent variables, in terms of proportion of variance. Again, given the age and diffusion of R^2, a wealth of studies about it has populated the scientific literature of the last century; in fact, for the standard linear regression model the coefficient of determination, R-squared (R^2), is a widely used goodness-of-fit measure whose usefulness and limitations are more or less known.

The R-squared is the square of the multiple correlation coefficient R. This number claims how good is the model and its range is from 0 to 1.The closer the R-values are to 1, the more reliable the model will tend to be, while if the values tend to zero, the lower the correlation between the parameters correlated.

Usually, the larger the value of the R^2, the more the model has a high predictive power. The larger the R-squared is, the linear regression model explains the more variability.

This coefficient is defined as:

(1.9)

$$1-\frac{\sum_{i=1}^{n}(y_i-\hat{y}_i)^2}{\sum_{i=1}^{n}\left(y_i-\bar{y}\right)^2,}$$

Where:

y^i denotes the value of the objective variable (y) predicted by regression for the ith data point. The second term of this expression is the residual sum of squares divided by the sum of squares of y. Because the residual sum of squares has the value between 0 and the sum of squares of y, the coefficient of determination can have the value from 0 to 1, or 0 to 100% (Kasuya, 2019).

More general terms it can be defined as:

(1.10)

$$R^2=\frac{SSR}{SST}=1-\frac{SSE}{SST}$$

Where:
SSE is the sum of squared error, *SSR* is the sum of squared regression, and *SST* is the sum of squared total.

3.7.2 Multiple linear regression

Another type of linear regression is the multiple linear regression. Multiple regression is an extension of simple linear regression. It is used to predict the value of a variable based on the value of two or more other variables. The variable we want to predict is called the dependent variable. The variables we are using to predict the value of the dependent variable are called the independent variables. The distance-elevation parameters as a function of seismic noise were thus considered. A special script has been created to extract the corresponding graphs. This was done for each frequency band and component.

Chapter 4

Data analysis

4.1 Seismic ambient noise a spectral analysis

The results of evaluating ambient seismic noise levels are shown and McNamara and Buland (2004) and Peterson (1993) method are applied. McNamara and Buland (2019) reproduce their method that recalled Probability Density Function of Power Spectral Density (PSDPDF), describing in details a better way to visualize the spectral characteristics and numerous sources of seismic noise.

Probability Density Function of Power Spectral Density of all 233 station selected within the 0.025 - 30 Hz frequencies range has been computed for the Z and H channels, according to these methods. For each station, its vertical component will be displayed.

As described above, at first SQLX software was used, but for a better graphical return is been created a Matlab code.

The seismic noise powers are reported in dB and referred to 1 $(m/s^2)^2$ /Hz). The vertical grey lines represents the boundaries among the four frequency bands. Instead, the colours scale suggests the seismic noise in terms of probability density, i.e. the variability of noise levels at the respective frequencies.

All PDFs have a confidence interval where the data are presented (thin red lines), a median value that is the central value of the numerical data (thick red line) and modal value (green line) is the most frequently occurring value.

Noise levels are compared within the new low-noise model (NLNM) and new high-noise model (NHNM) of Peterson world reference models (1993), and they are represented with two black curves.

Ambient seismic noise is different in different seismic data acquisition environments: for this reason, spectra with different characteristics depending on their sources have been identified, but the purpose of this spectral analysis is mainly to identify natural sources.

For all stations PSD and PDF have been generated, but the spectral characterization has not been

analysed and described in detail for each location. Only some cases have been selected, having particular spectral characteristics.

In fact, several PDFs related to some stations representative of the National Seismic Network are presented: specifically, spectra are shown of stations rising at high altitudes, near the coastline, windy areas and volcanic districts.

Some examples of anthropic noise in urban environment also are reported to make a comparison. Of course, natural and anthropic sources can overlap in the same settings in the intermediate bands. Artifacts related to self - noise at very low frequencies can be included too.

Two reference PDFs, referred FAGN (Fagnano) and ACER (Aceranza) stations are displayed in Fig. 26. They are characterized by a satisfying ambient noise that suggests how ambient noise falls for a good part within the reference models of Peterson, maintaining a good trend at all periods. Although they are both far from the sea, these stations confirmation in low frequency bands two peaks linked to microseisms (between -120 dB and -160 dB).

Although FAGN station (Fig.26, upper panel) is close to a little village, an optimal response of seismic noise even at high frequencies is showed.

ACER station (Fig.26, low panel) is more far from man-made activities and also present a good reaction (not exceeding -120 dB) as shown in the Figure 26 in the lower panel.

Similar plots are produced for all the 233 stations. For each of these stations has been ascertained their location in order to better distinguish the main sources. They have been subdivided in different categories to show the peculiar aspects. Only some particular classes will be shown below.

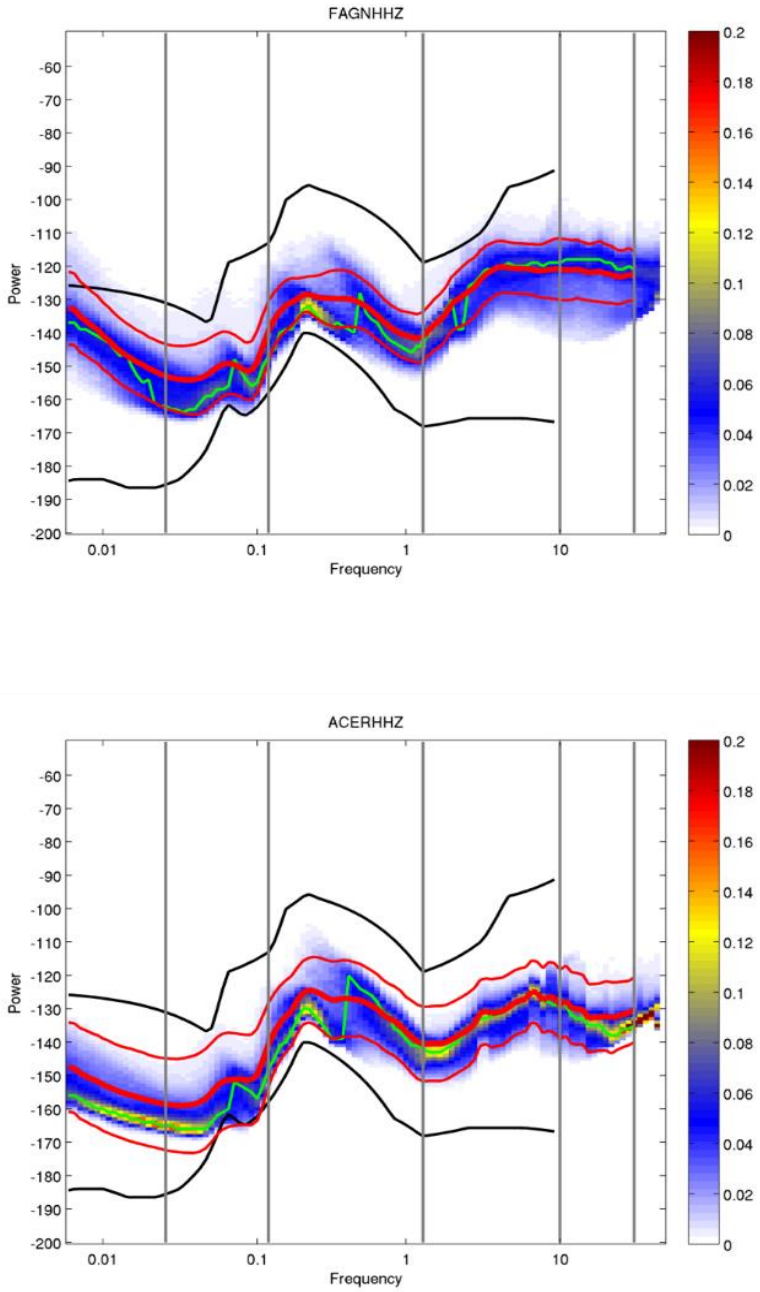

Figure 26: PDF of the vertical component of the FAGN station (top) and ACER station (bottom) are shown. Each panel was built using the corresponding PSD curves. These two stations show the good PDFs that fall within the Peterson reference models (black lines).

4.1.1 Case studies

Alpine environments

Among the different categories, the Alpine sites are chosen because being at higher altitudes and far from populated areas are less influenced by cultural noise and show less disturbed spectra by the overlapping of more sources, appreciating better the characteristics in all frequencies.

Four sites have been selected for almost the entire alpine region. Especially, the reported spectra belong to MABI, MRGE, BRMO, PTCC stations (Fig. 27); they are located in 1853, 1660, 1380, and 700 meters a.s.l. respectively. Except the BRMO station (located close to Bormio village), all stations are installed in a remote site. MABI station is located to next to the Bissina dam and this may be related to certain disturbance present in the spectrum.

In all four stations, the maximum noise level recorded not exceed -110 dB, and there are no peaks attributable to the local wind. This is probably due this is probably because the stations are located in sheltered places within valleys.

Overall, all four stations present low ambient noise spectra and all fit into the Peterson reference models.

As already explained in Chapter 1, microseisms are observed all over the world with greater amplitudes in the coastal sites than the continental sites (Bromirski, 2001) but being sites unaffected by additional sources, the primary and secondary microseismic peaks are distinguished very well in all four stations at low frequencies.

Alps are a complex and ever varying orogenic system but almost certainly, the low noise of the stations is related to their location and to the geological conditions of the area.

Coastal environments

Generally, if the continental sites can be predominantly are influenced by the cultural noises, the coastal sites are most affected by the microseismic noise. Especially, ambient noise in the middle bands strongly is affected by geographic location mainly due to proximity of the station to coastlines (Mcnamara and Buland 2004 and 2019).

To better explore the interaction between Italian coast and seismic noise, four stations are analysed (Fig.28).

Especially, only stations located near the coast and on land (the farthest station is 1.4 kilometres from the coastline) have been chosen, ruling out those sited on the small islands and treated separately. In addition, many stations located very near the coastline in the Pozzuoli area were discarded cause main volcanic component.

In all four stations, microseisms contributions are clearly identifiable, being close to the coast.

In the literature, the primary (or single-frequency) and secondary (or Double Frequency - DF) microseisms are affected by the ocean waves, and data coming from the Italian stations are in agree with this correlation. In fact, microseisms are continuously recorded in the 0.04 to 2 Hz frequency band by seismic sensors (Essen et al., 2003; Bromirski et al., 2005).

Also Italian data fall between Very Low Frequencies band (0.025 - 0.012 Hz) and Low Frequencies band (0.012 - 1.2 Hz). Precisely, according to Cessaro (1994) and others, the primary peaks microseisms are recorded for frequencies < 0.1 Hz and are due to far away sources (such as swell from distant storms).

Instead, secondary microseisms are found around 0.1 and 0.5 Hz, in agreement to Cessaro (1994) and Barruol et al. (2006). These PDF peaks probably are associated to sources located near the coast (such as waves induce by local wind) and corresponding to short period microseisms (Stephen et al., 2003; and Bromirski et al., 2005).

Explicitly, MILZ and HAGA stations (Fig. 28, upper left and low left respectively) are located on the coast in Milazzo and Brucoli sites respectively (Sicily), while PESA and AOI stations are positioned along the Adriatic coast in Conero Mount, and not far Pesaro urban centre (Marche region) at a distance from 500 meters and 1.4 kilometres from the coastline.

In addition, all stations show a “third” peak in the middle band probably related to the local wind (in MILZ station is most dispersed). Especially PESA and AOI stations (Fig.28, upper right and low right respectively) are more exposed to meteorological agents being located at 221and 530 meters above sea level respectively.

High frequencies are probably characterized by cultural noise, as the stations are located not far from towns or roads. The MILZ station is located on the sea (Milazzo peninsula) at few meters from the coastline and possibly local winds can strongly influence a broader frequency spectrum, showing a wider powers range (until about -80 dB) than others do stations.

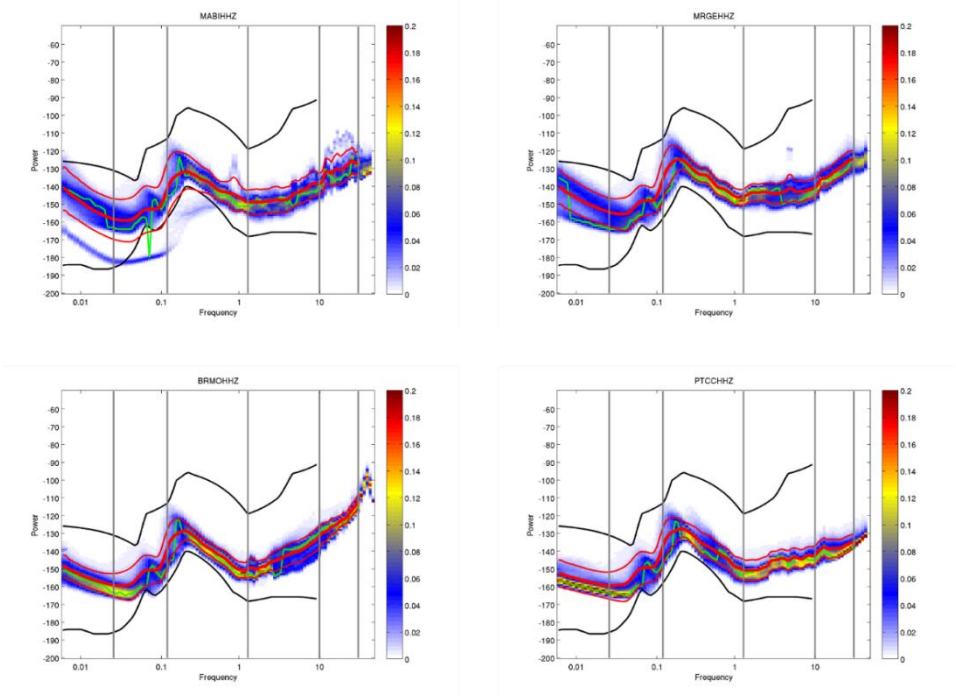

Figure 27: Low ambient noise is displayed in PDFs of selected spectra in the Alpine area. In the intermediate bands the two microseismic peaks are evident.

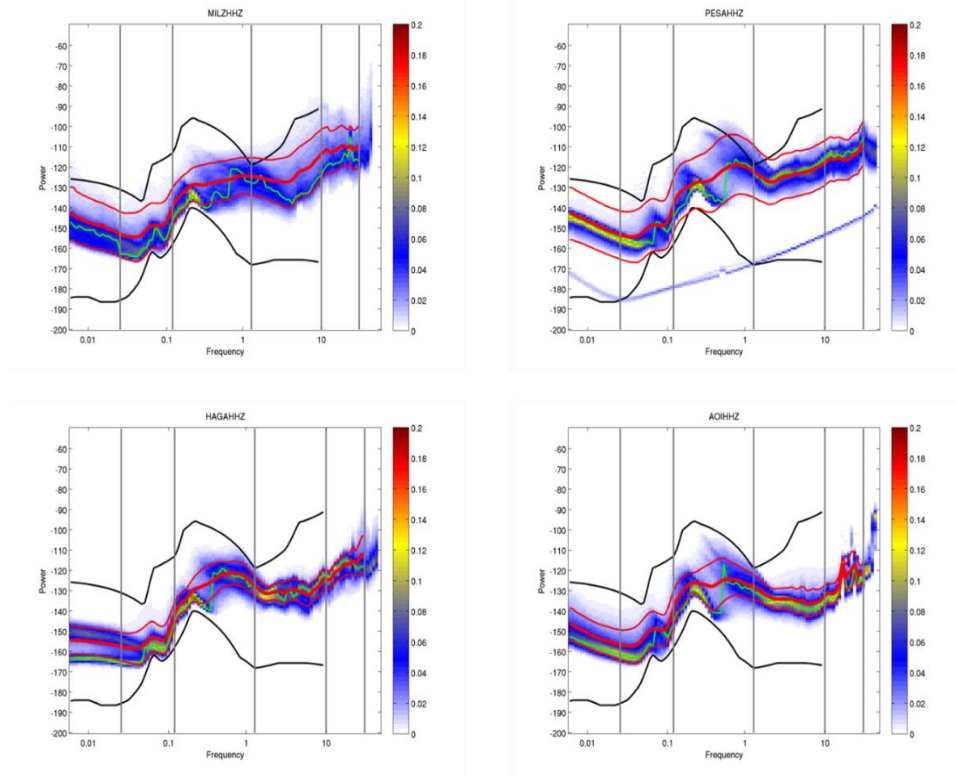

Figure 28: MILZ, HAGA, PESA and AOI stations are the four sites chosen for a better appreciation of single and double microseismic peaks. Their PDFs are shown. High noise relative to local wind around 1 Hz it is evident in all stations.

Volcanic environments

Others interesting sample stations have been found in volcanic sites. It is clearly demonstrated that in these environments the main sources noise are correlated to volcanic activity as confirmed as well by literature.

For two stations at Mt. Etna volcano (Southern Italy - Sicily), especially Serra La Nave and Monte Spagnolo stations (ESLN and EMSG stations codes) seismic noise shows within the Peterson reference models except around 1 Hz frequencies where higher noise levels occurred (Figure 29).

This characteristic trend detected, probably is correlated to the continuously volcanic tremor at the volcano and several sequence of paroxysmal episodes occurred. Generally the dominant frequencies of volcanic tremor are 1 - 5 Hz (2 - 3 Hz is most common) similar to LF (Low - Frequency) events (Lee et al., 2002).

This seismic noise occurs at frequencies of around 1 Hz and with powers between - 130 dB and - 100 dB. In fact, according to Cannata et al., 2017, volcanic tremor frequency content at Mt. Etna is generally contained between 0.5 and 5.5 Hz. In addition, also Raphael et al., 2019 states that between 1 and 2 Hz the most of Etnean volcanic tremor energy is contained. From about 5 Hz a decrease in background noise is observed with values less than -120 dB.

Being ESLN station (Fig.29, left panel) is located on the southern slope of the volcano (at 1787 meters a.s.l.), while EMSG stations (Fig.29, right panel) sited on NW of Etna sector (at 1435 meters a.s.l) and both stations are far from populated areas. For this reason, high frequency range could always be justified to the volcanic source and attributed to HF (High - Frequency) events with dominant frequencies generally between 5 - 15 Hz (Lee et al., 2002).

A different volcanic context is Vesuvio volcano (Southern Italy - Naples). Although Vesuvio is one of the most dangerous volcanoes in the world, particular spectra not found. Almost all stations exhibit high seismic noise levels for Very Low and Low Frequencies, certainly mainly attributable to the quiescent volcanic activity of the volcano but also the proximity to the coast and the speed of the local wind may overlap.

In particular, two sample stations have been preferred (Fig. 30). Especially for the VCRE station (Fig.30, right panel) of the Osservatorio Vesuviano, intermediate values between -145 and -120 dB are distributed with high probability density in the low frequency classes.

In addition, CRTO (Fig.30, left panel) station have similar high noise levels (-150 to -120 dB) for low frequencies. In this circumstance could also be related to artifacts of the sensor.

Surely, volcanic processes contributes on all frequency bands maintaining high levels of noise, especially for high frequency bands (between -120 to -80 dB).

Instead, the near Campi Flegrei volcanic district has proved to be a more disturbed area, as

demonstrated by the relative PDFs.

Nine broadband stations (CPIS, CSFT, CSOB, CMSN, CAAM, COLB, CPOZ, CFMN, CAFL station) in this area are equipped. High noise levels are detecting for both low and high frequencies in all stations.

Campi Flegrei is an inhabited volcanic caldera bordering Naples and to be considered as one of the most alarming areas for its volcanic criticality in the world, despite its strong anthropization. This area is considerate a capped geothermal system (Vanorio & Kanitpanyacharoen, 2015; De Siena et al., 2017). Pressurized fluids movements occur in depth involve deformations and stress and cause noise. In addition, possible meteorological and ocean swells conditions for the low frequency seismic noise occur and especially sea and wind interact constantly with the caldera waves producing (Vassallo et al., 2008; Zaccarelli and Bianco, 2017; Petrosino and De Siena, 2021).

This is a very complex area and several natural sources overlap (crustal changes related to variations in hydrothermal, earthquake occurrences, or magma injections at depth).

This characterizes the high levels of noise at low frequencies. Instead, the outlier noise conditions, for low frequencies, can also due as artefact of the instruments response.

Unlike the stations located in the summit of Vesuvius that are far from the populated areas, Campi Flegrei stations are all affected by cultural noise because distributed in a densely populated area. According to Bianco et al. (2010), high frequencies are related to anthropic activities being so densely inhabited area. Therefore, both sources (volcanic contribution and anthropic noise) would contribute to high noise values for these stations for high frequencies.

As will also be shown in the next paragraphs, Campi Flegrei stations represent the noisiest group of stations in Italy for both low and high frequencies. Many small earthquakes have high probability to be undetected due to e high background noise levels (Del Pezzo et al., 2013).

Among all these, two particular stations (CPIS and CSOB stations) from the Solfatara - Pisciarelli area (Pozzuoli - Naples) were taken as sample stations (Fig. 31). Spectral levels are high over the entire analysed range (0.025-30 Hz).

Especially CPIS station (Fig. 31, left panel) is the noisiest station in this area, as well as being the noisiest in Italy. CPIS station is located in Pisciarelli Fumarole area and its PDF appears to be totally outside of the world Peterson reference models.

The minimum noise is above -130 dB (low frequencies) and reaches its maximum that exceeds -60 dB (for high frequencies around 10 Hz).

It is also possible to see how for low frequencies there is an increase in noise certainly linked to natural sources but can also include artifacts related to self - noise at very low frequencies. Instead, CSOB station (Fig.31, right panel) was chosen for a better spectrum than other stations and no for

its proximity to the CPIS station.

At low frequencies, the secondary microseism peak is well observed while the medium-high frequencies do not exceed the -90 dB of power being part of the Peterson reference models.

According Giudicepietro et al., (2021), Solfatara and Pisciarelli vents emit from 2000 to 3000 tons/day of CO_2 in the atmosphere and this could justify the high ambient noise at low frequencies in adding to the other sources indicated.

Being a very complicated and high-risk area, from nine to 26 March 2009 was carried out the "UNREST" experiment on the recording of seismic noise in the volcanic area of CampiFlegrei. The experiment purpose was to define important elements for the levels of seismic detection that may be generated during a phase of resumption of volcanic activity (Bianco et al., 2010).

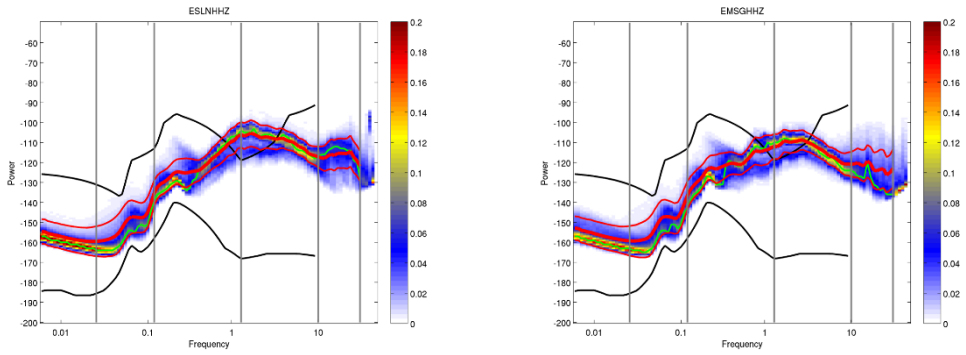

Figure 29: PDFs of ESLN (left panel) and EMSG (right panel) stations located on Etna volcano. In a both stations, a peak around 1 Hz related to volcanic tremor is detected.

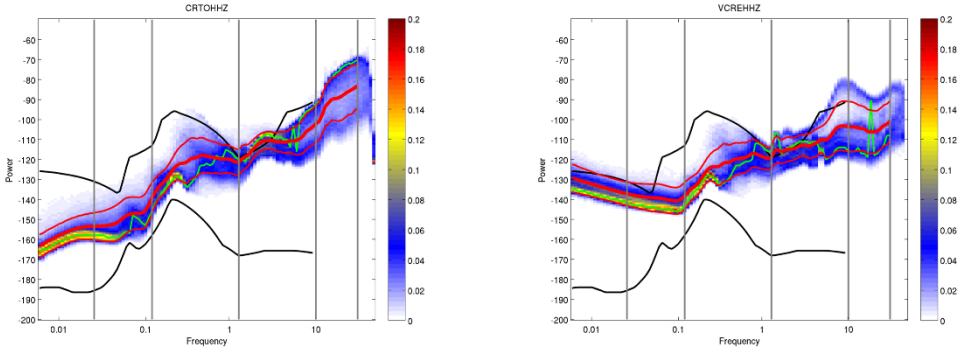

Figure 30: PDFs of CRTO (left panel) and VCRE (right panel) stations located on Vesuvio volcano. An increase in seismic noise is shown by increasing frequencies. This is attributable to the activity of the volcano.

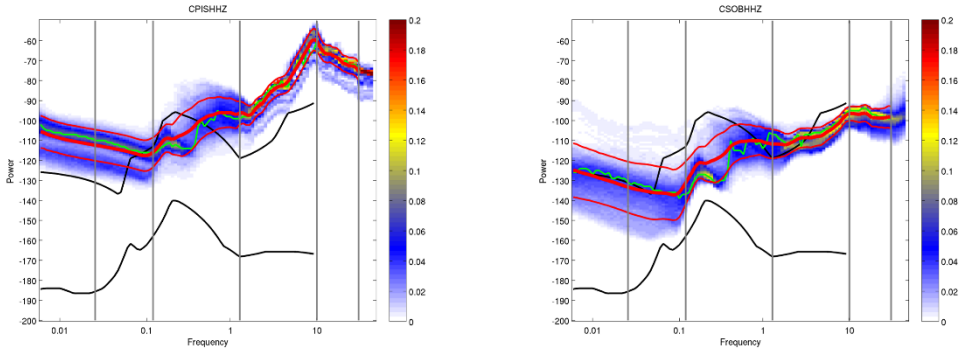

Figure 31: PDFs of two stations located on Campi Flegrei district. CPIS (left panel) is the noisiest station in this area but also the noisiest station of all 233 stations selected. Both stations are very noisy for all four frequency windows. This is strongly influenced by the multiplicity of overlapping natural and anthropic noise sources in the areas.

Island environments

Other particular contexts where several mainly natural sources can interact with each other are small islands. Seismic stations near coasts or islands are generally characterized by a high seismic noise level (McCreery et al., 1993).

The following are the PDFs of two smaller islands (Figure 32) such as Ustica (USI code) and Lampedusa (LPDG). At the he low frequencies the microseismic peaks is linked to the wave motion as well noted. High distribution is in both cases linked to the second peak (yellow).

In addition, at middle frequency 0.012 Hz and 1.2 Hz, it is possible to notice a high noise level certainly due to the wind as per the literature. As already mentioned in Chapter I, Withers et al. (1996) showed a strong correlation between wind speed greater than about 3 m/s and short-period (< 1 s) seismic noise. In addition, Young et al. (1996), Mucciarelli et al. (2005), Bormann and Wielandt (2013), and others, observed a correlation between wind and noise in the similar range. Although the literature suggests this, it is not easy to analyse the frequency band related to phenomena such as wind if you do not have more detailed analysis. In fact, according to Sydney et al., (2015) and Lott et al., (2017), wind can vary significantly across short distances, and wind-generated noise could behave differently in high-noise environments. High frequencies, on the other hand, are related to the anthropic factors. Although the station of Ustica (Fig.32, right panel) is located at 285 meters a.s.l. and away from the populated area, exhibit high levels of noise although probably part of the source can be given at high wind speeds that insist on high frequencies, as also supposed by Sydney et al., (2017). Instead, Lampedusa station (Fig.32, left panel) is located at 50 meters a.s.l. In these case, a supplementary noise for the higher frequencies because of the anthropogenic factor. In fact, compared to the island of Ustica is more densely populated and there is an airport that definitely

contributes to other frequencies of cultural noise.

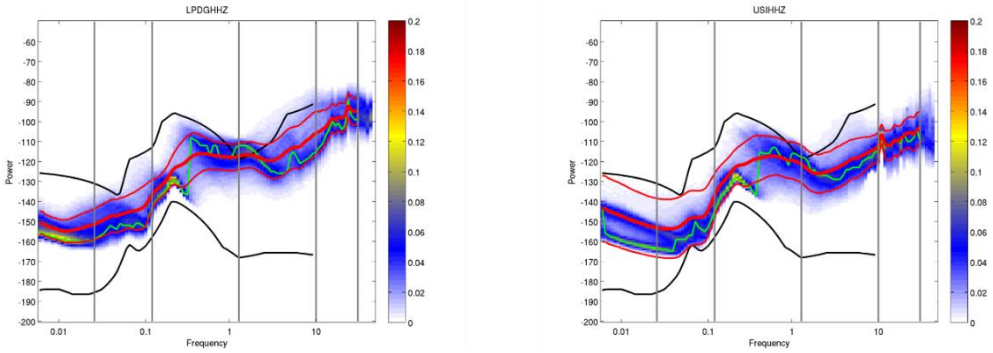

Figure 32: Probability density functions of two stations located on Lampedusa (left panel) and Ustica (right panel) islands. High ambient noise is recorded on much of the frequency window, except the lower band. Especially high noise in the middle band is related to local wind conditions

Volcanic islands environments

Volcanic islands, unlike the previous category, volcanic sources add, in addition to the standard seismic noise component related to ocean waves, storm and local wind.

For this aim, stations in the Aeolian Islands have been chosen. Among all the Eolian islands, two stations of Stromboli and Vulcano have been selected.

The Stromboli stations (ISTR and IST3 codes) are displayed in Figure 33: probably the overlap of multiple sources is shown here. As it is clearly visible, in both sites, at the Very Low Frequencies are very high powers (between -150 and -140 dB), and then increasing again from 0.1 Hz up to higher frequencies. Stromboli is other particularly volcanic contexts: explosions typically occur at a rate of 3 - 10 events per hour (Chouet et al., 1997) with occasional swarm activity reaching 20 - 30 events per hour (Chouet et al., 1999). Hence, sustained tremor and discrete explosions are superimposed on the background noise constantly, as in Etna volcano. This is observed with a constant noise for medium and high frequencies. Especially 0.1 - 1 Hz secondary microseisms is observed but also the frequencies associated to the local wind and volcanic phenomena overlap. Especially, De Lauro et al. (2006), analysed the intermediate 0.1 - 0.5 Hz frequency band of Very Long Period (VLP tremor) suggesting that this frequency band is largely affected by ambient noise, and microseismic noise influences the signals. Therefore, they ascribe the microseismic noise source to Scirocco wind. In addition, the higher frequency signals as due to Strombolian volcanic tremor and explosion quakes (>0.5 Hz) in according with Ciaramella et al., (2004) and De Lauro, (2008). This almost certainly affects the high frequencies, as it is not attributable an anthropic factor.

As for the stations chosen for Vulcano Island, a similar trend is shown. For values greater than 0.1 Hz, a continuous increment is displayed. IVGP and IVPL stations (Fig.34) are located in remote areas. At the intermediate frequencies, more sources are superimposed (sea waves, local wind). The noise related to volcanic aspects are present on almost the entire window of frequencies, including high frequencies.

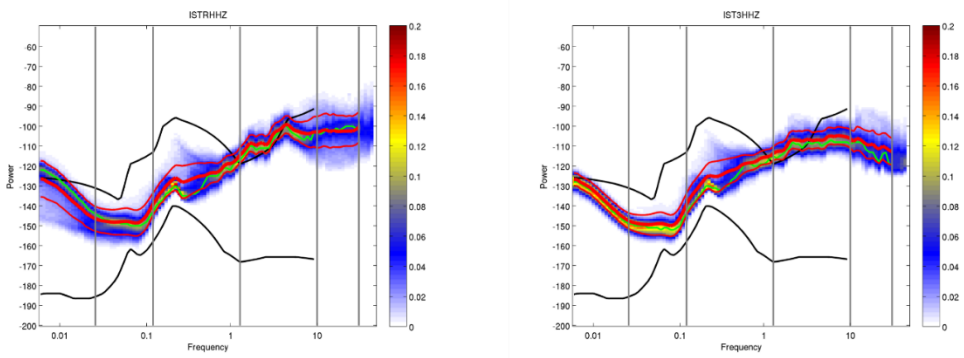

Figure 33: PDFs of ISTRI (left panel) and IST3 (right panel) stations located on Stromboli Island. The ambient noise related to volcanic aspects are present on almost the entire window of frequencies, including high frequencies. This is remarkable for the persistent activity that characterizes this volcano with intermittent explosion-quake and VLP signals.

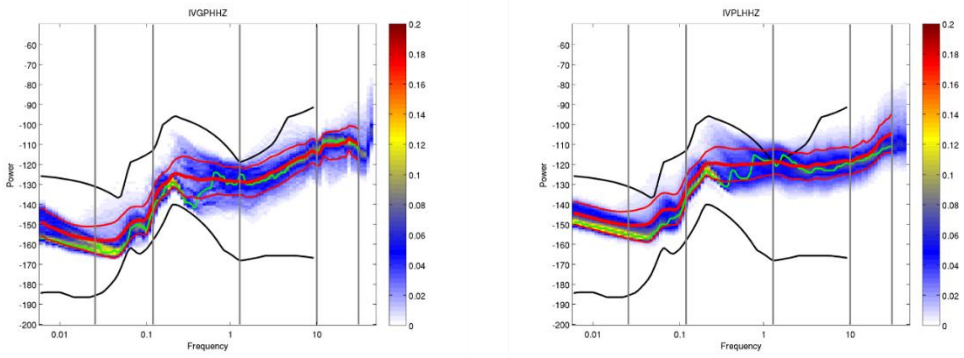

Figure 34: Probability density functions (PDFs) of IVGP (left panel) and IVPL (right panel) stations. The ambient noise related to volcanic aspects are present on almost the entire window of frequencies, including high frequencies**.**

Geological conditions

As already mentioned, the boundary between microseisms and microtremors is close to 1 Hz, but the 1 Hz however, is not a universal limit. It may vary from site to site depending on the soil frequency, i.e. geological conditions, and as already dealt with are several works in the literature that state that geological conditions can affect the power of noise (Seo 1997; Marzorati and Bindi, 2006). More advanced investigations have to be done to define the exact frequency limit between microseisms and microtremors, and determine the possible role played by the soil geological characteristics for ambient noise.

The stations of the Italian seismic network are installed on different geological contexts: most are installed on rocky outcrops, others on sedimentary soils. This means that the role played by geology is crucial in order to detect noise levels and hence, depending on the geological characteristics of soil, the power of the noise can be affected. For instance, Marzorati and Bindi (2006) highlight the differences of noise levels in different stations examined of north central Italy with different geological conditions.

For this reason, two sample stations (Fig. 35) have been chosen where the geological conditions probably influence the background noise at low frequencies. In both situations, thicknesses of thick sedimentary deposits persist.

In the left panel CLTA stations and in the right panel ORZI station are shown. The first station is installed in southern Sicily in the territory of Licata village and the second station is located in Orzinuovi village in the north-western part of the Po Valley. Both have values greater than -110 dB at low frequencies (0.012-1.2 Hz). In addition to the presence of DF peak, probably at these frequencies thick sedimentary deposits present in these two areas determine high noise levels.

As for the high frequencies (> 1 Hz), it is possible to notice a modest noise levels in CLTA station (it is located in a remote area and distant from anthropic sources). Instead, ORZI station, besides being in a geological area subject to site effects, it is strongly influenced by man-made activities and extensive industrialization.

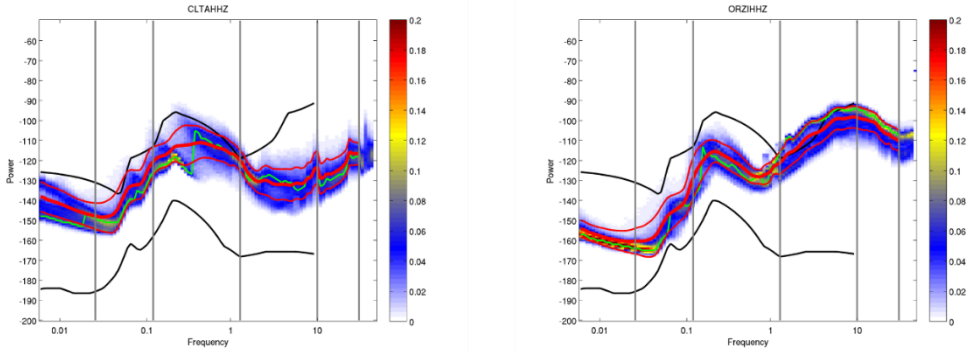

Figure 35: Probability density functions (PDFs) of CLTA (left panel) and ORZI (right panel) stations. They are two stations located in geologically particular areas and subject to site effects. At frequencies around a 1 Hz can be traced back to such effects.

Cultural noise

Numerous stations of the Italian National Network are installed within urban areas or in neighbouring areas in different settings (inside buildings, in built-up areas, near roads, cemeteries, dams, radio bridges). In most stations, anthropogenic factors increasing considerably noise levels and they are the dominant sources of high frequency noise. The noise power in the high frequency range are strongly different from site to site. The highest noise levels are observed for those stations located close to areas with high density of industries, infrastructures and densely populated areas. Cultural noise is not the real focus of this research and has been taken less into account than natural sources. As already mentioned, the cultural noise presents the range of high frequencies from 1 Hz onwards. Only two cases samples are take in account and the analysed PDFs are in agreement with the literature; in fact, for values greater than 1 Hz in both stations is clear a strong increase. The two stations are positioned in small villages and both stations are located in the Po Valley. In Figure 36, the two relative PDFs are shown. In the left panel, CAVE station is presented: this is located in the astronomical observatory of Cavezzo (where the powerful instruments surely increase the noise), while NDIM station (right panel) is sited in Novi di Modena village. In both spectra, the minimum power range is about -130 dB (for values greater than 1 Hz) and you get to exceed -90 dB (especially for NDIM station). For frequencies lower than 1 Hz are visible microseismic peaks. Especially more evident is the DF peak, as observed in the Po Plain by Marzorati and Bindi (2006).

A problem that persists in this area studied by Marzorati and Bindi (2006) is certainly related to the geological conditions of the Po Valley, as already discussed. Probably the site effects also affect the two stations, being installed over a thick sedimentary cover in the Po plain. This could be amplify the ambient noise at the two stations at middle-high noise levels.

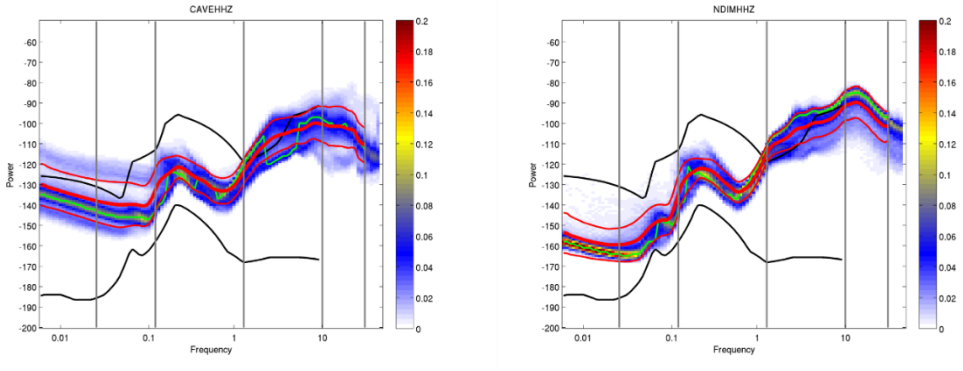

Figure 36: Probability density functions (PDFs) of CAVE (left panel) and NDIM (right panel) stations located in urban environments. It is immediately observed how high frequency stations show high cultural noise.

4.1.2 New Italian seismic noise model

Regional study of Italian seismic noise have been carried out in the past (Vassallo et al.2012; Marzorati et al., 2011; Marzorati & Bindi, 2006 and others).

These models provide a more detailed study than global studies but a model has not yet been proposed for Italy as has been done for other parts of the world as Mcnamara (2004 and 2019); Dimitrova and Nikolova, (2010); Grecu et al., (2012); Soliman, (2013); Custódio et al., (2014); Melosantos et al., (2015); Anthony et al., (2015) ; Guo and Aydin, (2015); Demuth et al., (2016), Jana et al., (2017).

The great amount of data in possession and the respectable coverage of the National Seismic Italian Network on territory, can therefore allow you to propose a good Italian model.

For this reason, the ambient noise level of the different Italian broadband stations was analysed.

After extracting all the PSDs of each stations, all the mean of the each single PSD have been plotted into a single graph: in the Figure 37 is reported the Z component.

Each black line represents the mean PSD of each station in the 3-year period considered. The dotted red lines represents the Peterson model and represent the currently accepted standard for expected limits of seismic noise, and the dotted yellow line indicates the average of all the averages of 233 PSDs. The most PSDs are packed into Peterson reference models except for some very noisy stations. Italian ambient noise at low power falls within the minimum level Peterson model (NLNM) but it is higher than the lower baseline (NLNM). Instead, some stations have higher noise levels than world's top reference model (NHNM). Some of these stations as already seen are attributable to the volcanic district of the Campi Flegrei area and some stations exceed especially in the high frequencies (between 1 to 5 Hz and 10-30 Hz respectively). These sites are to the noisiest stations found on the Italian region. Among the extracted PDFs, have been obtain the lowest and the highest recorded noise. PDF of the end members stations belong to ROVR station (that is the lowest average that appears in the PSD graph) and CPIS stations (the upper average) as shown in Figure 38. ROVR station is the station with the lowest level of noise and it is sited in Rovere Veronese. In fact, it is possible to notice a higher density at very low frequencies. Surely, the station is affected by the microseisms it can detect quite well. The station is sited at 1316 meters a.s.l. and then in an undisturbed location and this justifies the low noise at high frequencies.

Instead, CPIS station has been widely discussed in advance. This is the only station to show high levels of noise even at low frequencies. It is the noisiest station of the entire Italian territory. As previously mentioned it is attributable to the actual complex volcanic context.

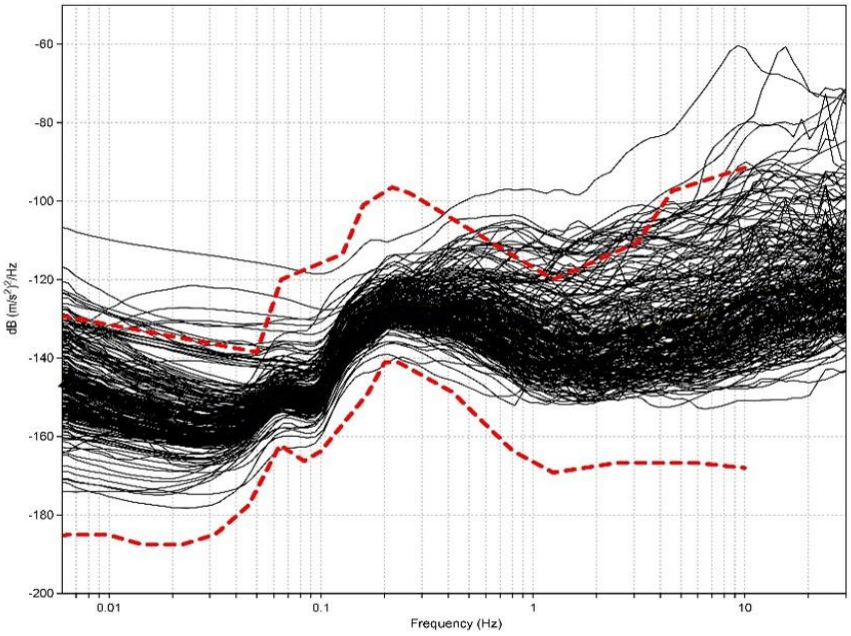

Figure 37: The overplot of the averages Power Spectral Density of all PSDs (vertical component). Each black line represents the average of each station. Red dashed-dotted lines are the Peterson reference model (1993).

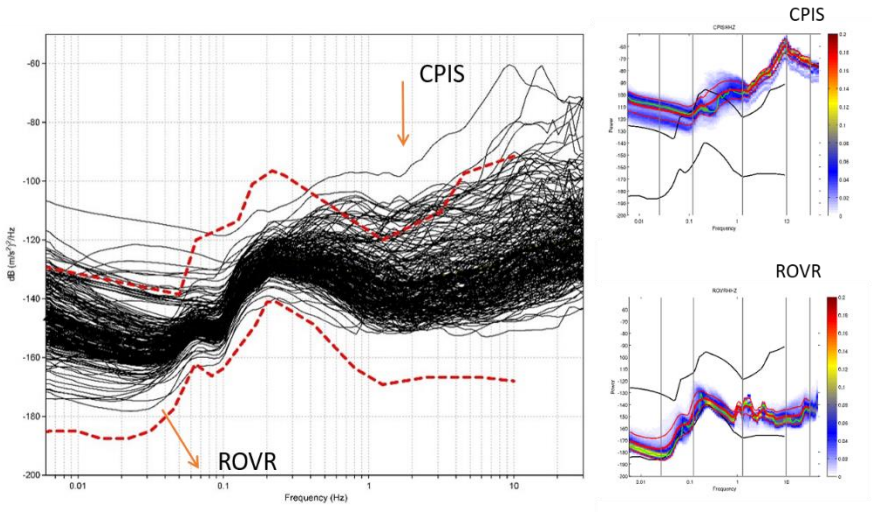

Figure 38: Averages Power Spectral Density curves for all Italian stations. The end members are represented by CPIS and ROVR stations. They are indicated with the two arrows in the PSD on the left, while the relative PDF are shown on the right.

Finally, the corresponding overplot of the average of all PDFs is extracted (Fig. 39b).
It is shown next to the overlay graph of all PSD of the stations (Fig. 39a).
The vertical grey dashed lines represent always the boundaries between the four frequency bands. This PDF is representative of all the analysed 233 stations for the vertical component and could be considered the PDF reference for the Italian territory.
This suggests better how the Italian noise largely falls within the reference models of Peterson. It is also possible to see how for low frequencies there is an increase in noise certainly correlated to natural sources but can also include artifacts. Therefore the highest probability density recorded is for very low frequencies (<1 Hz) with powers between -160 dB and -140 dB. In addition, many obvious appear always in the low frequencies, the two peaks microseismic (in yellow) with a density distribution of about 0.06. This states that natural sources linked to weather conditions, the sea and the wind affect a territory (entirely bathed by the sea) strongly influence the Italian background noise. Finally PDF and PSDs (Fig 39b), allows us to estimate both the overall stations quality and a baselines level of the Italian seismic noise.
As observed by other authors as well (Mcnamara and Buland, 2004; Berger and Devis, 2004 and others) also in the Italian territory baseline noise level is upper of the NLNM of Peterson (1993). In fact, in Italy the minimum threshold of noise levels is therefore higher than NLNM model. Even the upper baseline exceeds due to some stations the upper NLNM level.
These new baselines of the Italian background noise have been underlined as shown in Figure 40 (light blue lines). This model can be considered the reference model for seismic noise for the Italian territory. Especially Italian Low Noise model (ILNM) is the lower reference model and Italian High noise model (IHNM) is the higher reference model.

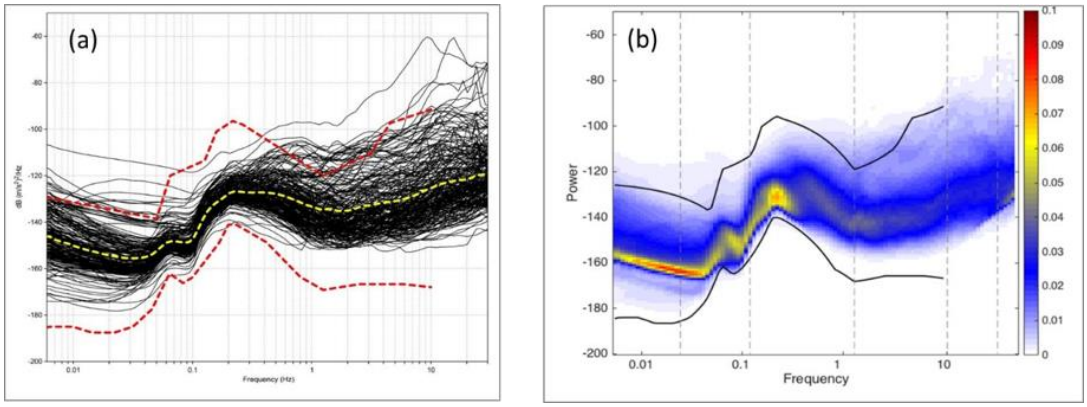

Figure 39: Overplot of the average of all PSDs (a) and the corresponding overplot of the average of all PDFs (b) determined for the vertical components of the 233 stations.

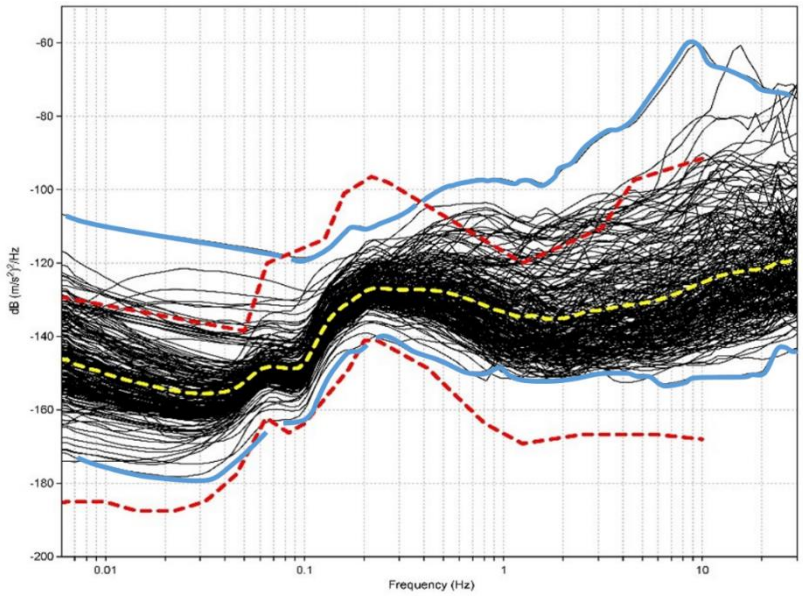

Figure 40: Italian reference models (ILNM and IHNM codes) are indicated with blue lines in the plot. Yellow dashed-dotted line is the average PSDs. The lower ROVR station falls in New Low Noise Model of Peterson while CPIS station is largely outside to the New High Noise Model of Peterson (1993).

4.2 Statistical Analysis

4.2.1 Seismic noise frequencies distribution

A first statistical approach was to assess the frequency distribution of noise density values at different Italian stations.

All means and standard deviation values have been extracted for each station over the three-year period for each component and frequency band and finally for each component and band was extracted the average value of the statistical indicators of means and standard deviations (Table 7 and 8).

From the analysis in each frequency band and component, frequency distribution histograms have been obtained.

Especially a bandwidth h = 5 is fixed for mean value and h=1 for standard deviation.

Histograms were carried out for all three components, but similarities were observable for the two horizontal components (Fig.41).

To verify this hypothesis (already observed also in the Table 7 and 8), the difference between the two means horizontal components (Fig.42) and their standard deviations (Fig.43) were computed. The means and standard deviation histograms are sufficiently symmetrical and centred towards zero. From the analysis performed, it has been decided to represent the average of horizontal components, referred to as H component for the four frequency bands.

Before studying the H component, a brief overview can be made on other calculated statistical indicators of all components.

In addition skewness, kurtosis, maximum and minimum parameters, for each component, and for frequency band have been considered. These statistical indexes are reported in Tables 9, 10, 11, 12, respectively.

All skewness values (Table 7) are positive (>0) and the highest values are reported for the first and last frequency band. The relative standard deviations are also reported in the same table. Kurtosis values (Table 8) are all positive as well. In this case, the highest values are for the first and the last bands, with a higher value (5.94) for band 0.025-0.012 Hz of the Z component.

The maximum and minimum values are displayed in the Tables 9 and 10. They are the values of the noisiest station (maximum value) and the least noisy one (minimum value) for each frequency band and component.

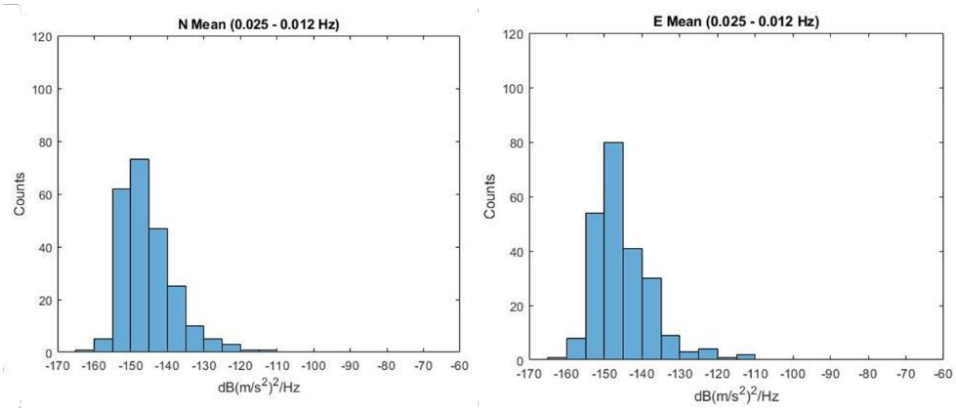

Figure 41: Histograms related to North and East components (0.025-0.012 frequency band). From this example, we observe the similarity of the frequency of distribution for the two components.

Frequency BANDS	Z Mean	N Mean	E Mean
0.025-0.012 Hz	-150.61	-145.24	-145.21
0.012-1.2 Hz	-130.18	-128.96	-129.13
1.2-10 Hz	-131.65	-129.11	-129.39
10-30 Hz	-121.77	-119.96	-120.19

Table 7: Means average values related to Z, N and E components for the four frequency bands. In the box the two horizontal bands showing very similar values.

Frequency BANDS	Z STD	N STD	E STD
0.025-0.012 Hz	10.49	9.66	9.61
0.012-1.2 Hz	8.15	7.94	7.97
1.2-10 Hz	8.19	7.37	7.35
10-30 Hz	7.98	7.85	7.83

Table 8: Standard deviation average values related to Z, N and E components for the four frequency bands. In the box the two horizontal bands showing very similar standard deviation values.

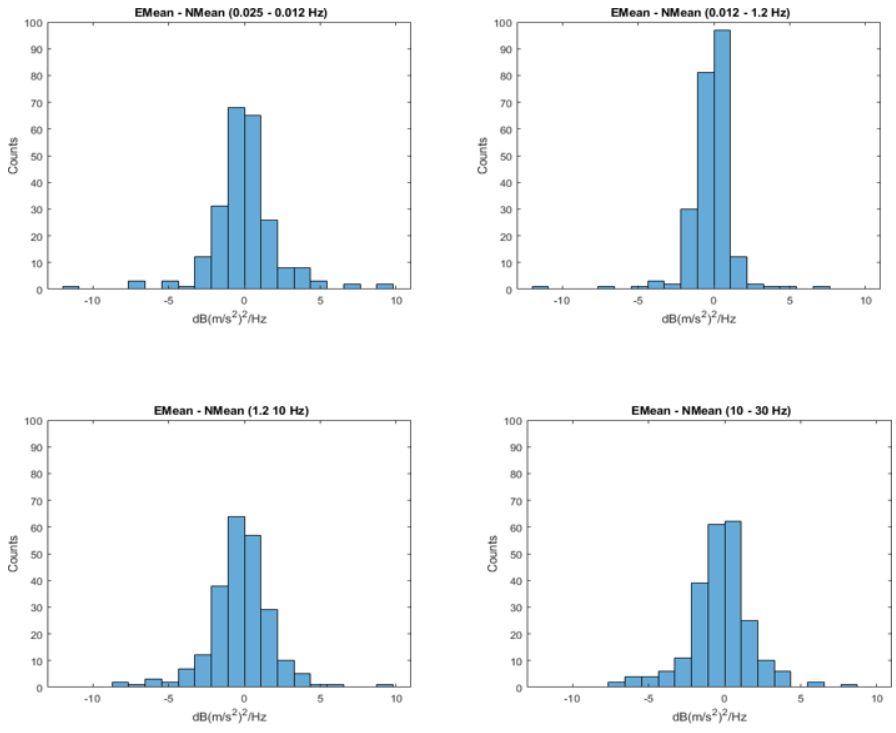

Figure 42: Histograms relative to the difference between the two horizontal components. They show symmetrical patterns.

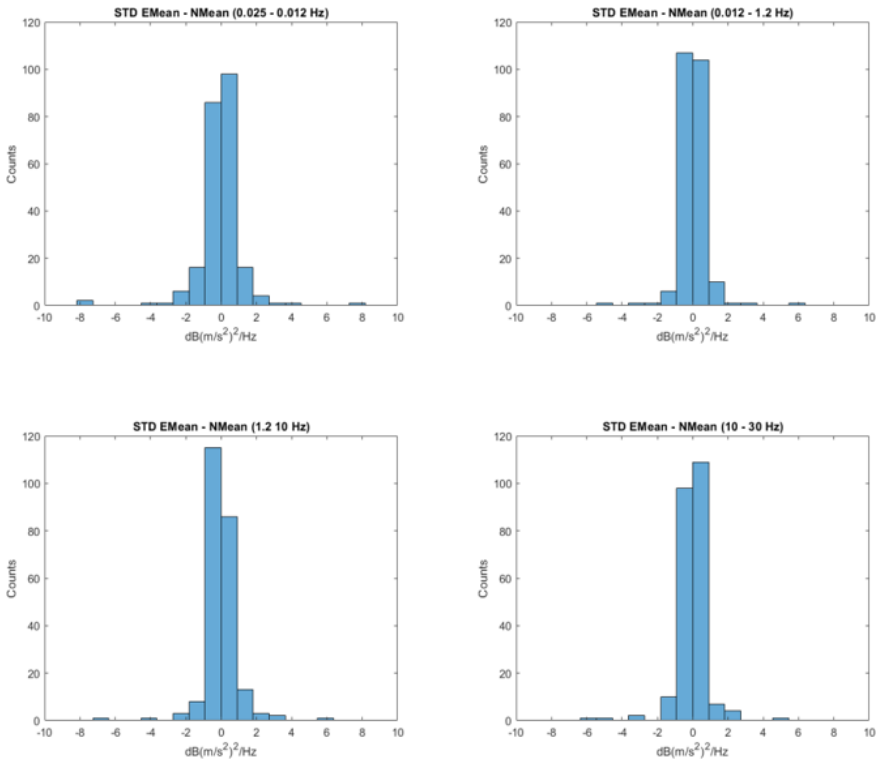

Figure 43: Histograms relative to the difference between STD of the two horizontal components.

Frequency BANDS	Z Skewness Mean	N Skewness Mean	E Skewness Mean	Z Skewness STD	N Skewness STD	E Skewness STD
0.025-0.012 Hz	1.80	1.39	1.48	1.43	2.11	1.69
0.012-1.2 Hz	0.88	0.83	0.87	1.69	2.35	2.16
1.2-10 Hz	1.07	0.88	0.97	1.30	1.58	1.56
10-30 Hz	1.17	1.10	1.12	1.07	1.24	1.05

Table 9: Skewness values related to Z, N and E components for the four frequency bands.

Frequency BANDS	Z Kurtosis Mean	N Kurtosis Mean	E Kurtosis Mean	Z Kurtosis STD	N Kurtosis STD	E Kurtosis STD
0.025-0.012 Hz	5.94	2.83	3.58	2.37	5.99	4.41
0.012-1.2 Hz	1.32	0.42	0.82	3.54	7.52	5.81
1.2-10 Hz	0.71	0.03	0.32	1.75	3.01	2.80
10-30 Hz	1.58	1.40	1.42	1.57	3.33	2.11

Table 10: Kurtosis values related to Z, N and E components for the four frequency bands.

Frequency BANDS	Z Max Mean	N Max Mean	E Max Mean	Z Max STD	N Max STD	E Max STD
0.025-0.012 Hz	-116.06	-113.54	-110.23	22.02	21.77	21.40
0.012-1.2 Hz	-104.00	-102.99	-102.69	16.75	18.03	17.43
1.2-10 Hz	-82.63	-96.03	-92.30	19.22	17.48	16.84
10-30 Hz	-69.85	-72.86	-72.39	18.00	20.74	17.73

Table 11: Maximum values related to Z, N and E components for the four frequency bands.

Frequency BANDS	Z Min Mean	N Min Mean	E Min Mean	Z Min STD	N Min STD	E Min STD
0.025-0.012 Hz	-166.50	-161.11	-160.96	3.87	4.77	4.11
0.012-1.2 Hz	-143.56	-143.26	-143.56	4.90	5.22	4.93
1.2-10 Hz	-148.48	-147.81	-147.57	3.76	3.75	3.71
10-30 Hz	-148.08	-143.90	-143.21	2.71	2.97	2.91

Table 12: Minimum values related to Z, N and E components for the four frequency bands.

Before showing the Z and H components results, the new statistical indicators calculated for the H component are shown below.

The Tables 13 and 14 show the mean values and their relative standard deviations of the H component compared the Z values previously seen. Skewness (Table 15) and kurtosis (Table 16) values remain always positive.

Maximum and minimum values in the Tables 17 and 18 are agree with the spectra previously seen. In fact, for the Z component the maximum value is represented by the CPIS station (-116.06 dB) while the minimum is ROVR station (-166.50 dB). For H component, the same stations have values -111.88 dB (maximum) and -161.03 dB (minimum).

Frequency BANDS	Z Mean	H Mean
0.025-0.012 Hz	-150.61	-145.23
0.012-1.2 Hz	-130.18	-129.05
1.2-10 Hz	-131.65	-129.25
10-30 Hz	-121.77	-120.07

Table 13: Means average values related to vertical and horizontal components for the four frequency bands.

Frequency BANDS	Z STD	H STD
0.025-0.012 Hz	10.49	9.63
0.012-1.2 Hz	8.15	7.96
1.2-10 Hz	8.19	7.36
10-30 Hz	7.98	7.84

Table 14: Standard deviation average values related to vertical and horizontal components for the four frequency bands.

Frequency BANDS	Z Skewness Mean	H Skewness Mean	Z Skewness STD	H Skewness STD
0.025-0.012 Hz	1.80	1.42	1.43	1.84
0.012-1.2 Hz	0.88	0.83	1.69	2.19
1.2-10 Hz	1.07	0.93	1.30	1.50
10-30 Hz	1.17	1.11	1.07	1.10

Table 15: Skewness values related to vertical and horizontal components for the four frequency bands.

Frequency BANDS	Z Kurtosis Mean	H Kurtosis Mean	Z Kurtosis STD	H Kurtosis STD
0.025-0.012 Hz	5.94	3.23	2.37	4.85
0.012-1.2 Hz	1.32	0.56	3.54	6.3
1.2-10 Hz	0.71	0.16	1.75	2.64
10-30 Hz	1.58	1.42	1.57	2.63

Table 16: Kurtosis values related to vertical and horizontal components for the four frequency bands.

Frequency BANDS	Z Max Mean	H Max Mean	Z Max STD	H Max STD
0.025-0.012 Hz	-116.06	-111.88	22.02	21.25
0.012-1.2 Hz	-104.00	-102.84	16.75	17.73
1.2-10 Hz	-82.63	-94.17	19.22	16.40
10-30 Hz	-69.85	-72.65	18.00	19.24

Table 17: Maximum values related to vertical and horizontal components for the four frequency bands.

Frequency BANDS	Z Min Mean	H Min Mean	Z Min STD	H Min STD
0.025-0.012 Hz	-166.50	-161.03	3.87	4.92
0.012-1.2 Hz	-143.56	-143.33	4.90	5.23
1.2-10 Hz	-148.48	-147.69	3.76	3.73
10-30 Hz	-148.08	-143.01	2.71	2.94

Table 18: Minimum values related to vertical and horizontal components for the four frequency bands.

After showing the numerical values of the averages and standard deviations of the two components is shown below the frequency of distribution of the PSD both of the average values and of the relative standard distributions.

0.025-0.012 Hz frequency band

The averages frequency distribution for the Z component (Fig. 44, upper left) it is very clear how the most sites (115 stations) are characterized by PSDs values between -155 and -150 dB $(m/s^2)^2/Hz$.
Little more than thirty stations (32) have a range between -155 and -160 dB $(m/s^2)^2/Hz$. Other 53 stations are represented by means values between -150 to -145 dB $(m/s^2)^2/Hz$, while the remaining (27) are characterised by higher noise levels (-145 and -115 dB $(m/s^2)^2/Hz$range). Only six sites have very low noise levels (from -160 to – 170 dB $(m/s^2)^2/Hz$).
As regards the horizontal component (Fig. 43, lower left), the PSDs means values of the most representative eclass (78 stations) have a range between -150 and -145 dB $(m/s^2)^2/Hz$.
While 56 stations have a range between -155 and -150 dB $(m/s^2)^2/Hz$, others 45 stationspresent including a range of -145 to -140 dB $(m/s^2)^2/Hz$ means values.
Most stations (46) are spread to the right of the histogram and they are divided intosubclasses up to -110 dB $(m/s^2)^2/Hz$. Only eight stations represent the stations with minimum PSDs means values (< -160 dB$(m/s^2)^2/Hz$).

Analysing their standard deviation of a both components (Fig.43, upper and low right) it possible observe a high variability of the data up to 22 dB $(m/s^2)^2/Hz$. For a both components, the higher frequencydistribution of standard deviation is between 8 - 9 dB $(m/s^2)^2/Hz$ for 63 stations of Z component and for 74 stations of H component. This allows confirming a fair reliability of the average of the subclass, while it is increasing for the remaining subclasses (up to 22 $dB(m/s^2)^2/Hz$). Eleven stations for H component are characterised by a good average reliability between (4 and 7 dB $(m/s^2)^2/Hz$)) while Z component 8 station between 5 and 7 dB $(m/s^2)^2/Hz$ and one station show values between 3 and 4 dB $(m/s^2)^2/Hz$.

It is possible to observe and as mentioned above, how the average is dispersed to the right of the histograms; the skewness values are > 0 with 1.80 and 1.42 for Z and H components respectively (Table 13). In addition, kurtosis are positive (>0) for both components with 5.94 and 3.23 values for Z and Hcomponents respectively (Table 14), showing a Leptokurtic distributions. Finally, it is possible to deduce that for this frequency band the highest distribution frequency has a range from -155 to -145 dB $(m/s^2)^2/Hz$ with standard deviation from 8-9 dB $(m/s^2)^2/Hz$.

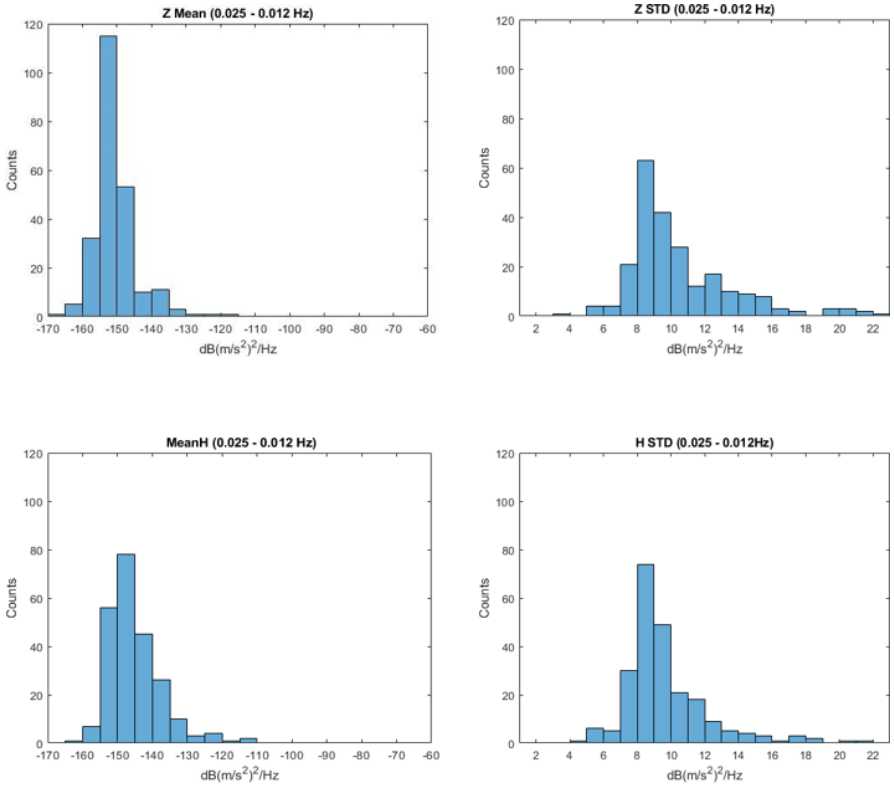

Figure 44: Histograms relative to frequency distributions of the density values for vertical and horizontal components and relative standard deviations for the 0.025-0.012 Hz frequency band.

0.012-1.2 Hz frequency band

A similar distribution regarding to the second frequency band. Histograms are displayed forboth Z and H components (Fig.45).

For vertical component more than 80 stations (85) have a PSDs means values in a range between -135 and -130 dB$(m/s^2)^2$/Hz, presenting the class with the highest distribution frequency about the Z component. Other important classes are represented by 42 stations with means values from -140 to -135 dB $(m/s^2)^2$/Hz, and 60 stations showing a range between -130 and -125 dB $(m/s^2)^2$/Hz. Only six stations are the least noisy stations for this frequency band (-145 to -150 dB $(m/s^2)^2$/Hz. While only a few classes have higher PSDs means values and are noisiersites (– 125 and -110 dB $(m/s^2)^2$/Hz). Only one station has the lowest PSD (between -105 and 100 dB $(m/s^2)^2$/Hz).

Similar is the behaviour for the H component: the highest distribution frequency (75 stations) have PSDs between - 135 and -130 dB $(m/s^2)^2$/Hz, while more than 50 stations (55) are included between -130 and -125 dB $(m/s^2)^2$/Hz. PSDs values of 39 stations from -140 to -135 dB $(m/s^2)^2$/Hz while the least noisy stations are seven with PSDs values -145 and -140 dB $(m/s^2)^2$/Hz. The remaining stations (57 stations) are distributed between -125 and -100 dB $(m/s^2)^2$/Hz. In addition, in this case both histograms are shifted to the left and show a positive asymmetry withvalues always > 0 especially 0.88 and 0.83 for Z and H components respectively (Table 13). Again, theyshow a kurtosis > 0 especially 1.32 value for Z and 0.56 value for H (Table 14). A small difference of standard deviations is shown for the two components (Fig. 44)

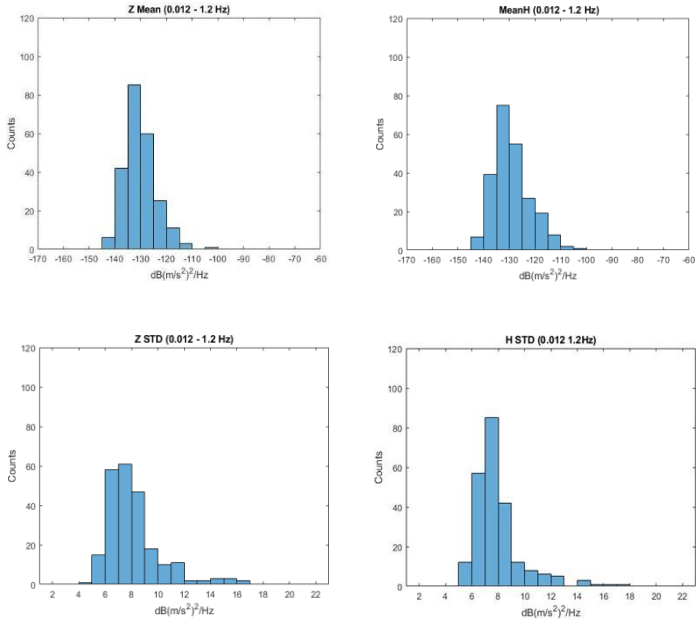

Figure 45: Histograms relative to frequency distributions of the density values for vertical and horizontal components and relative standard deviations for the 0.012-1.2 Hz frequency band**.**

1.2-10 Hz frequency band

In the 1.2-10 Hz frequency band both components show a distribution frequency tendingtowards noisier PSDs values (Fig 46).

Most stations have ranges between - 140 and -135 dB $(m/s^2)^2/Hz$ (number of stations 54stations) for both components. Only 10 stations with a range between -145 and -150 dB $(m/s^2)^2/Hz$ occur while the rest ofthe stations have a noise between -130 and -95 dB $(m/s^2)^2/Hz$. Only one class of stations represents the noisiest one (-85 and -80 dB $(m/s^2)^2/Hz$). The highest frequencies distribution for the horizontal component are to be considered in a range between -140 and -130 dB $(m/s^2)^2/Hz$ (102 stations). Thirty stations have PSDs values between -140 and -145 dB $(m/s^2)^2/Hz$, while 31 other stationshave between -130 and -125 dB $(m/s^2)^2/Hz$. The rest of the stations instead are distributed to increasingly noisy values (from -125 to – 90 dB $(m/s^2)^2/Hz$). Only six stations have a noise that does not exceed -150 dB $(m/s^2)^2/Hz$.

In the relative standard deviations, it is possible to observe that the most of station have a medium-low standard deviation. The skewness of the means PSDs shows positive values 1.07 (Z) and 0.93 (H) and being bothgreater than 0 they have a positive asymmetry. In addition, kurtosis parameter shows less peakness of the frequency distribution curve than the previous histograms especially for component H with a value of 0.16, while kurtosis is 0.71 for Z component.

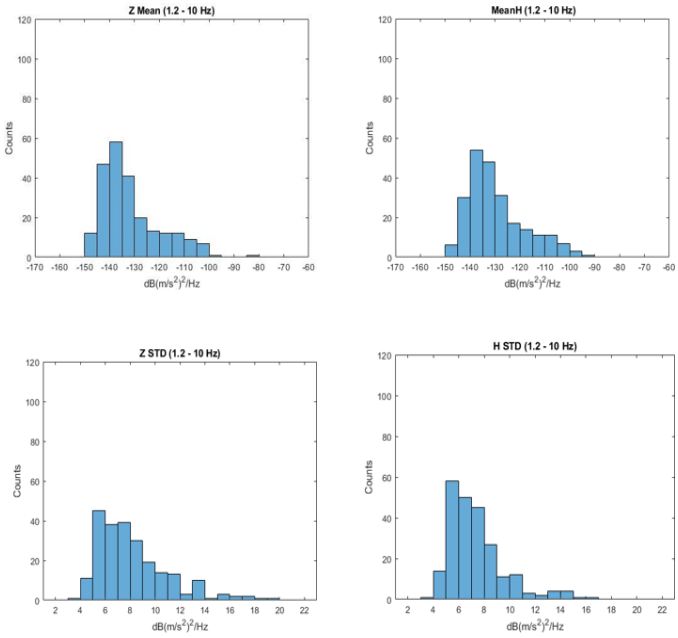

Figure 46: Histograms relative to frequency distributions of the density values for vertical and horizontal components and relative standard deviations for the 1.2 - 10 Hz frequency band.

10-30 Hz frequency band

For High Frequency of the Z component, the average value of all the averages of the Italian statins is -121.7 dB $(m/s^2)^2$/Hz with 7.9 standard deviation value.

Kurtosis and Skewness parameters are positive (1.5 and 1.1 respectively).

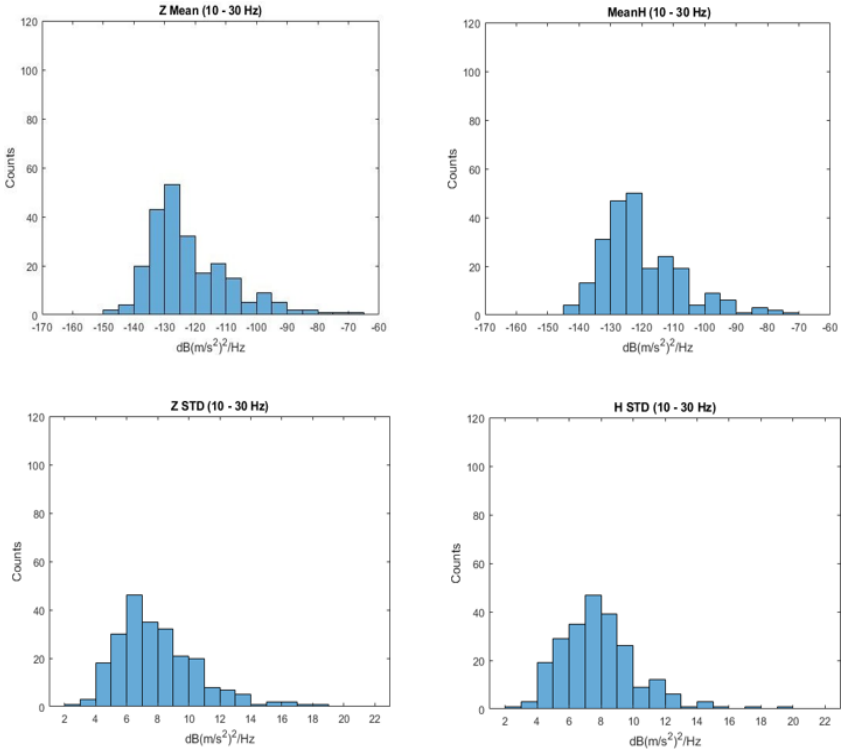

Figure 47: Histograms relative to frequency distributions of the density values for vertical and horizontal components and relative standard deviations for the 10-30 Hz frequency band.

4.2.2 Power Spectral Densities ratio

The averages and standard deviations ratios between the PSDs of horizontal and vertical components has been performed (Fig. 48 and 49).
It is possible to notice that the higher frequency distribution oscillates in a power range between 0.9 and 1 for all frequency bands (Fig. 48).
Only the first frequency band has a greater dispersion for values less than 0.9 and a slightly negative skew. Instead, the other distributions are distributed more or less around the centre 0 with a Gaussian distribution, except the 10-30 Hz frequency band that present a slightly symmetrical distribution with a positive skew.
In general, most stations are concentrated around a ratio of about one resulting in good ground-to-sensor coupling. This means that a good part of the sensors is distributed in suitable sites and a good signal-to-noise ratio is found. The standard deviations ratios (Fig.49) show for the most of stations a trend focused at 1 value, especially the 0.012-1.2 Hz frequency band. All others two bands show a higher dispersion (0.025-0.012 Hz and 1.2-10 Hz frequency bands).

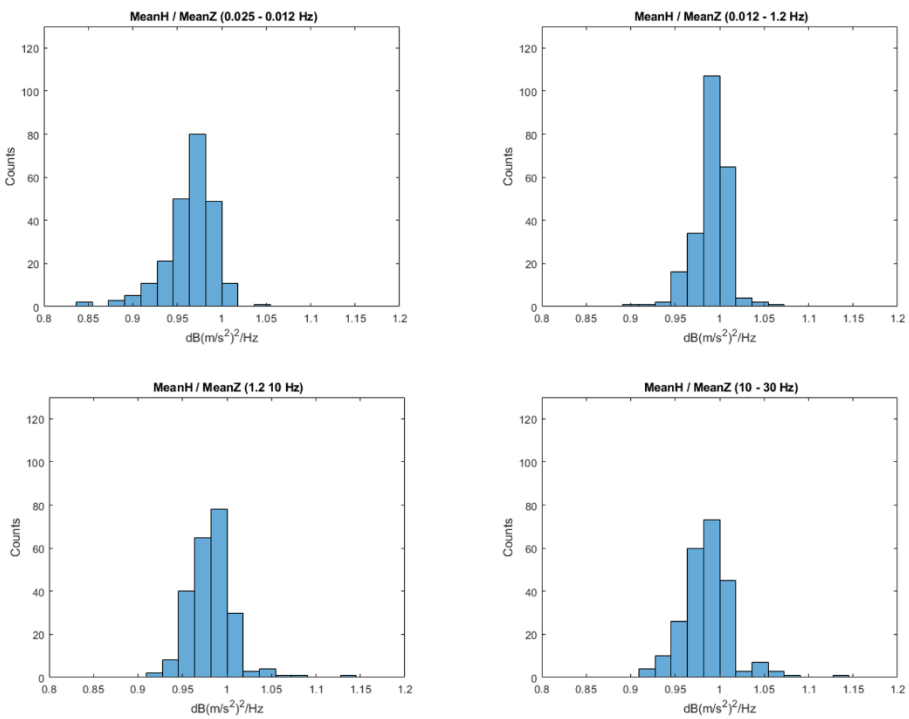

Figure 48: Histograms relative to PSD ratios for horizontal and vertical components and for all four frequency bands.

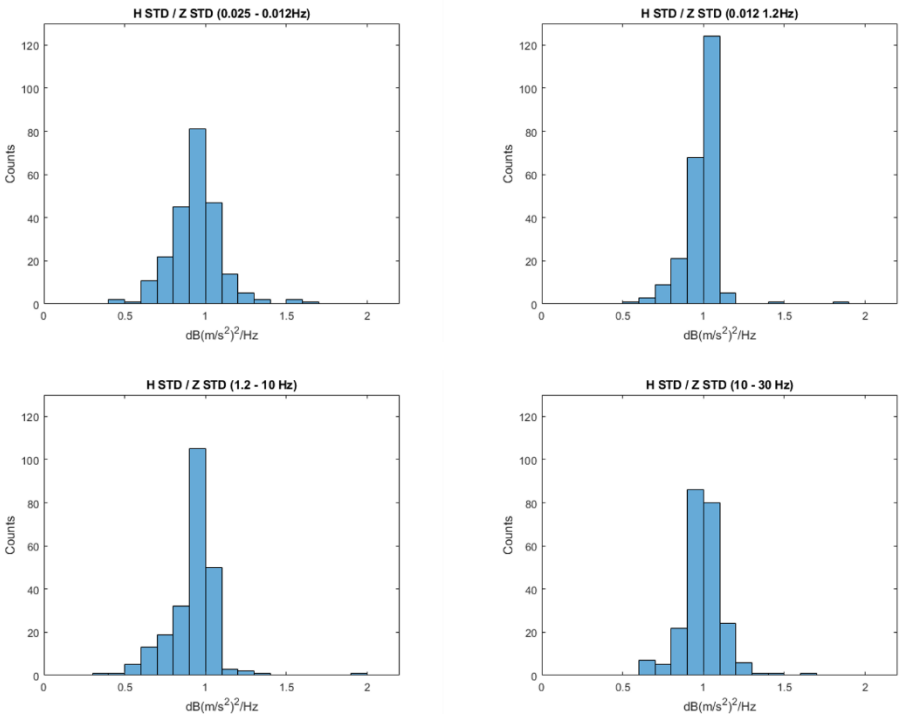

Figure 49: Histograms relative to PSD ratios standard deviation for horizontal and vertical components and for all four frequency bands.

4.2.3 Kernel distribution analysis

In order to exceed the limits of the histograms representation and for a more refined and statistically robust representation, among all the estimation methods, it has been decided touse a kernel method using Matlab software applying *ksdensity* function.

In this analysis, the data previously displayed as histograms, so now with this method are shown.

A density trace can also be combined with a histogram to give a more realistic impression of the data distribution. In Figure 50 is compared the histogram pattern of the Z component related to the frequency band 0.025-0.012 Hz, and its relative smoothed line with the Kernel method (blue trace).

Moreover, density traces are better suited for comparing data distributions than histograms because they can easily be plotted on top of one another and in different colours. In fact, for vertical and two horizontal components, plots was realized that show the estimation of the density distribution for every frequency bands (Fig. 51).

Generally, all Kernel curves smoothed show an apparent Gaussian distribution but no have a symmetrical distribution. In fact, the three components have all positive Skewness and Kurtosis. Especially all curves show a positive Skewness (tilted to the right) showing always a dispersion toward higher noise values. Positive kurtosis (especially for lower frequency bands that show high peakness) demonstrate that at most of stations, the average values PSDs have high density distribution even though it is lower in the higher frequencies (1.2-10 Hz and 10- 30 Hz).

It turns out to be interesting the plot relative to the Z component (Fig. 51, upper panel) while the other N (Fig. 51, middle panel) and E (Fig. 51, lower panel) two components obviously show more similar trends.

In the plot related to the Z component to observe that, for the 0.025-0.012 Hz frequency band (blue trace), ambient noise levels are medium lower regarding the other frequency bands. It has a low

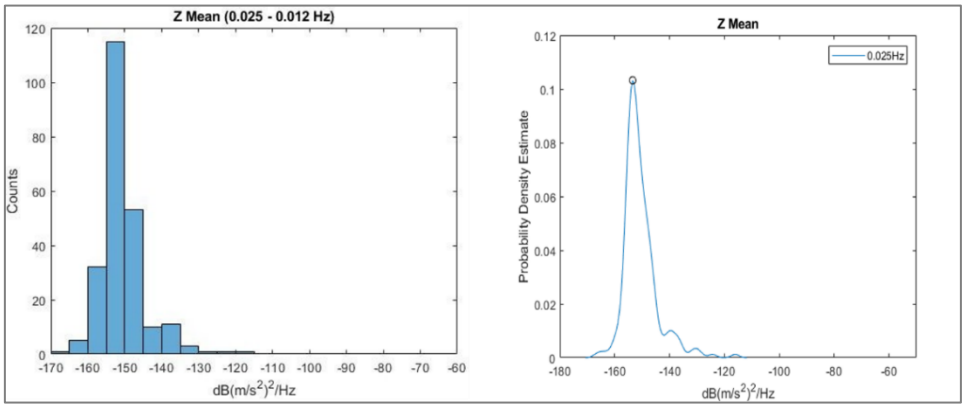

Figure 50: Histogram displayed as smoothed kernel trace for 0.025-0.012 Hz frequency band (Z component).

variability (small variance) and the distribution is much contracted with more than 0.1 of density estimate (a high peakness is displayed). This is the highest probability density for most stations with a mean value of about -155 dB.

Instead, in the others three bands, the noise values turns out to be at higher powers (with an average value of about -130 dB) showing a much wider variability (wide variance) and more dispersed. These frequency bands have a much broader values distribution above all for the higher frequency bands where reaching the maximum power value recorded (-66 dB) for the 10-30 Hz frequency band (violet trace). Especially, the second 0.012- 1.2 Hz frequency band (orange trace) is less dispersed than others does not exceed more than -100 dB; it has a higher probability density around 0.07, while the largest frequency bands do not exceed 0.04.

As far as the higher frequencies, on the other hand, as already mentioned, have a greater variability than the lower frequency bands: this means that the large-scale phenomena related to lower frequency bands have a less variability than the anthropic noise (higher frequencies) that can vary more being localized.

Instead, the Probability Density Estimates of the horizontal components N and E (Fig. 51, middle and lower panels) are very similar. Unlike the Z component, here the frequency band 0.025-0.012 Hz, has a lower estimate as for the frequency band 0.012- 1.2 Hz (about 0.07) and showing an average value always of -155 dB but with a poorly dilated variability of the data. Instead the high frequency bands (1.2 -10 Hz and 10-30 Hz) continue to always confirmation a probability density estimate around 0.04 and to show a wide variability in its PSDs (as for the Z component) with minimal differences and always showing an average peak around -130 dB.

As mentioned above, all curves have a dispersion towards higher noise values, but most stations concentrate within less noisy PSD values (around -150 and -120 dB). This confirms once again how much of the noise in the Italian territory falls within the terms of a medium noise as already seen in the spectrum of the Italian model (previous Fig. 39).

In particular, the frequency band 0.025-0.012 Hz, in addition to being the least noisy band, for the Z component, has the highest estimated density. This means that most of the stations for this component, suffer a lot from natural sources that overlap and act on a large scale continuously over time.

In general, it can be said that for 0.025-0.012 Hz and 0.012 – 1.2 Hz frequency bands, natural sources are the main cause and have a higher probability density. On the other hand, the noise sources of the major frequency bands, being more connected to anthropic sources, are more localized and present a lower probability density.

Instead, the relative standard deviations in Figure 52 are shown. It is possible to observe how the

lowest frequency band (0.025-0.012 Hz) have a wide dispersion (up to about 22 dB) than others three frequency bands. This is observable for all three Z, N and E components.

In addition, most stations for all three components have a lower dispersion (less 20 dB). Finally, it can be stated that the average is reliable and representative of the data because most of the data fall within a standard deviation of 15 dB.

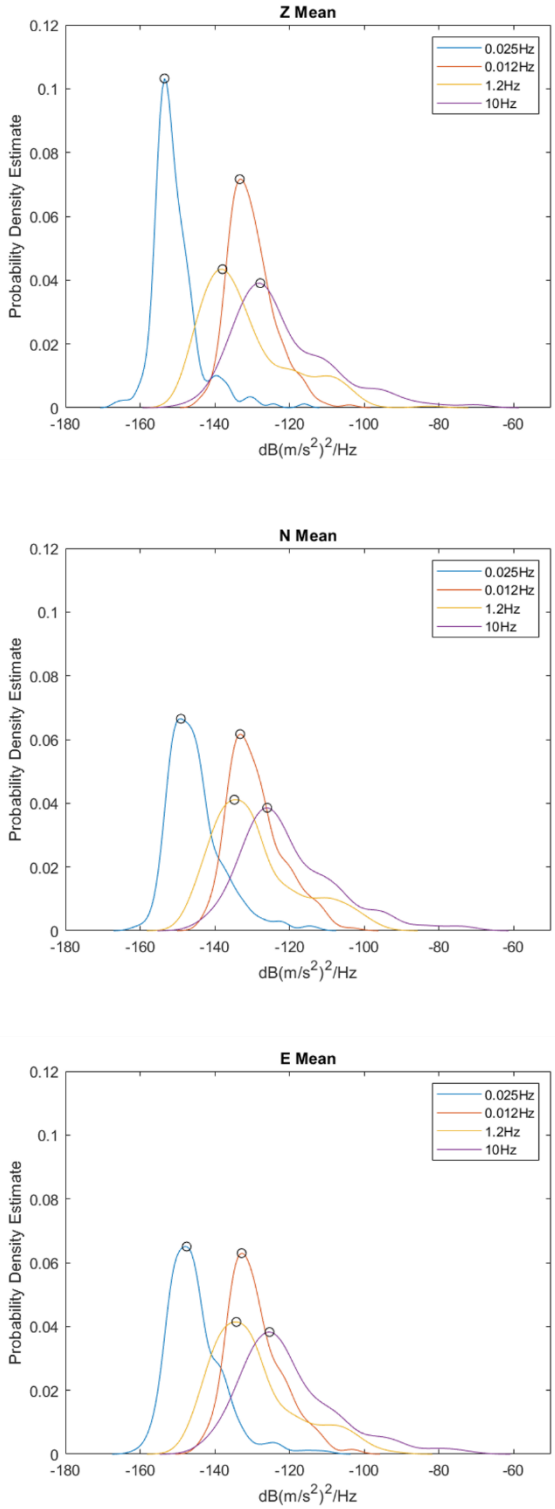

Figure 51: smoothed traces of the PSDs means for the Z, N and E components. The colours indicate the four frequency bands. The empty dots indication the maximum of each curve.

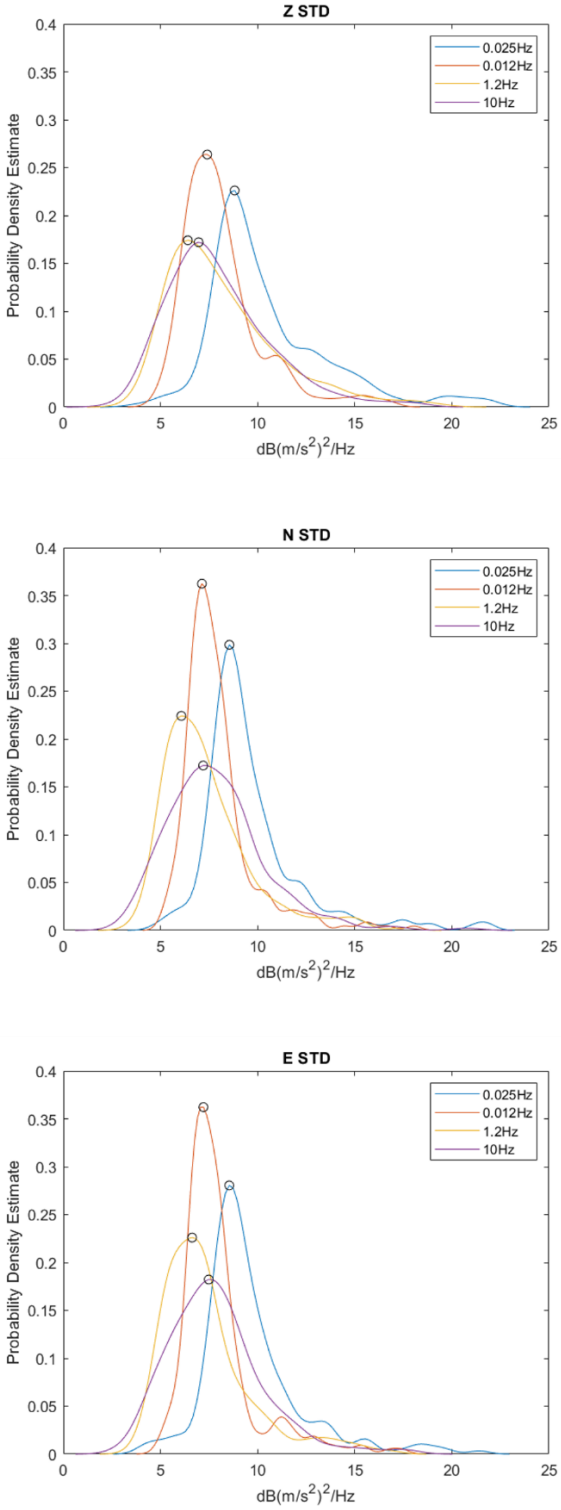

Figure 52: smoothed traces of the PSDs standard deviations for the Z, N and E components. The colours indicate the four frequency bands. The empty dots indication the maximum of each curve.

4.2.4 Mapping spatial noise power data

In order to explain the ambient noise powers distribution, a spatial analysis was performed as well and average noise power maps have been realized. Analysing the maps, an increase of the noise levels from the lowest to the highest frequency bands of the noise seismic are displayed for both components (Figures 53 and 54). Maps are produced using the same scale for all frequency bands.

The spatial distribution of seismic noise power shows for the lower frequency ranges (0.025 - 0.012 Hz and 0.012 - 1.2 Hz) roughly homogeneous trend along all the Italian peninsula, (except for some stations), while the higher bands a more heterogeneous trend is express (Fig. 53). From maps produced, it is possible to make considerations that are more detailed.

The noise range affected in first band (0.025-0.012 Hz) is between -166.5 dB up to -111.3 dB (Fig. 53, upper left). Especially in this frequency range several noisy stations occur: SAMA and LRP stations (Lazio), NARO station (Umbria), GATE station (Molise), CLTA station (Sicily) and some stations in Campania region. The highest levels of noise are recorded by the CPIS station (Campania). Instead, the 0.012-1.2 Hz frequency band (Fig. 53, upper right) confirmations still quite homogeneous distribution but higher noise powers (from -139 dB and within 97.5 dB). For this band, new noisy sites are added: OPPE and ORZI stations (upper Po Valley), OFFI and TRTR stations close to Adriatic Sea, together Aeolian Islands stations and many Sicilian stations (located in the southern and eastern sides). The Lazio and Campania sites are still present. CPIS is the noisiest station in this frequency band as well.

Mainly thanks to these low frequencies maps it possible to observe the stations that have higher noise levels due to natural sources. The detailed observation of these maps that represent the lowers frequencies, demonstrate that the large-scale meteorological phenomena and ocean wave along the coast always occur in all national territory. This makes the distribution on the maps more homogeneous, especially in the first frequency bands. Others several natural sources occur in these frequency bands such as local wind, geological conditions and volcanic sources. Especially, at the 1 Hz boundary, natural phenomena (as well as the wind or geological conditions) and cultural noise may be overlaps and in some cases could make each source recognition difficult.

Nevertheless, from these frequencies (>1 Hz) main noise source is related mainly to cultural sources. In fact, from 1.2 Hz, new noisy sites added in the map (Fig. 53, lower left panel) such as some stations located in the north central Italy. Besides, even noisier are the sites of Aeolian Islands, eastern sector of Sicily and Lazio and Campania are confirmed again. The highest values reach up to 69.8 dB for the 1.2-10 Hz frequency band.

Increasing the frequencies range (10-30 Hz), high noise levels are recorded more visibly throughout the country (Fig 53, lower right panel), and they are related to cultural sources almost exclusively.

Especially, in the high frequencies field, more noisy stations in northern Italy are observed: these stations are located in are extremely urbanized and industrialized areas. In addition, the stations near Rome and Naples cities have reasonably the highest noise levels because are strongly densely populated areas.

The same holds the horizontal component that exhibits similar maps: minimum differences characterize the four frequency bands of the horizontal component maintaining more or less the same trends of the vertical component (Fig. 54).

Standard deviation maps of both components are also shown to demonstrate the dispersion present for each frequency band (Figures 55 and 56). As already shown in the kernel curves, we noted a greater variability for the first frequency band (especially for Z component). More stations have higher standard deviations for low frequencies while the others bands show lower variability (except for a few stations).

Finally, distribution maps correlate the studied noise level of each station to the main source that characterizes it.

Besides, as already mentioned, the kernel curves relative to the 0.025-0.012 Hz and 0.012 – 1.2 Hz frequency bands have higher probability of density cause the large-scale phenomena. Instead, in the others two higher frequency bands (1.2-10 Hz and 10-30 Hz), phenomena are more local and for this a greater dispersion was shown.

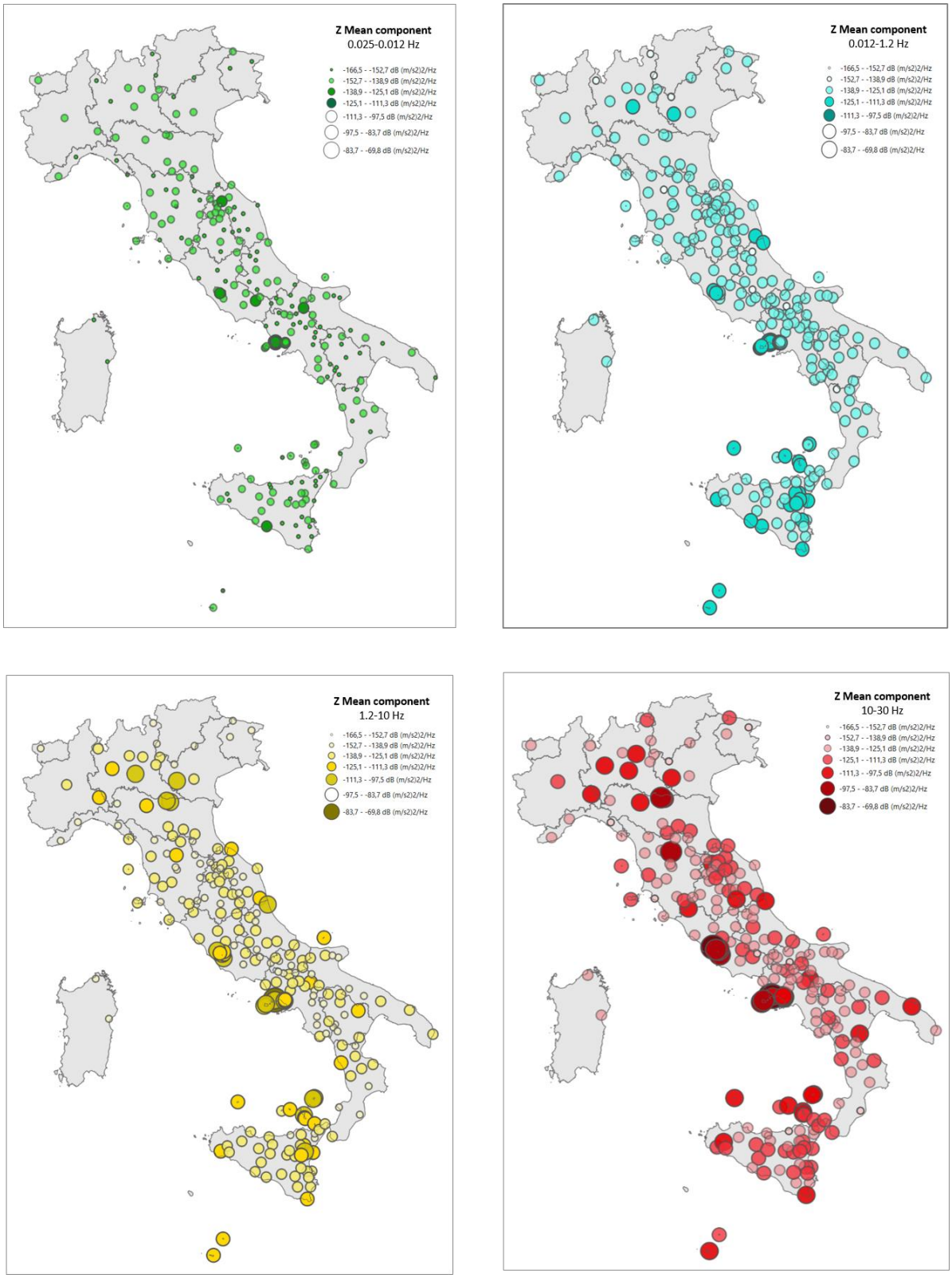

Figure 53: Spatial noise power distribution of vertical component for the frequency ranges analysed. Each map represents a several frequency that is indicated into the box. Each frequency band is divided into seven subclasses each of which is indicated with a circle of different sizes. Empty circles represent lacking frequency ranges.

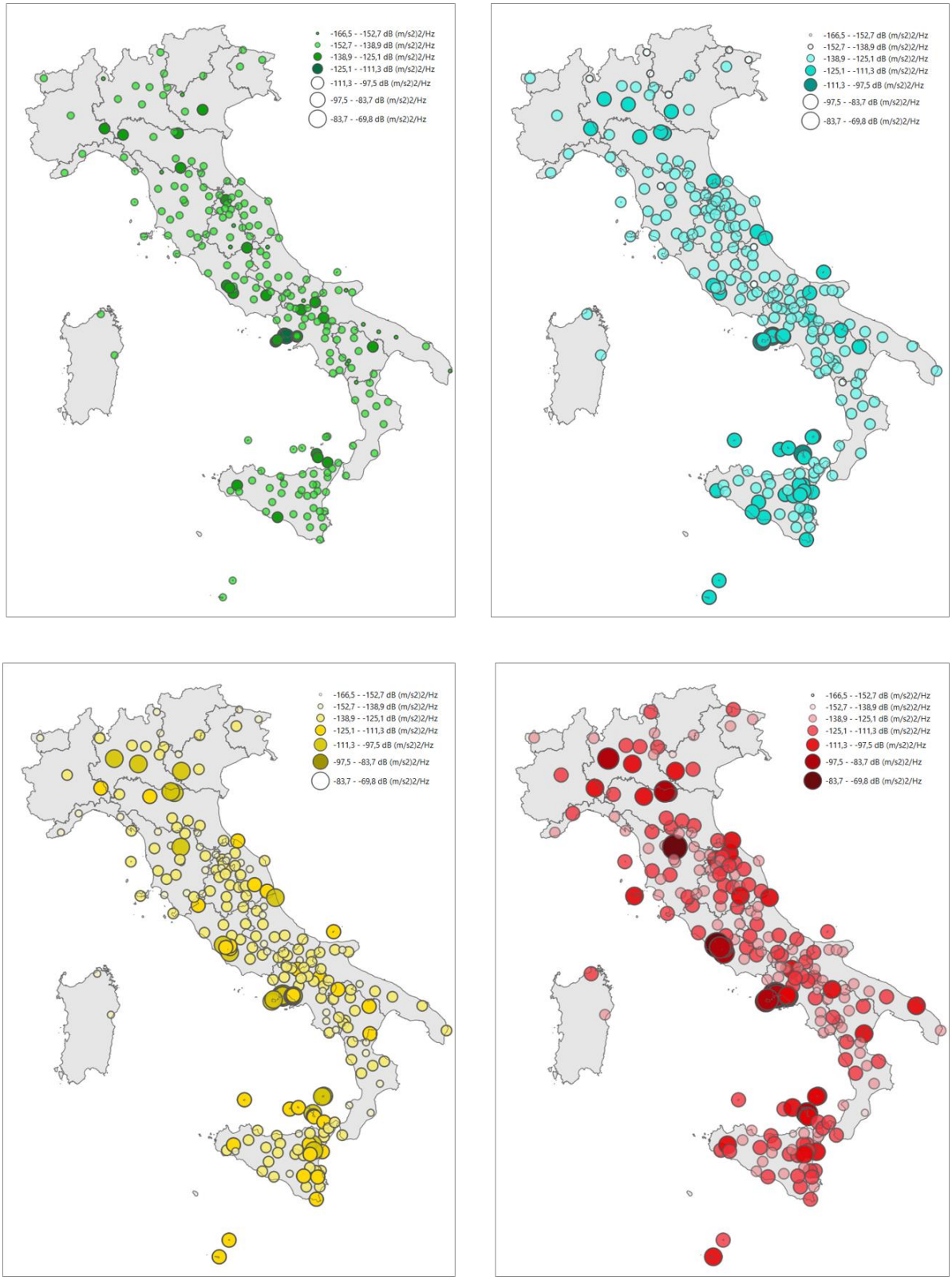

Figure 54: Spatial noise power distribution of horizontal component for the frequency ranges analysed. Each map represents a several frequency that is indicated into the box. Each frequency band is divided into seven subclasses each of which is indicated with a circle of different sizes. Empty circles represent lacking frequency ranges.

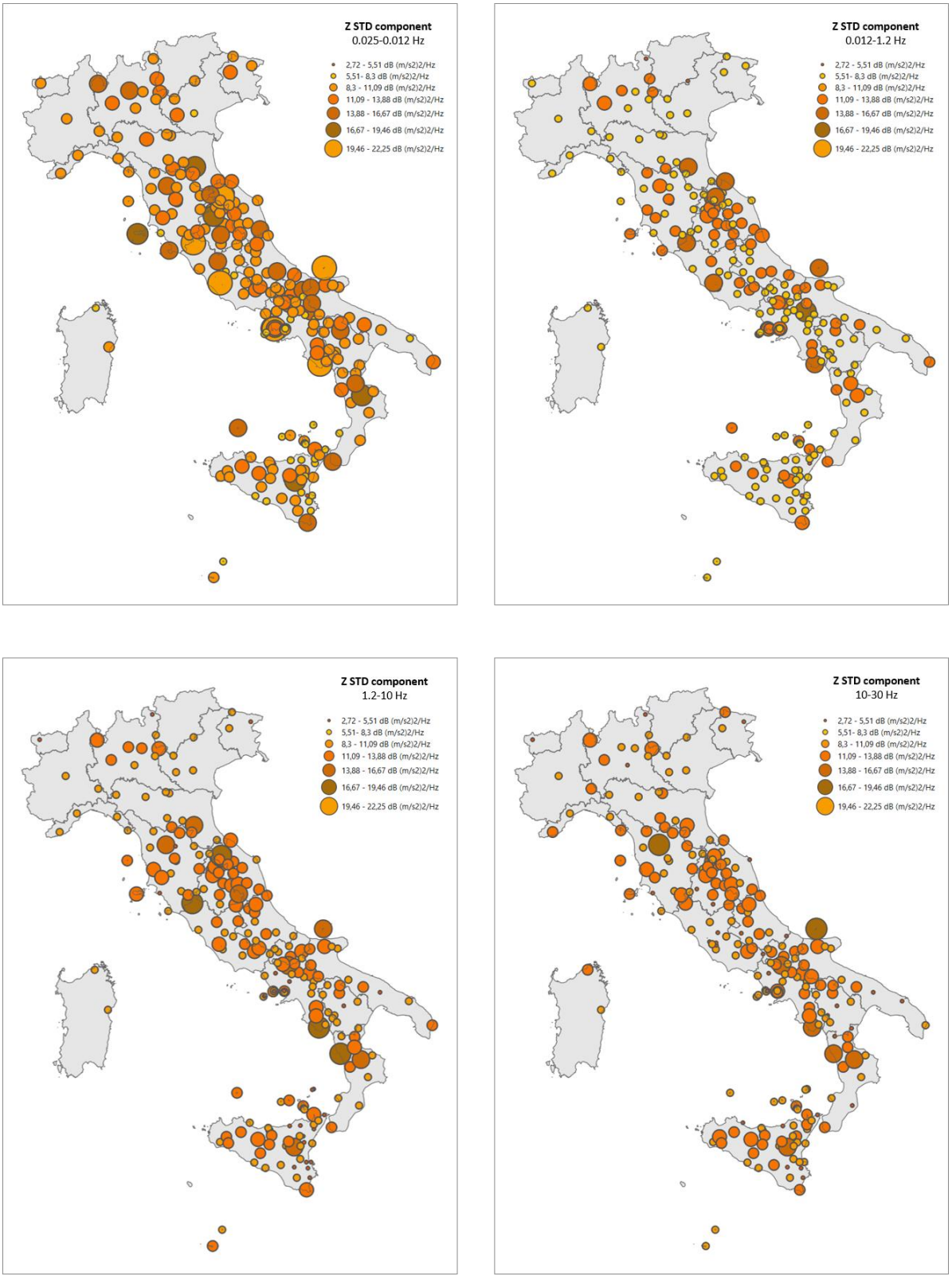

Figure 55: Spatial distribution of standard deviations of vertical component for the frequency ranges analysed. Each map represents a several frequency that is indicated into the box. Each frequency band is divided into seven subclasses each of which is indicated with a circle of different sizes. Empty circles represent lacking frequency ranges.

Figure 56: Spatial distribution of standard deviations of vertical component for the frequency ranges analysed. Each map represents a several frequency that is indicated into the box. Each frequency band is divided into seven subclasses each of which is indicated with a circle of different sizes. Empty circles represent lacking frequency ranges.

4.2.5 Interpolation analysis of spatial noise power distribution

The spatial data structure provide important information about the factors or processes influencing the observed concentration of the elements and interpolation techniques allow building maps with interpolated points. Spatial analysis is the process of manipulating spatial information to extract new information from the original data. Therefore, the data in possession of seismic noise in Italy can be calculated using interpolation.

In previous maps, it was possible to observe the distribution of noise levels at each station, while here; entire interpolation maps are discussed using points with known values to estimate values at other unknown points.

The colour scale indicates the variation of seismic noise from less noisy areas (blue) to highest noise levels (red) and the frequency ranges chosen by the same algorithm have been left.

What already has been observed in previous maps is better here delineated: a greater homogeneity for the low frequency bands and a greater heterogeneity for the higher frequency bands. In particular, observing the first frequency band of the vertical component, (Fig. 57, upper left) it is possible to highlight a homogeneous trend throughout the country while the least noisy stations (blue points) and the noisiest stations (red points) are highlighted. In all intermediate ranges (green-yellow areas) fall spaces with noise mediated by the IDW method. For instance, in this first band, among the noisiest sites, it is evident, as well as the area of Rome and the area near Naples, the site in Sicily near the CLTA station has been noted.

In the second frequency band (Fig. 57, upper right) changes slightly except for Sicily, which appears much noisier on the eastern and southern side.

Above all, it is for intermediate and high frequencies (Fig. 57, lower left and right) that a clear distinction between the least noisy and noisier stations is notable and noise levels are more pronounced.

As already deduced from the noise distribution maps, it is important to better notice that in north central Italy stations and stations located near the towns of Rome and Naples are the noisiest sites at high frequencies. In addition, also FIR station (located inside a building in Florence) shows high values for the 10-30 Hz frequency range. For the 1.2-10 Hz frequency band the Etna volcano presents its own noise. All minor islands are involved in the low and intermediate frequency bands: they show significant values especially in the 0.012- 1.2 HZ at 1.2 -10 Hz frequency bands.

It has been observed that especially Linosa (LINA station) and Lampedusa (LPDG station) show high noise value especially in the 0.012-1.2 Hz frequency band. In the case of Aeolian Islands is also added to the volcanic component especially in the 1.2-10 Hz range.

Similar maps are also shown for the horizontal component (Fig. 58) although the frequency band

0.012-1.2 Hz has noisier values especially in the north central Italy and in stations near Rome city. Sicily is also involved in an increase in ambient noise in this frequency band more than the vertical component.

All is comparable with the case studies that have been taken into account in the section on spectral analysis.

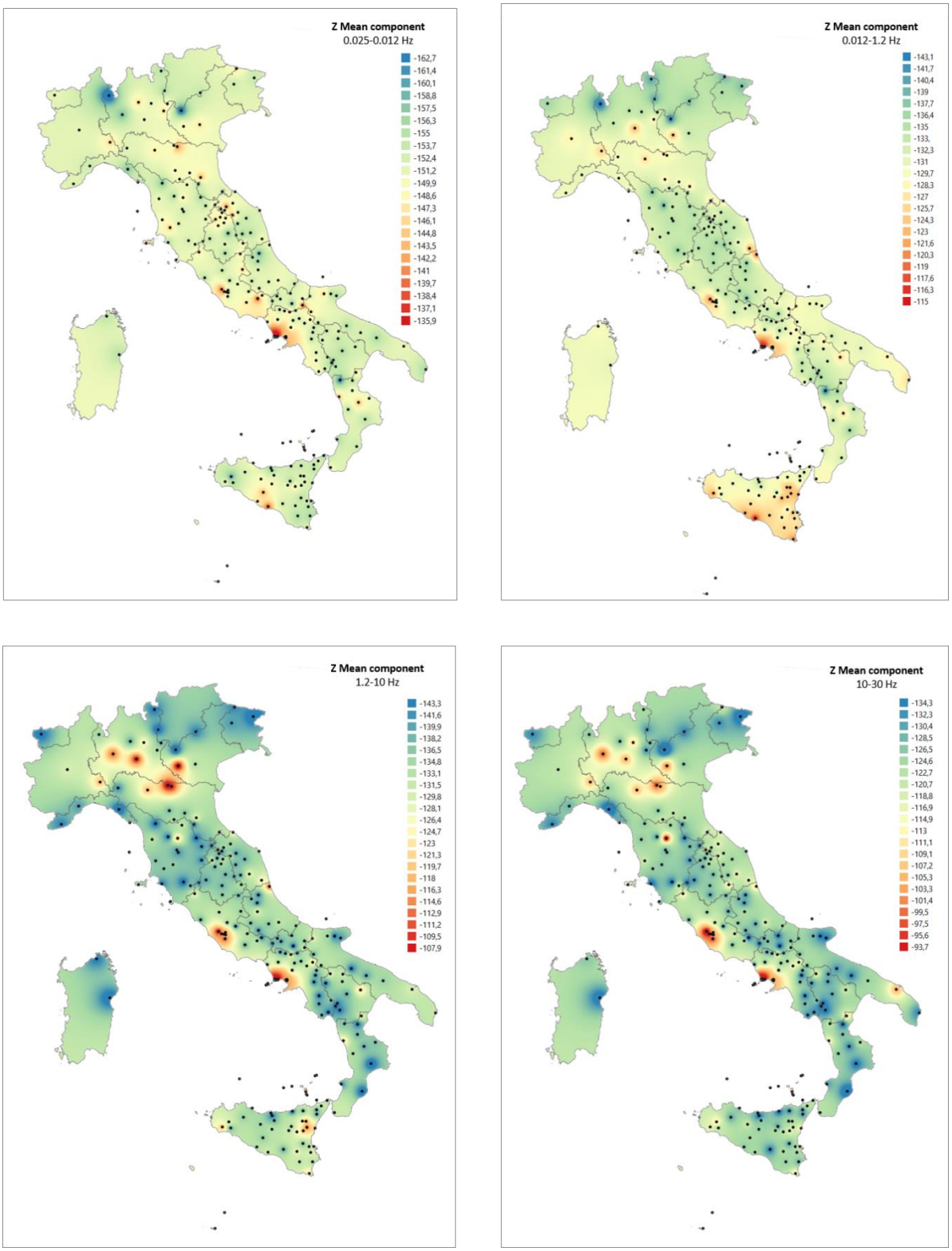

Figure 57: IDW interpolation maps for vertical component. Each map represents a different frequency band. The colour scale indicates the variation of the noise levels from lower noisy areas (blue points) to noisier ones (red points). The values of colours scale are not equal and represents the noise values for each frequency band represented.

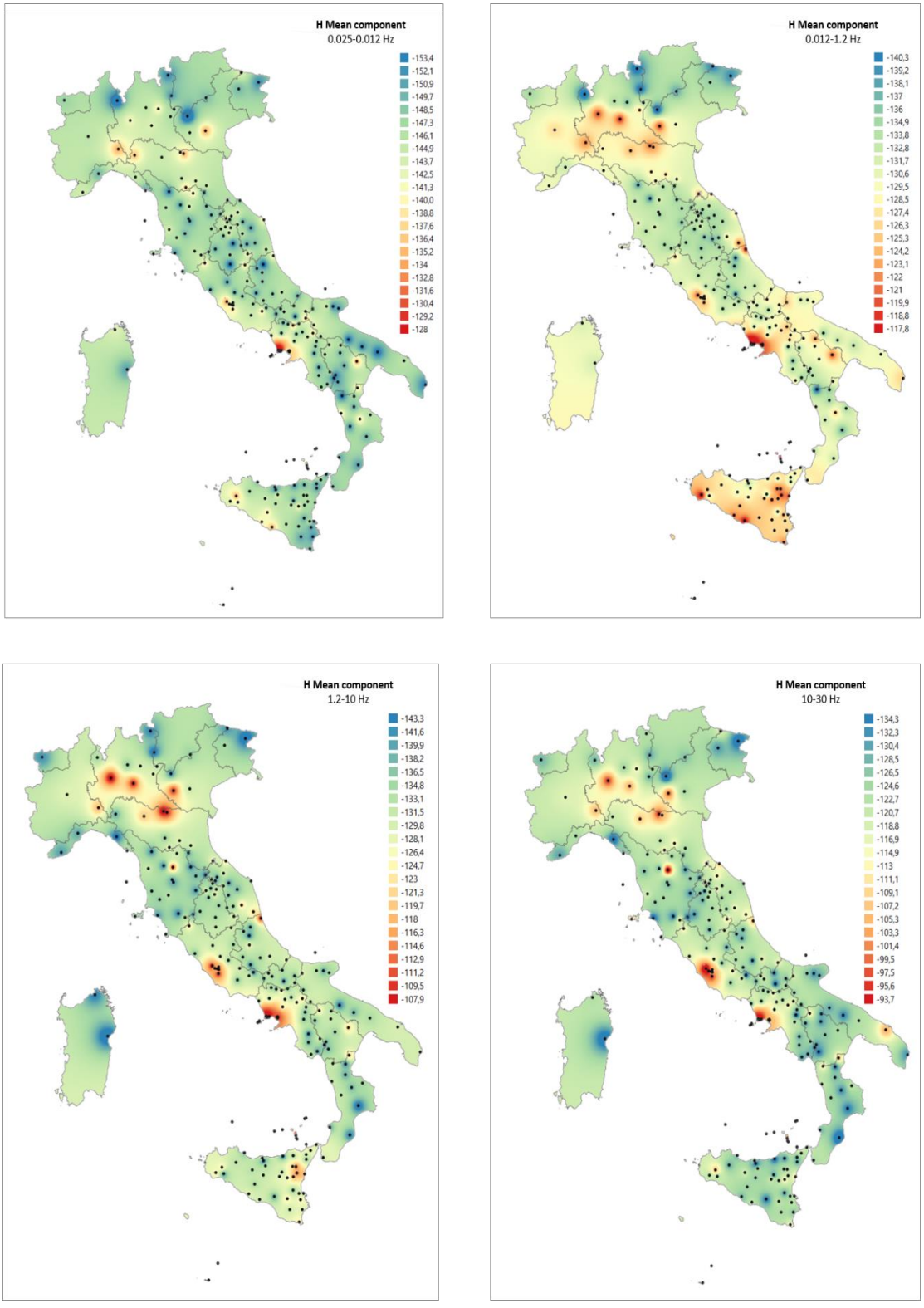

Figure 58: IDW interpolation maps for horizontal component. Each map represents a different frequency band. The colour scale indicates the variation of the noise level from lower noisy areas (blue points) to noisier ones (red points). The values of colours scale are not equal and represents the noise values for each frequency band represented.

4.2.6 Interpolation 2D filters analysis

Filters have been applied to interpolated data, to separate regional trends from local anomalies.
High and low pass filters have been applied: Low frequencies (referred to as Low) highlight regional trends in power value, while high frequencies (High) instead represent the difference (deviation) compared to the regional trend highlighting the anomalies for each individual station. Regional trends are more interesting than maps filtered with a high-pass filter reproduce local trends of lesser importance; these are used for a visual comparison and each Low map is associated to a High map. The two maps will obviously have different ranges because two different filter types are used. Regional trends show stimulating results and show in detail the hypotheses of the unfiltered interpolations maps.
At very low frequencies (0.025-0.012 Hz), a homogeneous trend is returned throughout the Italian peninsula (Fig. 59). Meteorological perturbations effects that characterize these frequencies act on a large-scale in the same way varying in the space. Only two especially anomalies are presented: the positive anomaly (blue area) represents a low noise station (VARE station) while the area with the most negative anomaly is located in Campania (CPIS station). Po Plain, Lazio, and south-western Sicily represent the other noisy sites for this band.
In the second frequency band (0.012 – 1.2 Hz) anomalies affected especially the Alps and the central Apennines areas (Fig. 60). In fact, in these areas major anomalies are found with lower noise values. Ocean waves along the coast are present in the second frequency band and these areas are farther from the coast suffering less of these phenomena. On the contrary, higher values are found along the Italian coasts, while in the area of the Po Valley the geological contribution is certainly relevant.
For the frequency band 1.2-10 Hz (Fig.61), in addition to the contribution of natural sources that can still insist on this band (example wind and volcanic and geological phenomena), also begin to overlap anthropic factors. In fact, an important negative anomaly emerges in the central-northern area of the Italian peninsula while they begin to be even more marked the area near Rome and that near Naples.
The highest frequency band (10 - 30 Hz) includes almost exclusively anthropogenic sources (Fig. 62): the regional trends highlight here the areas in northern Italy and the densely populated areas of Rome and Naples cities, i.e. the most urbanized areas with high industrialization.
Similar maps are also shown for the horizontal component.
Generally, all this corresponds to what has already been observed with spectral analysis: the areas that suffer most from higher levels of natural noise are the coastal, volcanic areas and more critical geological areas (such as sedimentary deposits, while for high frequencies are almost exclusively covered anthropic sources

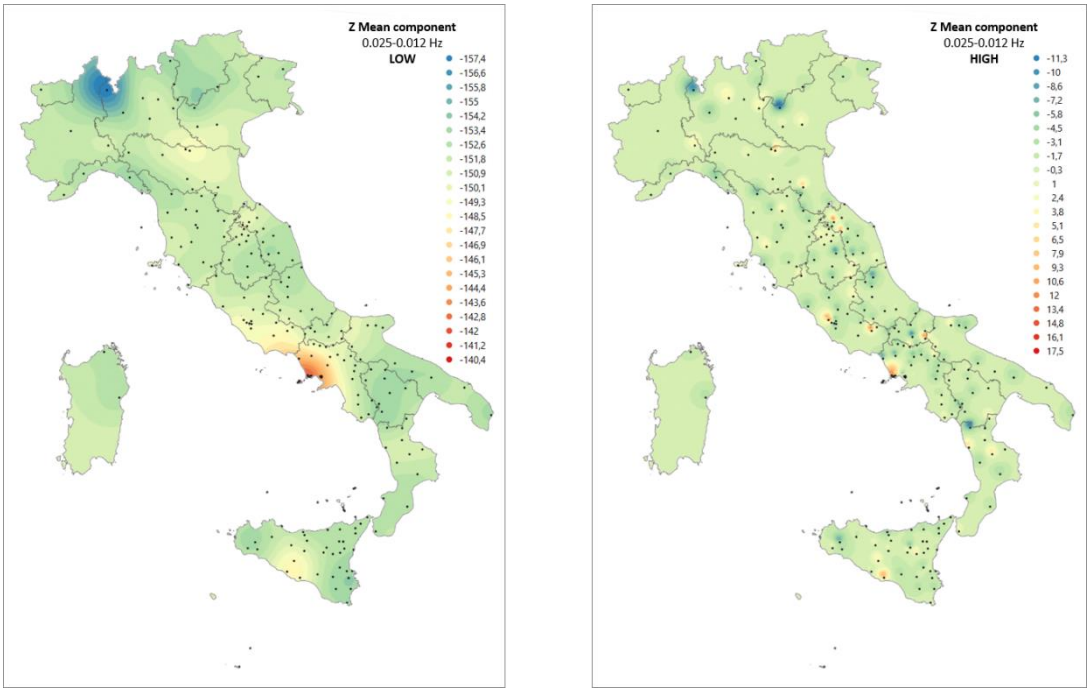

Figure 59: Interpolation filter maps (vertical component) are shown for 0.025-0.012 Hz frequency band. Low pass filter displays the regional trends (left panel) and high pass filter displays the local trends (right panel). The colour scale indicates the variation of the noise levels from lower noisy areas (blue points) to noisier ones (red points). Obviously two different scales of values are adopted for the two types of filters.

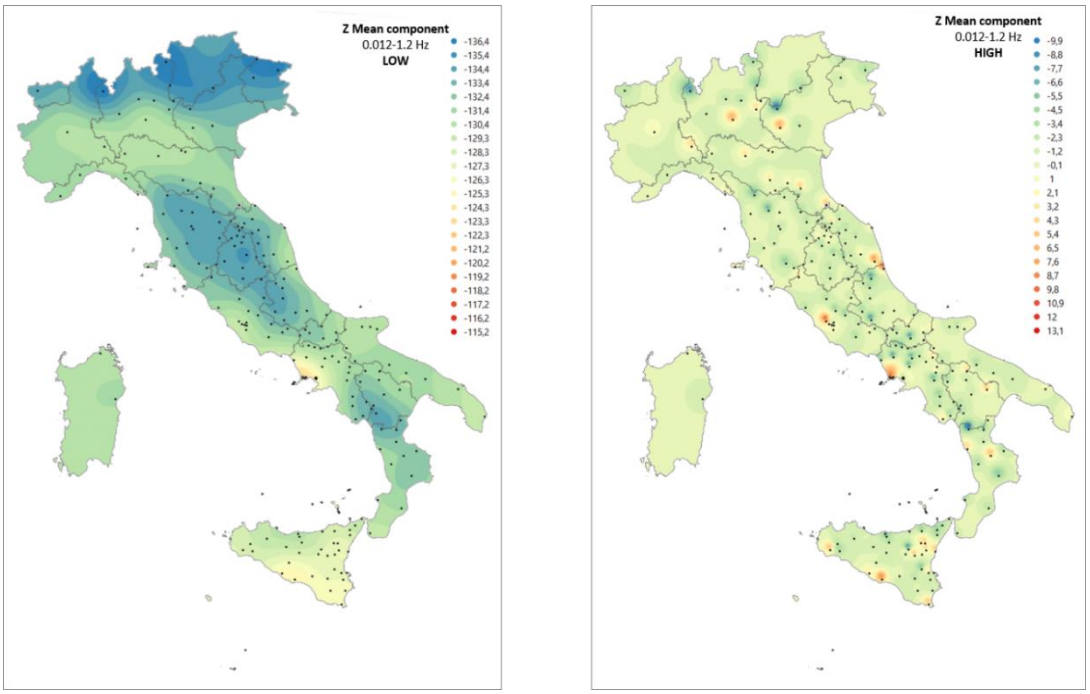

Figure 60: Interpolation filter maps (vertical component) are shown for 0.012-1.2 Hz frequency band. Low pass filter displays the regional trends (left panel) and high pass filter displays the local trends (right panel). The colour scale indicates the variation of the noise levels from lower noisy areas (blue points) to noisier ones (red points). Obviously two different scales of values are adopted for the two types of filters.

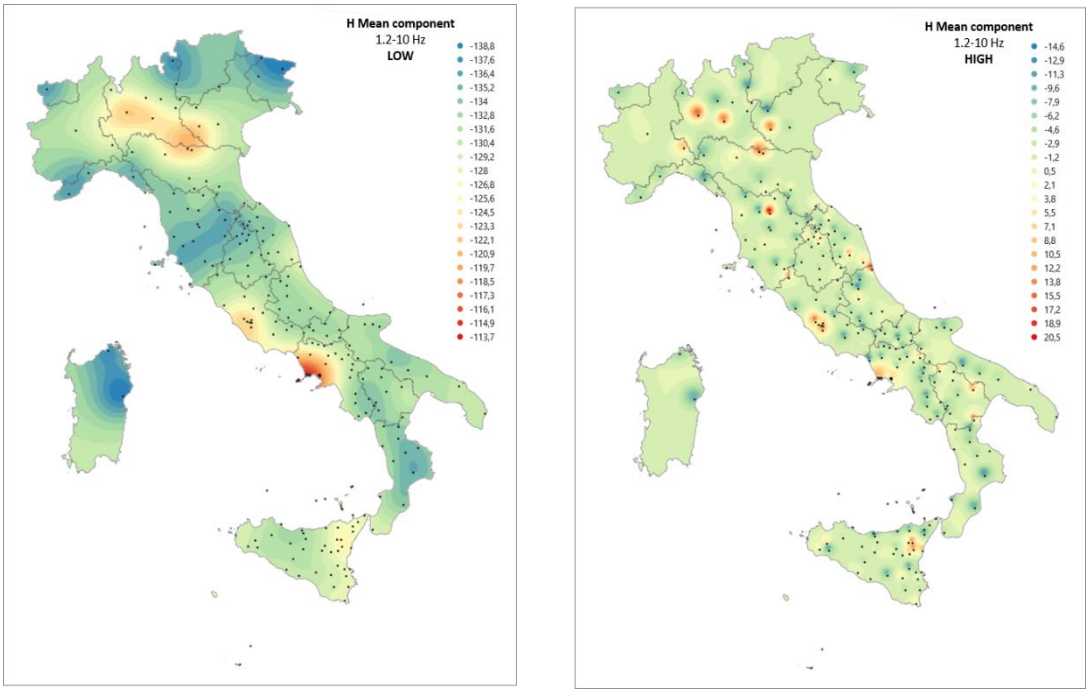

Figure 61: Interpolation filter maps (vertical component) are shown for 1.2-10 Hz frequency band. Low pass filter displays the regional trends (left panel) and high pass filter displays the local trends (right panel). The colour scale indicates the variation of the noise levels from lower noisy areas (blue points) to noisier ones (red points). Obviously two different scales of values are adopted for the two types of filters.

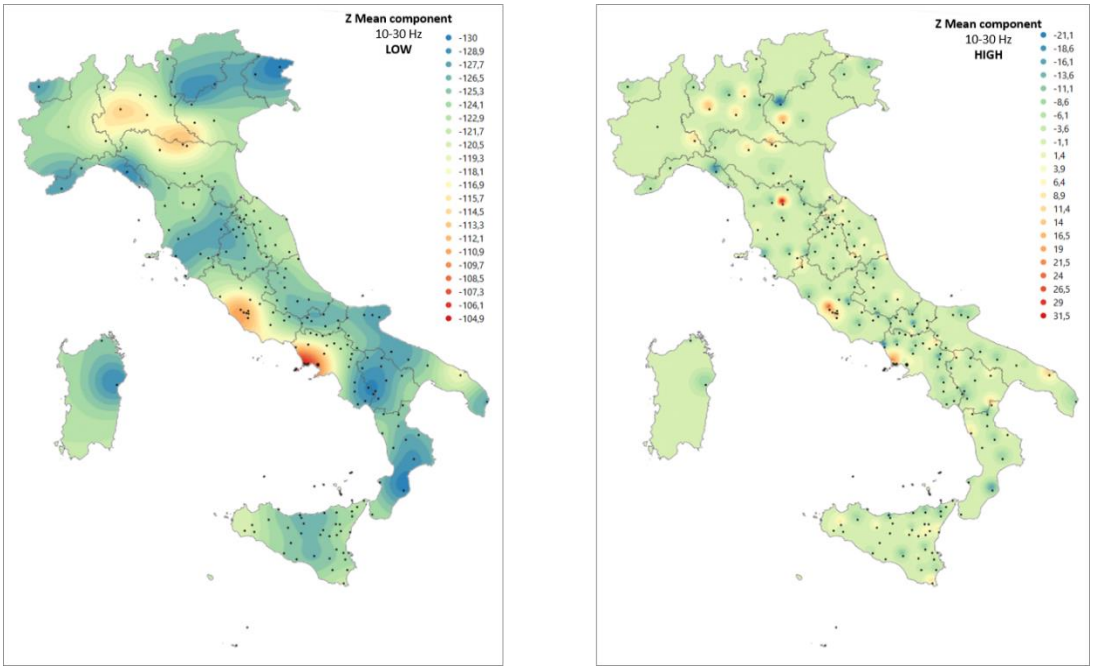

Figure 62: Interpolation filter maps (vertical component) are shown for 10-30 Hz frequency band. Low pass filter displays the regional trends (left panel) and high pass filter displays the local trends (right panel). The colour scale indicates the variation of the noise levels from lower noisy areas (blue points) to noisier ones (red points). Obviously two different scales of values are adopted for the two types of filters.

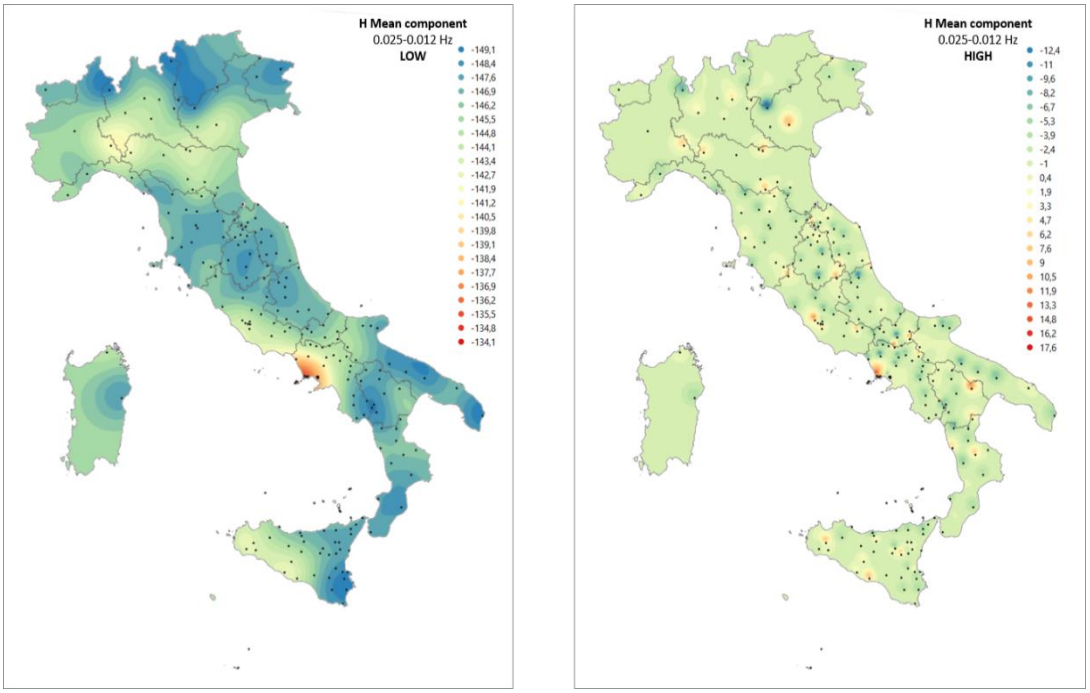

Figure 63: Interpolation filter maps (horizontal component) are shown for 0.025-0.012 Hz frequency band. Low pass filter displays the regional trends (left panel) and high pass filter displays the local trends (right panel). The colour scale indicates the variation of the noise levels from lower noisy areas (blue points) to noisier ones (red points). Obviously two different scales of values are adopted for the two types of filters.

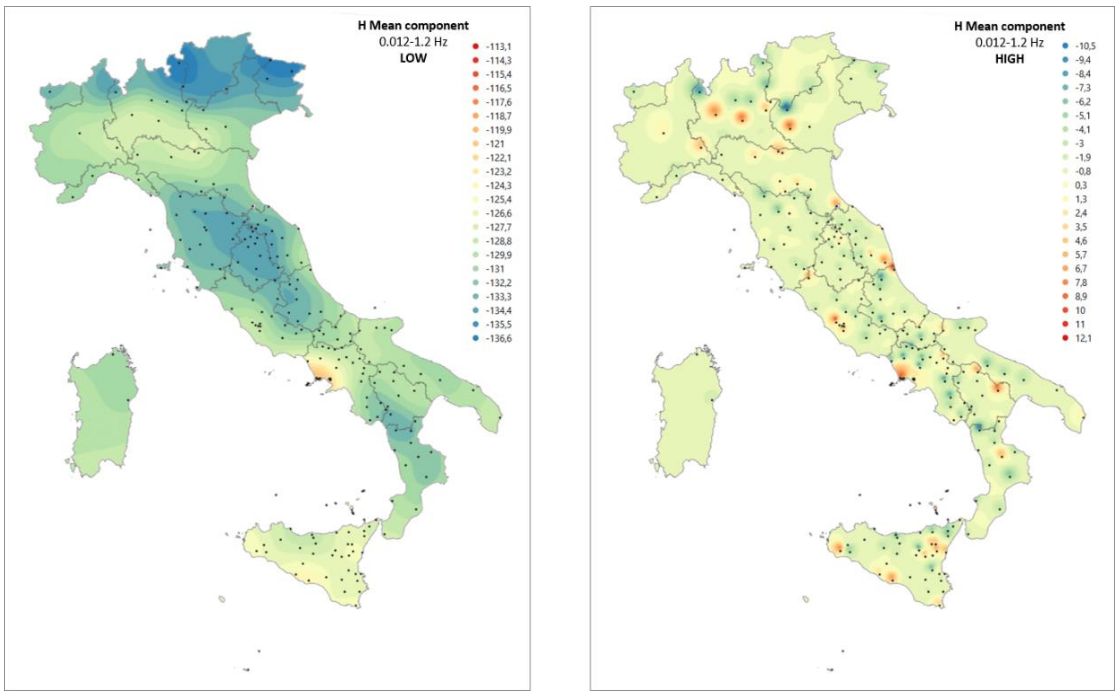

Figure 64: Interpolation filter maps (horizontal component) are shown for 0.012-1.2 Hz frequency band. Low pass filter displays the regional trends (left panel) and high pass filter displays the local trends (right panel). The colour scale indicates the variation of the noise levels from lower noisy areas (blue points) to noisier ones (red points). Obviously two different scales of values are adopted for the two types of filters.

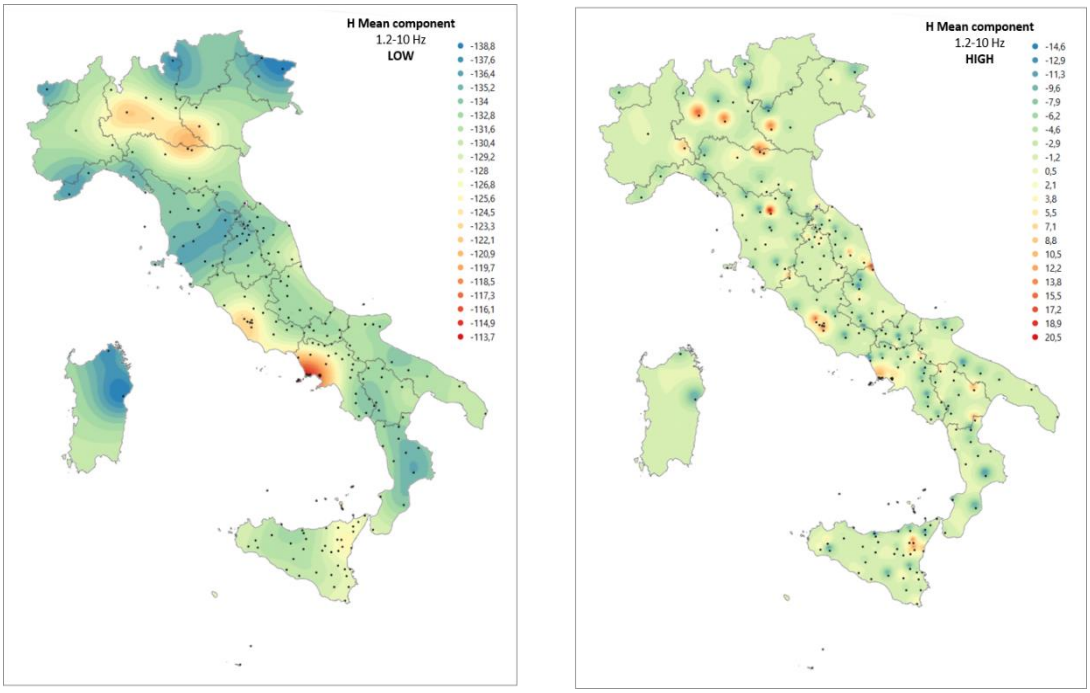

Figure 65: Interpolation filter maps (vertical component) are shown for 1.2-10 Hz frequency band. Low pass filter displays the regional trends (left panel) and high pass filter displays the local trends (right panel). The colour scale indicates the variation of the noise levels from lower noisy areas (blue points) to noisier ones (red points). Obviously two different scales of values are adopted for the two types of filters.

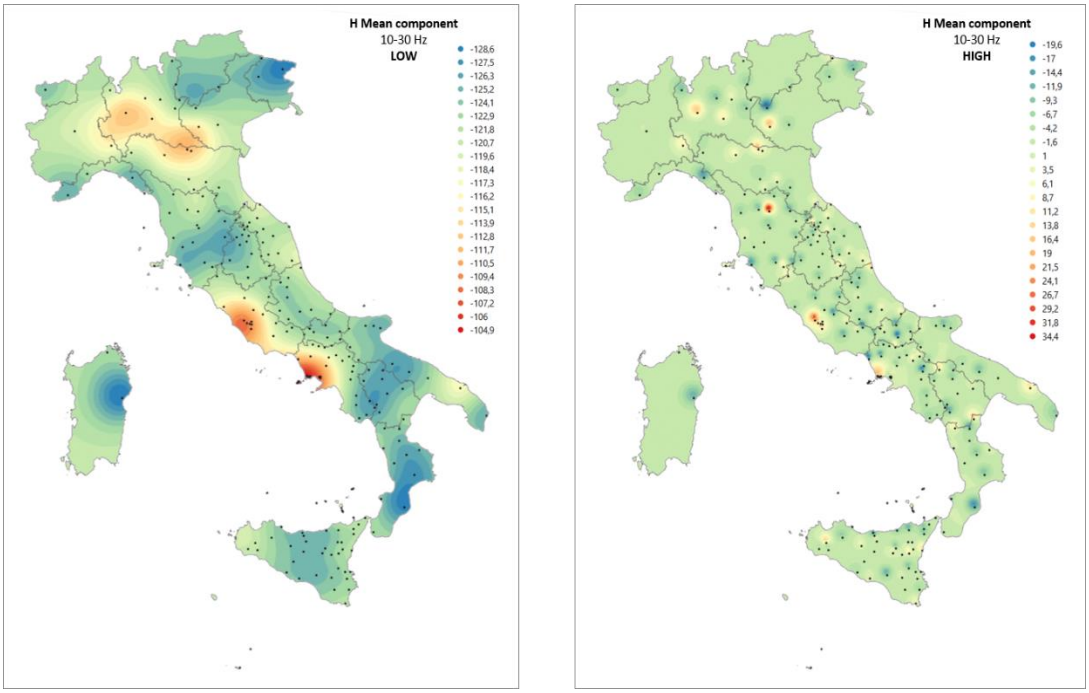

Figure 66: Interpolation filter maps (horizontal component) are shown for 10-30 Hz frequency band. Low pass filter displays the regional trends (left panel) and high pass filter displays the local trends (right panel). The colour scale indicates the variation of the noise levels from lower noisy areas (blue points) to noisier ones (red points). Obviously two different scales of values are adopted for the two types of filters.

4.2.7 H/Z Ratio distribution and effect site

Seismic noise study is a method normally used to assess the quality of recording sites and performance of stations. In addition to the style of installation of the instrument, the regional environment and local geology are known to affect local noise recorded by seismometers, particularly on the horizontal components (Murdoch et al., 2017; Tape et al., 2017).

The investigated area included throughout the Italian territory and geological factors can easily influence as natural sources.

Site response is understood in terms of different frequency distribution of energy due to amplification or attenuation properties. These effects are determined by local geological conditions (lithology, layers, thickness, morphology, etc.). As already noted in the first chapter, many studies affirm the role of geology on the different types of noise levels (Seo 1997; Marzorati and Bindi, 2006 and others).

The stations, as previous described, are located in different geographical and geomorphological contexts and for this reason, geology plays an important role on different sites. Italian territory is divided into flat and mountainous terrain: most stations are located in remote areas between hills and mountains.

In order to better observe the geological context on which the sensors are installed, the simplified geological map proposed by Bosellini has been adopted.

The outcropping formations are classified into three classes, from rock to soft soil, especially in the three categories of volcanic, metamorphic and sedimentary rocks (Fig. 67, right panel). The latter category is particularly divided into deposits ranging from the Palaeozoic to the Quaternary. It has been possible to observe that the stations are located (Fig. 67, left panel) on different surfaces and rest on sedimentary roofs while others rest on the crystalline, responding differently.

PSD ratio distribution maps of horizontal and vertical components have been extracted as shown in Figure 68. A procedure has been developed for calculating the spectral ratios taking into account the averages calculated at each station for each frequency band of the two components.

As already shown in the histograms (Fig.49) also here it can notice that the most of stations show a ratio about 1, especially values between 0.96 - 1.

In addition, some stations show values < 1 (0.84 to 0.96 values), but are not observable because are obliterated by circle with major size. Instead, for the all four frequency bands the most of stations present values between 0.96 and 1. A few stations display value > 1 (from 1 to 1.04) for the first band and up to values between 1.04 and 1.08 for the others frequency bands.

The report appears to be around 1 (especially 0.96 and 1) as evidence that almost all stations are

located on crystalline basement or discrete deposits. This demonstrates site effects (such as resonance phenomena) do not affect excessively. As described by Marzorati et al.2006, this is well known in the area of the Po Valley. In addition, as already seen in the distribution maps, important noise values are recorded in the upper Po Valley. In addition to the anthropic factor, the geological aspect plays a very important role in this area. On the other hand, crystalline basement and Mesozoic sedimentary rocks characterize the Alpine area. In these areas, they reply well and site effects are attenuated.

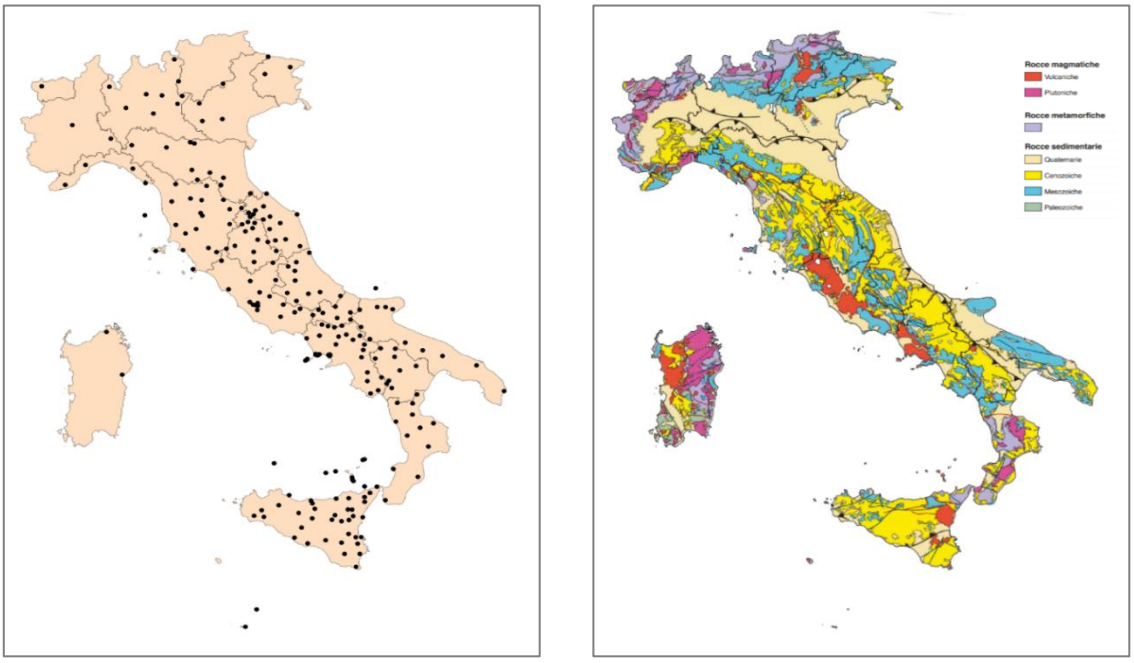

Figure 67: Spatial distribution map of the 233 seismic stations selected (left) and the simplified geological map of the Italian territory (right). The map has been given to us by courtesy by Professor Alfonso Bosellini and Zanichelli Publishing House. This image in contained in the book "Tettonica delle placche e storia geologica dell'Italia".

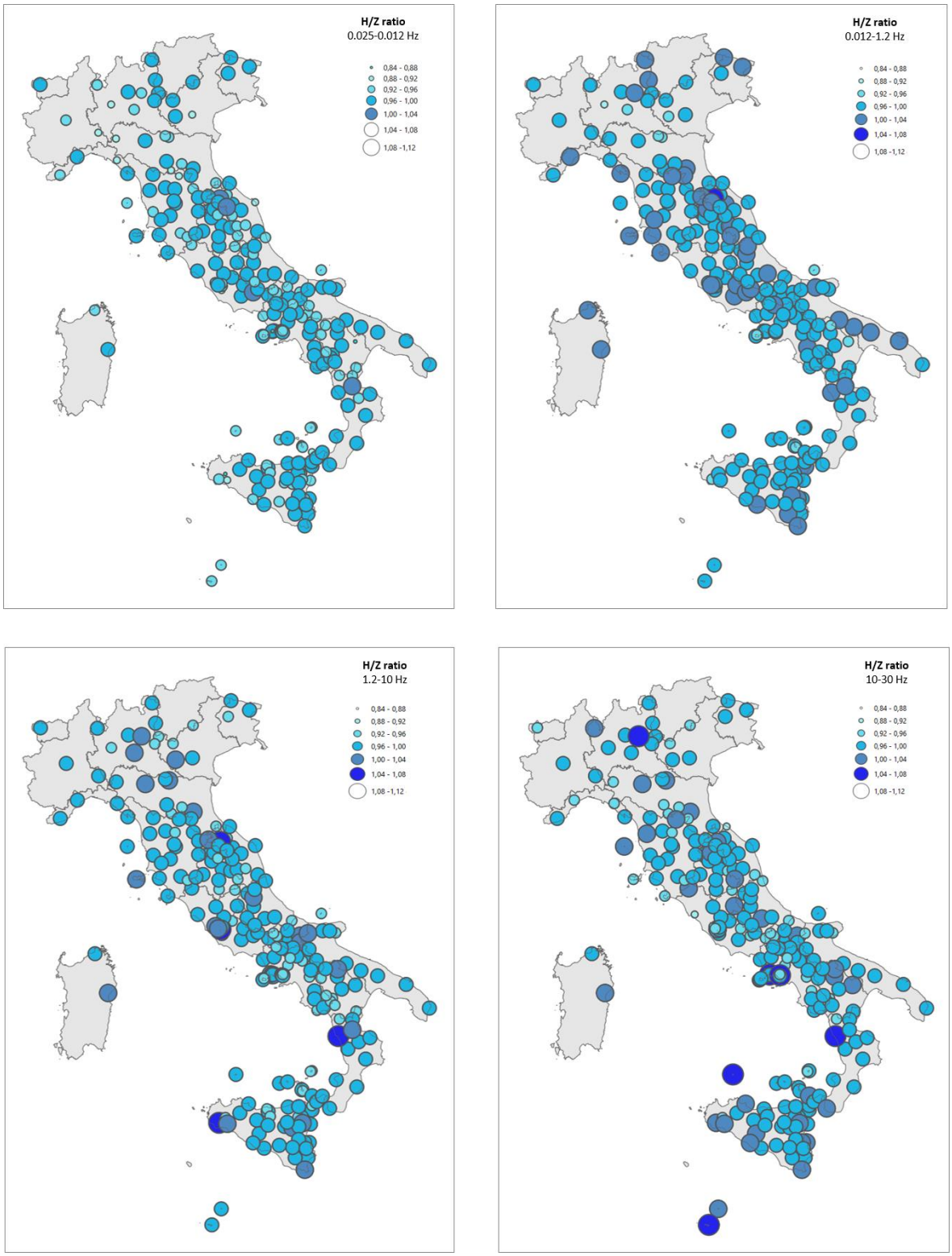

Figure 68: PSD ratio distribution maps of horizontal and vertical components are shown for the four frequency bands. Most stations have a ratio of between 0.96 and 1. Empty circles represent lacking frequency ranges.

4.2.8 Regression analysis

In this research, the regression analysis is intended to highlight any correlations between seismic noise anddifferent parameters that could affect its power. Between these parameters is selected the elevation, the distance minimal station-coast and the rainfall.
Seismic noise may vary depending on the altitude at which the station is located: usuallythe stations located on the areas furthest from the populated urban centres turn out to be lesssubject to the anthropic noise recording only the low frequencies.
The seismic noise can also be influenced by its distance from the coast and therefore be less affected by the ocean waves that can affect the sites near the sea more.
As for the rain, this can strongly affect the seismic noise, especially in areas where the rain is more abundant.
Several consideration are made about these regressions. The linear equation of degree II seems to respond better than the other degrees. To establish how strong predictive capacity, the coefficient of determination (R-squared) was used. These measurements estimate how much difference between the observed values of y in the sample and the values that the model has estimated for y.

Regression analysis: PSD – Elevation

The Italian Seismic Network stations are located at altitudes ranging from zero to 2000 meters above sea level. Most stations are distributed within 1000 meters of altitude, especially between 400 and 1000 meters a.s.l., as showed in the regression plots in Fig X. Only a few stations are above 1000 meters a.s.l.
Both vertical component (Fig. 69) and horizontal component (Fig. 70), a narrower interval confidence characterize the lower frequency bands, while the higher frequency bands exhibit higher dispersion. A negative regression with decreasing PSD values as the elevation increases was the initial hypothesis, but the results show a different trend from the expected model. For higher frequency bands, this behaviour is shown. Instead, negligible trends are observable for the 0.025-0.012 Hz and 0.012-1.2 Hz frequency ranges with an almost flats curves. In order to confirm the adequacy of the model and the statistical significance of the estimated parameters, coefficient of determination R-squared (R^2) is used for a good data prediction estimation. This displays the relationship that exists between the two variables. The best coefficient of determination R^2 is 0.40 for the 1.2-10 Hz frequency band; while the lower value recorded is 0.16 (for 0.025-0.012 Hz). The other bands show R^2 values of 0.37 (0.012-1.2 Hz) and 0.34 (10-30 Hz).
Since the coefficient of determination is a value between 0 and 1, prediction results obtained are all

medium-low values. Therefore, there is a statistically weak association between noise and altitude. Data is weak to predict a well-defined model. Especially, for the 0.025-0.012 Hz frequency band, the value is the lowest (0.16): probably the low frequencies are not much influenced by the elevation due to the sources related to large-scale meteorological phenomena. At the other frequencies there seems to be a significant reduction of ambient noise as the altitude increases within 1000 meters a.s.l. Instead, after 1000 meters a.s.l., a sensible increase is detected probably due to the atmospheric effects that occur at high altitude. This is more evident for higher frequencies, although the number of stations present at higher altitudes are few. The same behaviours are also occurred for the horizontal component, but in this case, the frequency band 0.012-1.2 Hz with a coefficient of determination of 0.35 gives the best.

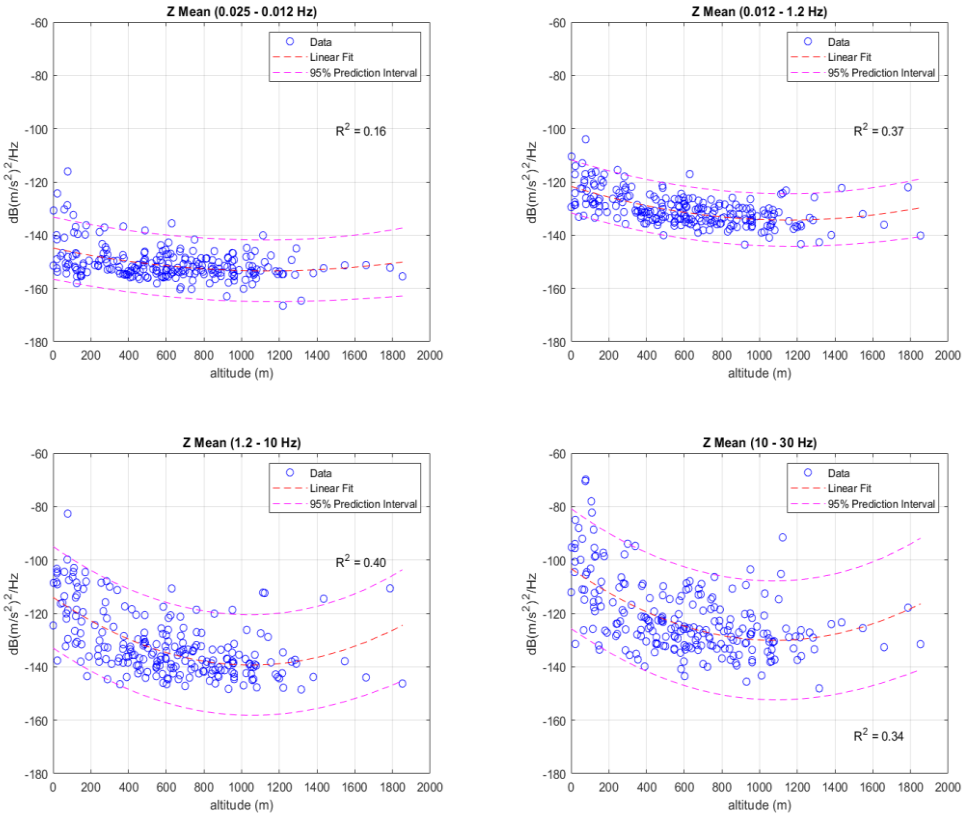

Figure 69: PSD - Elevation regressions trends (vertical component) are shown for the four frequency bands.

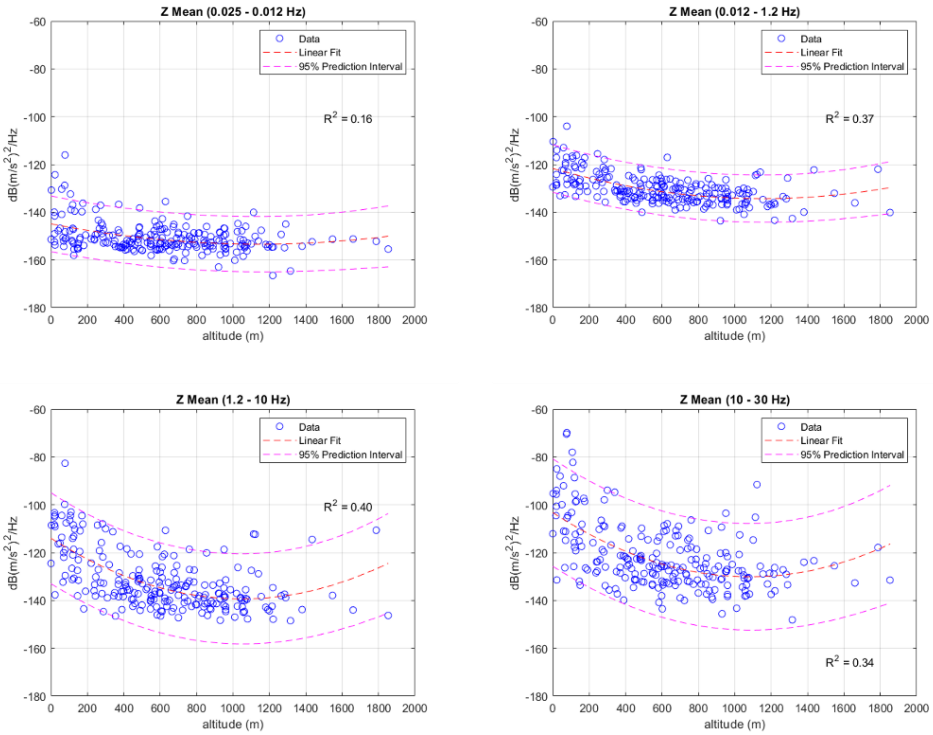

Figure 70: PSD-Elevation regressions trends (horizontal component) are shown for the four frequency bands.

Regression analysis: PSD – Minimum Distance to the coastline

The Italian Seismic Network stations are located at variable distance between 0 at 250 km to the coastline. Especially, most stations are located within 75-100 km.

As already observed in previous regressions, plots related to PSD-distance, have a narrow confidence interval at low frequencies while increases for the two highest frequency bands presenting a greater variability. For this parameter to the same bands are present similar trends (Fig.71). At low frequencies, an almost flat trend emerges to show that noise powers remain low despite increasing distance. At high frequencies (1.2-10 Hz and 10-30 Hz), a slight trend is present: it shows around 120 Km a slight increase. The coefficient of determination (R2) tends to zero values for all frequencies range, except for the second frequency band, which has a value R2 0.29. In this case, the correlation between the two variables is almost absent and a model cannot be defined. This means that the distance does not interfere on long distances, except for the frequency band 0.012-1.2 Hz where it shows a weak coefficient of determination 0.29 caused probably local sea wave effects occur in this band. Same behaviours occur for the horizontal component (Fig.72).

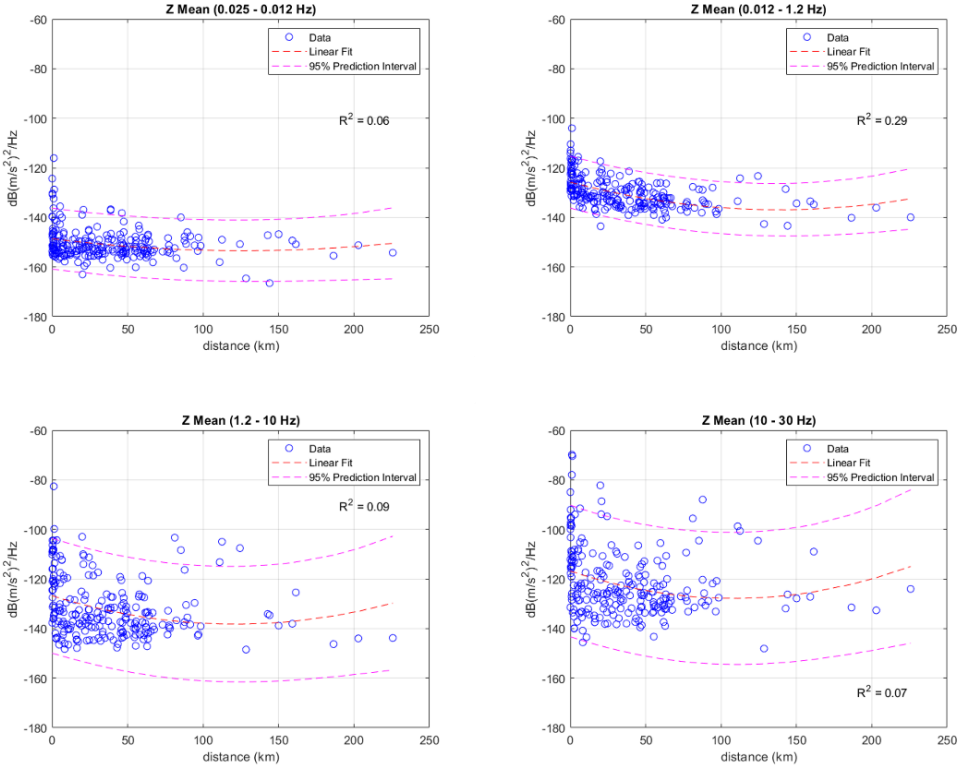

Figure 71: PSD-Distance to coasts regressions trends (vertical component) are shown for the four frequency bands.

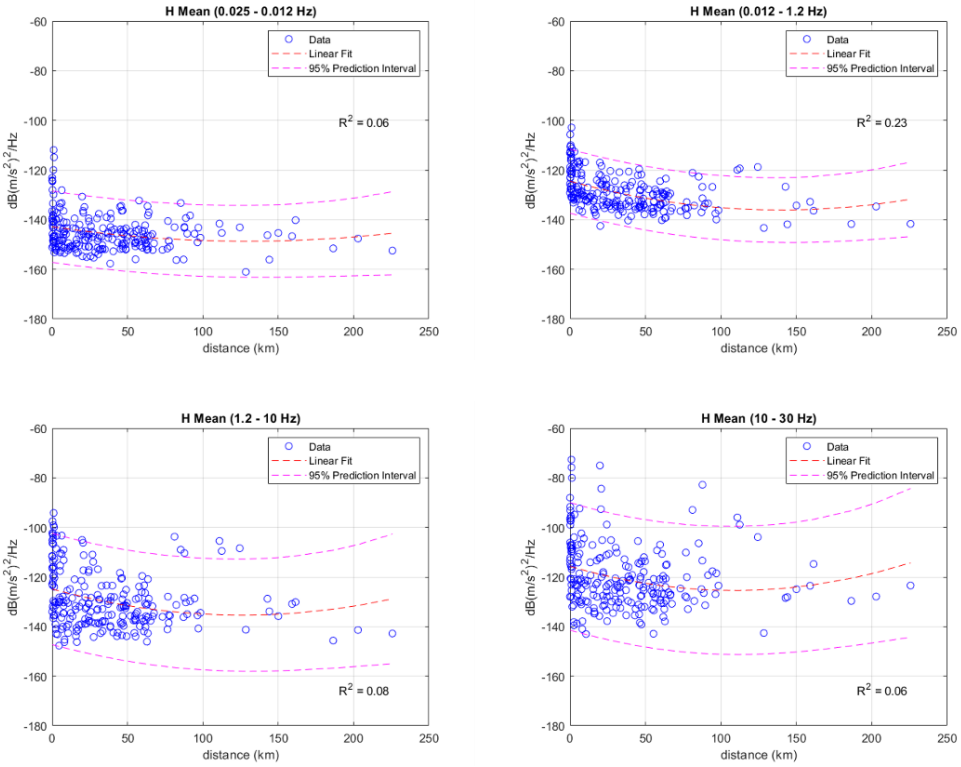

Figure 72: PSD-Distance to coasts regressions trends (horizontal component) are shown for the four frequency bands.

Regression analysis: PSD – Rainfall

It is known in literature that the local weather conditions also affect noise over 1.0 Hz frequency (Peterson 1993; Webb 1998).

For this reason, it has been suggested that a possible correlation between the power data and the rainfall could exist.

Especially, the precipitation rates (mm/y) derive from data averaged in the period 1961-2017 throughout Italy and they have been extracted from the ISPRA (Istituto Superiore per la Protezione e la Ricerca Ambientale) website. In the Figure X is shown a map what the average rainfall is in the different regions. The Seismic Network Stations (black points) are displayed on the map.

Not having available the rainfall data closest to each station, the data were obtained by median every range indicated by the ISPRA map. The database required for the analysis was thus created. The precipitation rate was not checked with the seasons. Only the data averaged based on three years in each station were taken into account.

As is well known, the rainiest areas are distributed along the mountain ranges of the Alps and the Apennines, while the most arid are some areas of Apulia, Sicily and Sardinia, and in the map, this is very evident.

In order to check whether a prediction model can be extracted between PSD and precipitation, a regression was performed. In order to analyse in detail how much the precipitation can affect the PSD would be necessary to make a further seasonal analysis but in this case, we have only been able to observe if the two parameters are dependent.

In Figure 73, it is evident that even for the rain parameter the low frequencies a lower dispersion is observed compared to the high frequencies that are instead characterized by a greater variability. In the plot (Fig. 74) is evident that even for the rain parameter the low frequencies a lower dispersion is observed compared to the high frequencies that instead are characterized by a greater variability.

For the lower frequencies of 0025-0.012 Hz and 0.012 Hz and 1.2 Hz, the stations are restricted to lower PSD values and have a narrow prediction range. Conversely, for the other two higher frequency bands, most stations have a much more varied PSD.

With regard to the coefficient of determination, little evidence of correlation is shown. In fact, the intermediate frequencies show better values (0.27 and 0.15). In the intermediate frequency bands are those where the noise determined by the rains can be recorded but anyway for all the frequency range the two parameters remain equally bound by an almost absent correlation. Have a weak correlation with seismic noise: probably a more accurate seasonal analysis could define a greater correlation. However, the time series of the noise level is not related to rare local precipitation.

In Fig. 75, the graphs related to the horizontal component are shown.

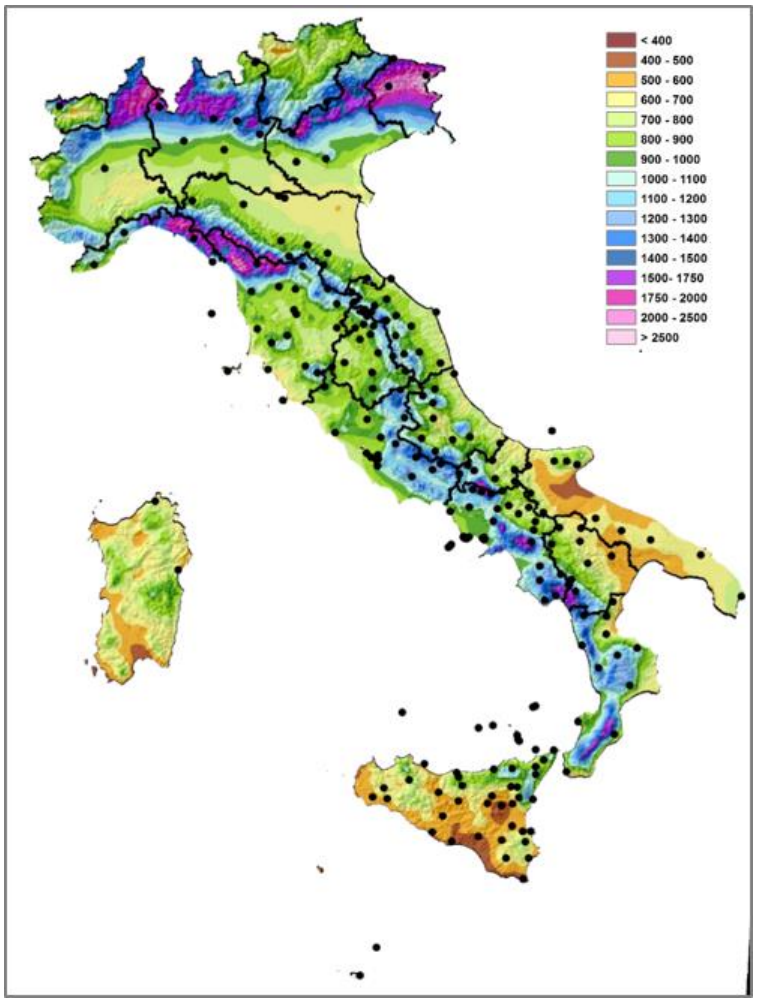

Figure 73: Distribution of the average annual precipitation height (mm) of the period 1961-2017.
Source ISPRA website (https://annuario.isprambiente.it/sys_ind/236).

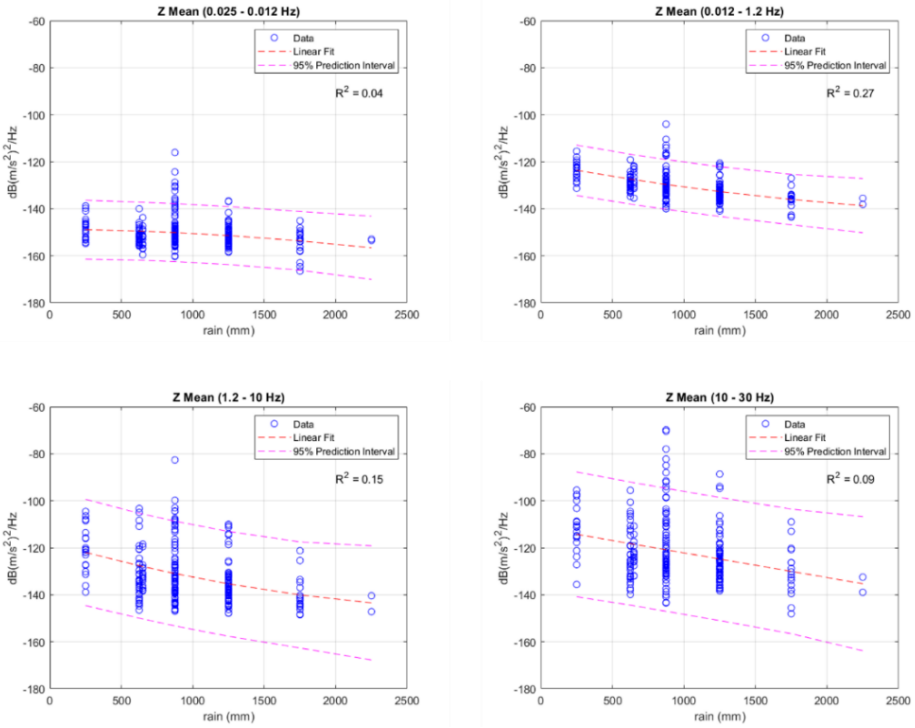

Figure 74: PSD-Rainfall regressions trends (vertical component) are shown for the four frequency bands.

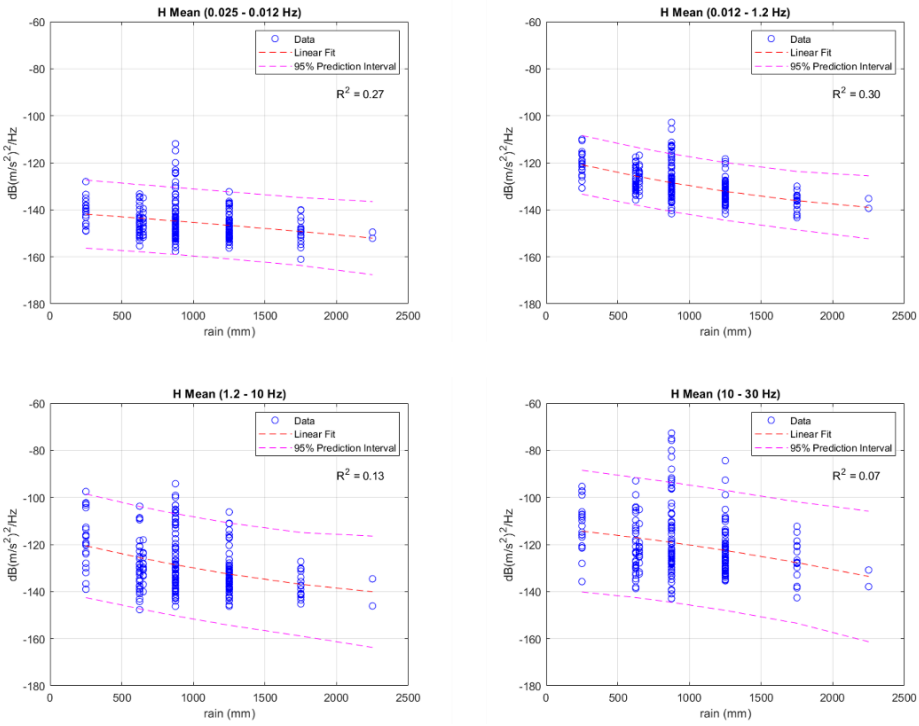

Figure 75: PSD-Rainfall regressions trends (horizontal component) are shown for the four frequency bands.

4.2.9 Regression analysis: distance - altitude analysis

A correlation model between the geographical parameters (altitude and minimum distance station-coast) has been attempted. The distribution of the stations is the same for all plots, as it represents the geographical location of each site. Different scales were used for every single frequency band. For this reason, it was not possible to extract a detailed model. As observed in Figures 76 and 77, no particular pattern is observable. This presumably depends on the high heterogeneity of the data and many variables contribute to each site. However, most of the stations are located within 1000 meters of altitude and not more than 100 km from the coastline.

For the other frequencies, for both components there is a class of six stations with higher power values located in a range of 100 km and at altitudes close to 0. These are maybe all stations located in plain areas and far from the coastline influenced by a high anthropic noise.

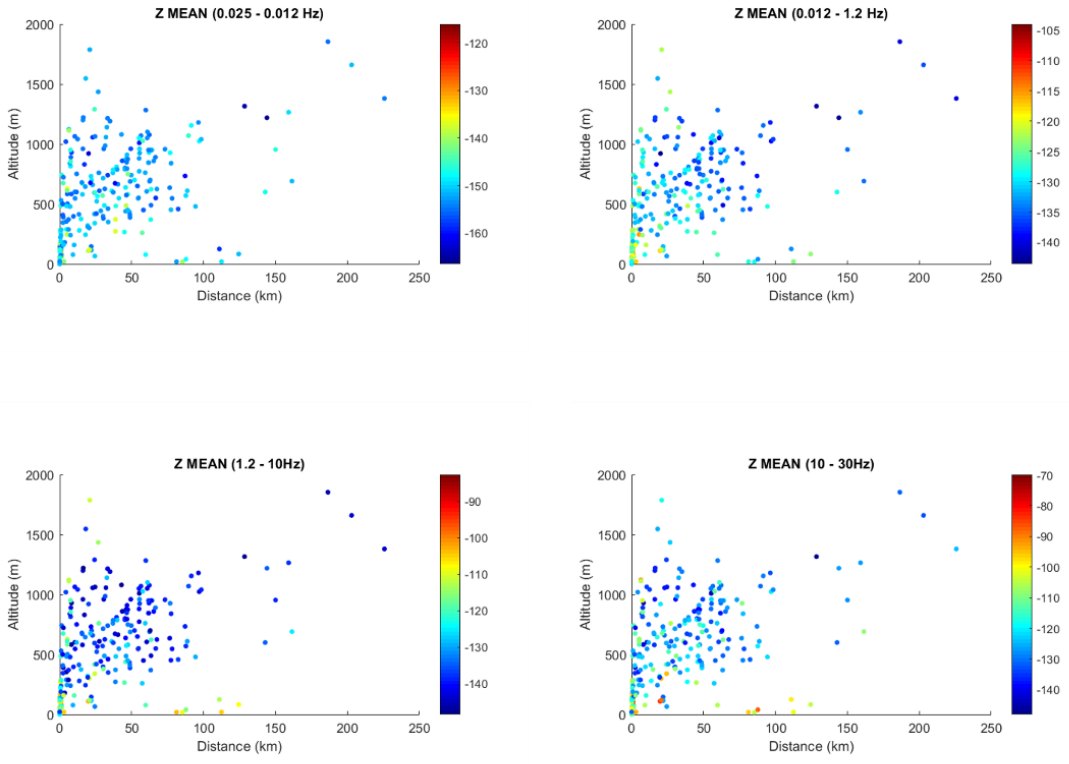

Figure 76: Elevation - distance plots for vertical component are shown. The colour scale represents the PSD in dB recorded for each frequency band.

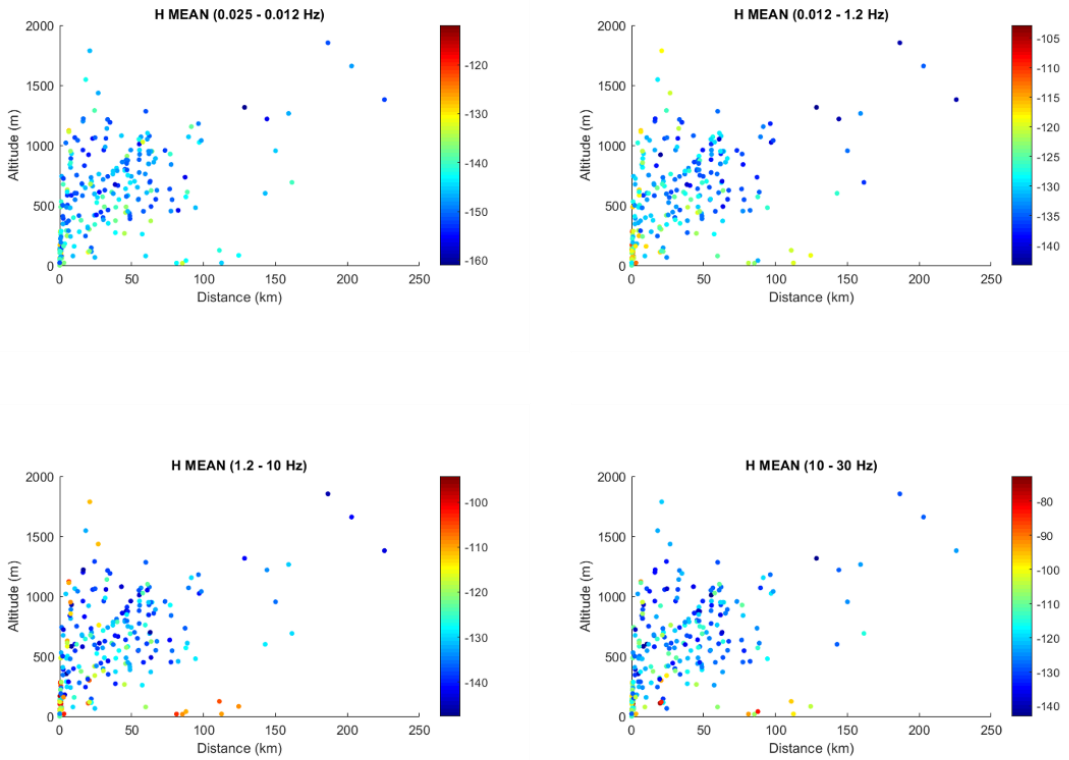

Figure 77: Elevation - distance plots for horizontal component are shown. The colour scale represents the PSD in dB recorded for each frequency band.

Chapter 5

Discussion

Nowadays almost every country in the world has its own national seismic network for earthquake detection and many stations have been equipped with broadband sensors for the detection of small seismic events and teleseisms. In recent years were also used for background seismic noise studies (Dimitrova and Nikolova, 2010; Grecu et al., 2012; Soliman, 2013; Custódio et al., 2014; Melosantos et al., 2015; Anthony et al., 2015; Guo and Aydin, 2015; Demuth et al., 2016; Jana et al., 2017).

In order to verify the background noise recorded in Italy by the Italian Seismic Network, 233 broadband stations were selected. All the stations that had anomalies have been removed and stations with clear noise reading were chosen. A three-year period was establish to have robust data.

The study of background seismic noise has been conducted through spectral analysis showing the different frequency contribution of the numerous signals that compose it.

PSD was used as an investigative tool to characterise noise spectral levels and for each station, the relative PDFs have been calculated using Peterson (1993) and McNamara & Buland (2004) approaches and results are plotted using MATLAB code.

PSDPDF for all stations have been generated producing a great catalog of seismic background noise spectra, but the spectral characterization has not been analysed and described in detail for each station.

Only some PSDPDF have been selected, where particular spectral characteristics were more significant. They are analysed and reported and the main type sources has been associated for each frequency bands according with the literature. Alpine environments have low ambient noise spectra in the all frequencies range. The low levels clearly show the microseismic peaks between 0.1 and 0.5 Hz, although generally, power in the primary and secondary microseism bands are highest at near-coastal stations and decay into the continental interior.

Microseismic peaks are clearly visible obviously along the coastline and in the islands environments, but in the selected sample stations, they appear less evident, surely for the overlap of meteorological effects that act (as the local wind). Especially in islands environments, the mains noise sources are meteomarine causes. Seismic noise in the 0,012-1.2 Hz frequency band is mainly attributable to

seawaves. As in literature, the primary (or single-frequency) and secondary (or Double Frequency - DF) microseisms are affected by the ocean waves and are recorded for frequencies < 0.1 Hz and 0.1 and 0.5 Hz respectively.

Other interesting data emerged from volcanic environments.

It is evident how volcanic areas represent the areas with greater natural noise. In particular, Etna and Stromboli show a seismic noise mainly correlated to their type of strombolian activity referring a special trend around 1 Hz correlated to probably the continuously volcanic tremor and explosion quake.

The region of Campania instead has high levels of noise for all the frequency range concerned, both for Vesuvius and especially for the Campi Flegrei. Probably its volcanic conditions represent a high source of noise (Petrosino and De Siena, 2021; Zaccarelli and Bianco, 2017), although possible meteorological and ocean swells conditions for the low frequency seismic noise can contribute. At high frequencies, high levels of noise are associated: in addition to the predominant volcanic aspect in the area, it is important to remember how the anthropic aspect is definitely imposing in the area of Naples.

Is worth noting that CPIS station located in the Pisciarelli area have continuously high noise levels throughout the all frequencies range.

Geological conditions play a fundamental role in the study of environmental noise. In fact, stations located in geologically steady areas (and possibly with a low anthropic impact) show normal noise values. While stations located in geologically less steady areas such as volcanic areas it has been found that noise levels increase even at medium-low frequencies . Another geological factor need to consider: thick sedimentary deposits may be the cause of increased noise levels. CLTA and ORZI station are considered.

These two sampling stations are located in sites characterized by thick soft sediment causing higher noise levels than bedrock. High noise levels were also documented in other studies in which the stations had same geological conditions (Seo, 1997; Marzorati et al., 2006; Grecu et al., 2012). These two stations show high noise level in the low frequencies (0.012-1.2 Hz)

Summing up the Alpine Arc record low seismic noise like a consequence of the geological characteristics and weak urbanization. Similar behaviour to occur in Sardinia but there are not enough stations for to confirm that the noise levels are very low for the same reasons. During the study of spectral analysis, the noisiest stations were evaluated: Campi Flegrei and Vesuvio sites remain the noisiest stations recorded throughout Italian territory for all frequency bands. In this region, fundamental role is given by the complex volcanic districts that characterizes the entire area.

It is worth noting like ordinary seismic natural noise exhibit considerable variations in the range 1-

15 Hz: several natural springs overlap each other depending on the context in which they occur. In fact, some natural sources can reach high levels of noise such as local wind speed can even reach 15 Hz as claimed by Young et al. (1996), or considerable volcanic process as has been remarked. Over 15 Hz we can almost certainly assume that the springs are almost exclusively anthropogenic in nature in all stations.

A total spectrum of all the 233 PSDs analysed allowed obtaining the first Italian seismic noise model. It is not noticed significant differences respect Peterson global standard baselines model (1993) to which individual station has been compared. Only low-noise threshold appear higher than NLNM reference model. It is worth noting that CPIS located in the area of Pisciarelli in the absolute the station with highest noise levels.

In addition to the total spectrum of all PSD averages, its overall PDF is also shown. This represents the statistical model of the noise of the entire Italian territory and is comparable with the model proposed by Mcnamara and Buland (2004) and Mcnamara & Boaz (2019).

A statistical analysis has helped to discriminate which is the distribution of frequencies to the different stations. A statistical analysis of four frequency bands was performed for both horizontal and vertical components. Several statistical parameters have been calculated to establish the distribution of mean values and standard deviations of PSD. Initially histograms were used but a more robust data was extracted using the Kernel technique. The kernel distribution reproduces in a more robust way the statistical data already described by the histograms. All Kernel traces smoothed show an apparent Gaussian distribution but no have a symmetrical distribution. They have a dispersion towards higher noise values, but most stations concentrate within less noisy PSD values (around -150 and -120 dB) and confirms once again how much of the noise in the Italian territory falls within the terms of a medium noise as already seen in the spectrum of the Italian model. In particular, the 0.025-0.012 Hz frequency band, in addition to being the least noisy band, for the Z component, has the highest estimated density. This means that most of the stations suffer a lot by natural sources that overlap and act on a large scale continuously over time. On the other hand, the noise sources of the major frequency bands, being more connected to anthropic sources, are more localized and present a lower probability density.

Finally, it can be stated that the average is reliable and representative of the data because most of the data fall within a standard deviation of 15 dB.

PSD data allowed as to generated distribution maps modelling. The noise power at each station in the four frequency bands has been viewed. Data distribution designates that the examined sites of the Network have more homogeneous noise values for low frequencies and more heterogeneous noise values for higher ones.

In general, these maps allowed us to identify areas of greater background noise. In fact, in accordance with D'Alessandro et al. (2010), the high noise levels are detected in the Po Valley, the Marche – Abruzzo coasts, Lazio, Aeolian Islands and Eastern Sicily, while values very low are present on almost all of the arc Alpine and on Sardinia.

Especially, the high noise of the Po Valley is probably due to the high thickness of recent sediments of the Po Basin and the presence of little sediment consolidated, with low wave propagation speed seismic, can give rise to resonance phenomena and consequently to a higher background noise (Marzorati and Bindi, 2006; D'Alessandro et al., 2010). Probably for the same reason also Marche-Abruzzo coastal area recorded a high noise levels that can be attributed to sediment recent of this area and in addition to the presence of many stations near the coast.

Instead, Lazio is affected by major noise levels even at medium-low frequencies probably connected to geothermal activity caused by residual volcanic activity passed. Instead, high density of urbanization is the cause of high background noise levels for the high frequencies.

The high noise level at the Aeolian Islands is probably a direct consequence of their geographical and geological nature and for the presence of volcano-seismic activity characterized from an intense volcanic tremor and explosion-quake, especially in Stromboli Island.

Regard as eastern Sicily sector, the seismic noise probably is due by Etnean volcano-seismic activity. Moreover, at low frequencies, especially in some southern areas of the island high noise values occurred for some geological conditions correlated thick sedimentary deposits that probably produced resonance or amplification effects. Especially this regional anomaly (for the 0.025-0.012 Hz frequency band) could be related to sedimentary deposits, in particular Neogene-Quaternary cover characterized by pre-evaporitic deposits, evaporitic and Trubi deposits and clayey deposits.

Finally, we can say that the Italian seismic noise in the first 0.025-0.012 Hz frequency band is associated to the large-scale meteomarine perturbation. In the second frequency band (0.012 – 1.2 Hz) the seismic noise is higher along the coasts (local sources) while the other natural sources are related to the volcanic districts and geological conditions for the 0.012 – 1.2 Hz and 1.2-10 Hz frequencies bands.

These results are useful to characterize the performance of the deployed broadband stations for detecting and could be relevant to choosing future locations of new stations and optimizing the distribution of local network stations.

The mean PSD values have been modelled also using IDW interpolation technique. It was possible to better observe the influence of ambient noise on the Italian territory and spatial variability. From interpolation maps, it is possible to analyse what had already been intuited with the previous maps of point distribution extracting points with known values to estimate values at other unknown points.

The result allows you to visualize how noise is distributed over the entire the Italian territory.
In addition, 2D spatial filters have been applied as well to understand on a large scale the behaviour of seismic noise in the Italian territory; it was possible to detect regional trends for each frequency band. Regional trends are very interesting and allow as contemplating the previous maps and PSD values detected. This 2D filters allowed to produce spatial Italian noise models for each frequency band.
We can therefore conclude that the spatial variability of the natural noise depend geographical features and local critical geological conditions of the Italian territory.
The Horizontal to Vertical Spectral Ratio can be used as a robust tool to determine the geological conditions of the sites where the stations are located. Values are about 1 (0.96-1 interval) indicating that the most of stations are advantaged by optimal geological conditions mainly characterized by bedrock consolidated.
Finally, regression analyses were carried out. The aim was to verify if there were particular correlations between the PSD values and the designated geographical and meteorological parameters. Regressions showed poor correlation. To ascertain this also the coefficient of determination (R^2) was considered. Although it is the best parameter to evaluate regression analyses, very low values have been found.
It is worth noting in this regard that is not possible to find a good pattern: noise is not strictly dependent on altitude or distance from the shoreline. As for the rainfall, it is not possible to establish any correlation, but it is probably necessary to plan a seasonal analysis. Finally, distance - altitude analysis have not extracted particular patterns because of the high quantity and heterogeneity of the available data on a wide territory characterized by multiple factors that make each site individual and with unique characteristics.

Chapter 6

Conclusions and Outlook

Analysing noise levels within four discrete bands that encompass different sources of natural, cultural, and instrument noise, it was broadly characterized the large-scale geographic distribution of seismic noise power in Italy.

Especially, this research is devoted to the careful analysis of background noise power recorded by the National Italian Seismic Network in the 3-yr period 2015-2017, considering it a sufficiently representative period.

Stations equipped by broadband sensors have been selected (233 sites) in order to obtain information about the properties of ambient noise in a wide frequency band between (0.025 Hz to 30 Hz). This broad range has been divided into four frequency bands that have been established roughly consistent with bibliographic information.

The study of background seismic noise has been conducted through spectral analysis showing the different frequency contributions of the numerous signals that compose it.

In fact, spectral analysis allowed getting the PSD and the relative PDF of each station characterizing the noise power in every sites and for the different four bands indicating the main sources.

A catalog of seismic background noise spectra has been obtained from spectral analysis and some cases selected have been evaluated for characterization.

In general, the PSD estimates show moderate noise levels at all stations falling within the high and low reference of Peterson (1993). The noisiest stations at low levels and high levels of noise in the sites of Vesuvius and Campi Flegrei probably reliable for the important volcanic system present. Instead, stations located at higher altitudes and far from densely populated areas seem to be less noisy. In these low-noise stations, the microseismic peaks are well evident at frequencies < 0.1 Hz (primary microseisms) and around 0.1 and 0.5 Hz (secondary peak) as in literature (Cessaro 1994; Barruol et al. 2006).

For the first time a new noise model for the Italian territory has been developed in the affected frequency range, that not exhibit significant differences respect Peterson model (1993). Especially, the minimum threshold of noise levels is therefore higher than NLNM model.

Statistical robust technique helped to discriminate the frequency distribution in stations, supporting spectral analysis.

Modelling the mean PSD values interpolation maps were extracted. These revealed the noise powers distributed over the whole territory. For medium-high frequencies (>1 Hz) overlaps of natural and cultural sources can occur while in the highest frequency (10-30 Hz) anthropogenic noise is the main source in almost all stations, especially in those densely populated and industrialized areas.

Especially, by applying 2D spatial filters, it was possible to detect regional trends for each frequency band.

Concerning the H/V ratio, good advantages are shown. In fact, the most of the resulting values are about 1 (0.96-1 interval) indicating that the most of stations are located on bedrock This means that the sites chosen for the stations enjoy good geological conditions adverse site effects (resonance and amplification effects).

Finally, statistical regressions have been attempted between PSD values and different geographical parameters. Weak correlations are observed. This means that the power of the background noise is not strongly influenced by the elevation or by the distance from the coastline. Roughly, not even the rainfall seems to show any influence on seismic noise.

Final remarks and potential improvements

Localizing and studying seismic events is the role of the Italian Seismic Network. Its efficiency and performance are mainly linked to the quality of the instrumentation and the choice of the site. This is important for detection thresholds for local earthquakes. In fact, the detection of seismic noise and the efficiency of the station are both significant. A very noisy site reduces the performance of the station and small events fail to be detected.

For this reason, optimal seismic station siting is important for reducing noise levels at short and long periods.

This research has allowed evaluating the performance of the National Seismic Network and the operating status of the sensors. Therefore, it was very important to select the stations with the highest ambient noise because allowed us to understand which sites can be improved, but others investigations will be useful. In fact, the results of this research can be a first step for new future surveys for to detect the locations of the microseism sources and for the evaluating the quality and capacity of each individual station to improve the estimation of station and network detection and location thresholds.

Bibliography

Abd el-aal, A. E. A. K. (2013). Very broadband seismic background noise analysis of permanent good vaulted seismic stations. Journal of Seismology, 17, 223-237.

Anthony, R. E., Aster, R. C., Wiens, D., Nyblade, A., Anandakrishnan, S., Huerta, A., & Rowe, C. (2014). The seismic noise environment of Antarctica. Seismological Research Letters, 86(LA-UR-14-28568).

Arai, H., Tokimatsu, K. (1998). Evaluation of local site effects based on microtremor H/V spectra. Proceeding of the Second International Symposium on the Effects of Surface Geology on Seismic Motion. Yokohama, Japan, pp. 673–680.

Arai, H., Tokimatsu, K. (2000). Effects of Rayleigh and love waves on microtremor H/V spectra. Proceedings of the 12th World Conference on Earthquake Engineering. Auckland, New Zealand.

Aki, K. (1957). Space and time spectra of stationary stochastic waves, with special reference to microtremors. Bulletin of the Earthquake Research Institute, 35, 415-456.

Aki, K. (1965). A note on the use of microseisms in determining the shallow structures of the earth's crust. Geophysics 30 (4), 665–666.

Ardhuin, F., Stutzmann, E., Schimmel, M. & Mangeney, A. (2011). Ocean wave sources of seismic noise, J. geophys. Res., 116, C09004, doi: 10.1029/2008JC005215.

Armstrong JS, Collopy F. (1992). Error measures for generalizing about forecasting methods:empirical comparisons. International Journal of Forecasting 08:69–80.

Asten, M.W., and Henstridge, J.D. (1984). Array estimators and use of microseisms for reconnaissance of sedimentary basins, Geophysics, 49, pp. 1828-1837.

Asten, M.W. (1978). Geological control of the three-component spectra of rayleigh-wave microseisms, Bull. Seism. Soc. Am., 68, pp. 1623-1636.

Banerji, S. K. (1924). Microseisms associated with the incidence of the south-west monsoon, Nature, 114-2868, 576.

Banerji, S.K. (1925). Microseisms and the Indian monsoon. Nature 116 (2928), 866.

Barruol, G., Reymond, D., Fontaine, F.R., Hyvernaud, O., Maurer, V. & Maamaatuaiahutapu, K. (2006). Characterizing swells in the southern Pacific from seismic and infrasonic noise analyses, Geophys. J. Int., 164, 516–542.

Barstow, N., G. H. Sutton, and J. A. Carter. (1989). Particle motion and pressure relationships of ocean bottom noise at 3900 m depth: 0.003 to 5 Hz, Geophys. Res. Let. 16, 1185-1188.

Berger, J., Davis, P. (2004). Ambient earth noise: a survey of the global seismographic network. Journal of Geophysical Research 109 (B11307)

Bernard, P. (1941). Sur certaines proprietes de la boule etudiees a l'aide des enregistrements seismographiques, Bull. Inst. Ocean 800, 1-19. ogr. Monaco

Bernard, P. (1941a). Etude sur l'agitation microséismique. PressesUniversitaires de France.

Bernard, P. (1941b). Etude sur l'agitation microséismique et ses variations. Annales de l'Institut de Physique du Globe de Paris 19, 77.

Bertelli, T. (1872). Osservazioni sui piccoli movimenti dei pendoli in relazione ad alcuni fenomeni meteorologiche. Bullettino Meteorologico dell'Osservatorio dell Collegio Romano, Roma, Italy, vol. 101.

Burrough, P.A. and McDonnell, R.A. (1998). Principles of Geographical Information Systems. Oxford University Press, Oxford, 333 pp.

Brown, S. H. (2009). Multiple linear regression analysis: a matrix approach with MATLAB. Alabama Journal of Mathematics, 34, 1-3.

Bianco, F., Castellano, M., Cogliano, R., Cusano, P., Del Pezzo, E., Di Vito, M. A., ... & Rovelli, A. (2010). Caratterizzazione del noise sismico nell'area vulcanica dei Campi Flegrei: l'esperimento" UNREST". Quaderni di Geofisica.

Bonnefoy-Claudet, S. (2004). Nature du bruit de fond sismique: Implications pour les études des effets de site. Ph.D. thesis, University Joseph Fourier, Grenoble, France.

Bonnefoy-Claudet, S., Cotton, F., & Bard, P. Y. (2006). The nature of noise wavefield and its applications for site effects studies: A literature review. Earth-Science Reviews, 79(3-4), 205-227.

Bonnefoy-Claudet, S., Cornou, C., Bard, P.-Y., Cotton, F., Moczo, P., Kristek, J. and Fäh, D. (2006). H/V ratio: a tool for site effects evaluation. Results from 1D noise simulations. Geophysical Journal International.doi:10.1111/j.1365-246X.2006.03154.x. (o 167.2 (2006):827-837).

Bonnefoy-Claudet, S., Cornou, C., Bard, P.-Y.and Cotton, F., (2004). Nature of noise wavefield. SESAME report, D13.08 (http:// sesame-fp5.obs.ujf-grenoble.fr).

Bormann, P. (2002). NMSOP – New Manual of Seismological Observatory Practice. IASPEI, GeoForschungsZentrum Potsdam, Germany.

Bormann, P., & Wielandt, E. (2002). Seismic signals and noise. New manual of seismological observatory practice, 2, 1-62

Bradner, H. and J. G. Dodds (1964). Comparative seismic noise on the ocean bottom and on land, J. Geophys. Res. 69, 4339-4348.

Cannata, A., Cannavò, F., Montalto, P., Ercoli, M., Mancinelli, P., Pauselli, C., & Leto, G. (2017). Monitoring crustal changes at volcanoes by seismic noise interferometry: Mt. Etna case of study. Journal of Volcanology and Geothermal Research, 337, 165-174.

Capon J. (1969). High-resolution frequency-wavenumber spectrum analysis. IEEE. 57 1408- 1419.

Capon J., R. J. Greenfield and R. J. Kolker. (1967). Multidimensional maximun-likehood processing of a large-aperture seismic array. IEEE 192-211.

Cessaro, R. K. (1994). Sources of primary and secondary microseisms. Bull. Seism. Soc. Am., 84, 1, 142-148.

Chicco, D., Warrens, M. J., & Jurman, G. (2021). The coefficient of determination R-squared is more informative than SMAPE, MAE, MAPE, MSE and RMSE in regression analysis evaluation. PeerJ Computer Science, 7, e623.

Chouet, B., Saccorotti, G., Dawson, P., Martini, M., Scarpa, R., De Luca, G., ... & Cattaneo, M. (1999). Broadband measurements of the sources of explosions at Stromboli Volcano, Italy. Geophysical research letters, 26(13), 1937-1940.

Chouet B., G. De Luca, G. Milana, P. Dawson, M. Martini and R. Scarpa. (1998). Shallow velocity of Stromboli volcano, Italy, derived from small-aperture array measurements of Strombolian tremor. Bulletin of the Seismological Society of America, 88-3, 653-666.

Cornou, C. (2002). Traitement d'antenne et imagerie sismique dans l'agglomération grenobloise (Alpes françaises): implications pour les effets de site. Ph.D. Thesis, University Joseph Fourier, Grenoble, France.

Cornou, C., Bard, P.-Y., Dietrich, M., (2003a). Contribution of dense array analysis to identification and quantification of basin-edge induced waves. Part I: methodology. Bulletin of the Seismological Society of America 93 (6), 2604–2623.

Cornou, C., Bard, P.-Y., Dietrich, M., (2003b). Contribution of dense array analysis to identification and quantification of basin-edge induced waves. Part II: application to Grenoble basin (french Alps). Bulletin of the Seismological Society of America 93 (6), 2624–2648.

D'Alessandro, A., Luzio, D., D'Anna, G., & Mangano, G. (2010). Valutazione della performance di localizzazione della RSN-INGV tramite simulazione numerica. Quaderni di Geofisica, 2010-06-24(83), 1-33

Darbyshire, J. and E. O. Okeke (1969). A study of primary and sec ondary microseisms recorded in Anglesey, Geophys. J. R. Astr. Soc. 17, 63-92.

De Lauro, E., De Martino, S., Del Pezzo, E., Falanga, M., Palo, M., & Scarpa, R. (2008). Model for high-frequency Strombolian tremor inferred by wavefield decomposition and reconstruction of asymptotic dynamics. Journal of Geophysical Research: Solid Earth, 113(B2).

De Lauro, E., De Martino, S., Falanga, M., & Palo, M. (2006). Statistical analysis of Stromboli VLP tremor in the band [0.1–0.5] Hz: some consequences for vibrating structures. Nonlinear Processes in Geophysics, 13(4), 393-400.

De Lauro, E., De Martino, S., Falanga, M., Palo, M., & Scarpa, R. (2005). Evidence of VLP volcanic tremor in the band [0.2–0.5] Hz at Stromboli volcano, Italy. Geophysical research letters, 32 (17).

Delfiner, P. (1976). Linear estimation ofnon-stationary spatialp henomenaI.n Advancedg eostatistics in the mining industry, ed. M. Guarascio, M. David, and C. Huijbregts, pp. 49-68. Dordrecht, Holland: Reidel.

Demuth, A., Ottemöller, L., & Keers, H. (2016). Ambient noise levels and detection threshold in Norway. Journal of seismology, 20(3), 889-904.

De Myttenaere A, Golden B, Le Grand B, Rossi F. (2015). Using the mean absolute percentage error for regression models. In: Proceedings of ESANN, 2015 - The 23rd European Symposium on Artificial Neural Networks, Computational Intelligence and Machine Learning. Louvain: Presses Universitaires de Louvain, 113.

Del Pezzo, E., Bianco, F., Castellano, M., Cusano, P., Galluzzo, D., La Rocca, M., & Petrosino, S. (2013). Detection of seismic signals from background noise in the area of Campi Flegrei: Limits of the present seismic monitoring. Seismological Research Letters, 84(2), 190-198.

De Siena, L., Chiodini, G., Vilardo, G., Del Pezzo, E., Castellano, M., Colombelli, S., ... & Ventura, G. (2017). Source and dynamics of a volcanic caldera unrest: Campi Flegrei, 1983–84. Scientific reports, 7(1), 1-13.

Demuth, A., Ottemöller, L., & Keers, H. (2016). Ambient noise levels and detection threshold in Norway. Journal of seismology, 20(3), 889-904.

Diaz, J., Villasenor, A., Morales, J., Pazos, A., Cordoba, D., Pulgar, J., Garcia-Lobon, J. L., Harnafi,M., Carbonell, R., Gallart, J., and TopoIberia Seismic Working Group (2010). Background noise characteristics at the IberArray broadband seismic network. Bulletin of Seismological Society of America 100(2), 618–628

Douze E. J. (1967). Short-period seismic noise. Bulletin of the Seismological Society of America, 57-1, 55-81.

Douze E. J. (1964). Rayleigh waves in short-period seismic noise. Bulletin of the Seismological Society of America, 54-4, 1197-1212.

Duennebier, F.K., Lucas, R., Nosal, E-M., Aucan, J. & Weller, R.A. (2012). Wind, waves, and acoustic background levels at Station ALOHA, J. geophys. Res., 117, C03017, doi: 10.1029/2011JC007267.

Ferretti, G., Zunino, A., Scafidi, D., Barani, S., & Spallarossa, D. (2013). On microseisms recorded near the Ligurian coast (Italy) and their relationship with sea wave height. Geophysical Journal International, 194(1), 524-533.

Frantti, G. (1963). The nature of high-frequency earth noise spectra. Geophysics 28 (4), 547– 562.

Frantti, G., Willis, D.E., Wilson, J.T. (1962). The spectrum of seismic noise. Bulletin of the Seismological Society of America 52 (1), 113–121.

Giudicepietro, F., Chiodini, G., Avino, R., Brandi, G., Caliro, S., De Cesare, W., ... & Macedonio, G. (2021). Tracking episodes of seismicity and gas transport in Campi Flegrei caldera through seismic, geophysical, and geochemical measurements. Seismological Society of America, 92(2A), 965-975.

Gramacki, A. (2018). Nonparametric kernel density estimation and its computational aspects (pp. 42-49). Cham: Springer International Publishing.

Grecu, B., Neagoe, C., & Tataru, D. (2012). Seismic noise characteristics at the Romanian broadband seismic network. Journal of Earthquake Engineering, 16(5), 644-661.

Guo, Z., & Aydin, A. (2015). Double-Frequency Microseisms in Ambient Noise Recorded in Mississippi. Bulletin of the Seismological Society of America, 105(3), 1691-1710.

Kasuya, E. (2019). On the use of r and r squared in correlation and regression (Vol. 34, No. 1, pp. 235-236). Hoboken, USA: John Wiley & Sons, Inc...

Haubrich, R. A. and K. McCamy (1969). Microseisms: coastal and pelagic sources, Rev. Geophys. Space Phys. 7, 539-571.

Haubrich, R. A., W. H. Munk, and F. E. Snodgrass (1963). Comparative spectra of microseisms and swell, Bull. Seism. Soc. Am. 53, 27-37.

Hasselmann, K. (1963). A statistical analysis of the generation of microseisms, Rev. Geophys. Space Phys. 1, 177-210.

Holcomb, L. G. (1998). Spectral stucture in the Earth's microseismic background between 20 and 40 seconds. Bull. Seismol. Soc. Am., 88(3), 744-757.

Horike M. (1985). Inversion of phase velocity of long-period microtremors to the S-wave- velocity structure down to the basement in urbanized areas. J. Phys. Earth, 33, 59-96.

Isaaks, E.H., Srivastava, R.M. (1989). Applied Geostatistics. Oxford University Press,

New York.

Iyer, H. M. (1958). A study of direction of arrival of microseisms at Kew Observatory, Geophys. J. 1, 32-43

Johnston, K., Ver Hoef, J. M., Krivoruchko, K., & Lucas, N. (2001). Using ArcGIS geostatistical analyst (Vol. 380). Redlands: Esri.

Kanai, K., Tanaka, T. (1961). On microtremors VIII. Bulletin of the Earthquake Research Institute 39, 97–114.

Köhler, A., Ohrnberger, M., Scherbaum, F., Wathelet, M., Cornou, C. (2007). Assessing the reliability of the modified three-component spatial autocorrelation technique. Geophysical Journal International, 168(2), 779-796. https://doi.org/10.1111/j.1365-246X.2006.03253.x.

Kravchenko, A. N. (2003). Influence of spatial structure on accuracy of interpolation methods. Soil Science Society of America Journal, 67(5), 1564-1571.

Krige, D.G. (1951). A statistical approach to some mine valuations problems at the Witwatersrand. J. Chem. Metall. Min. Soc. S. Afr. 52, 119e139.

Lacoss, R.T., Kelly, E.J., Nafi, T.M. (1969). Estimation of seismic noise structure using arrays. Geophysics 34 (1), 21–38.

Lam, N. S. N. (1983). Spatial interpolation methods: a review. The American Cartographer, 10(2), 129-150.

Laslett, G.M., McBratney, A.B., Pahl, P.J., Hutchinson, M.F. (1987). Comparison of several spatial prediction methods for soil pH. J. Soil Sci. 38, 325e341.

Lee, W. H., Jennings, P., Kisslinger, C., & Kanamori, H. (Eds.). (2002). International Handbook of Earthquake & Engineering Seismology, Part A. Elsevier.

Li, J., & Heap, A. D. (2014). Spatial interpolation methods applied in the environmental sciences: A review. Environmental Modelling & Software, 53, 173-189.

Li, J., & Heap, A. D. (2008). A review of spatial interpolation methods for environmental scientists.

Li, T.M.C., Ferguson, J.F., Herrin, E., Durham, H.B. (1984). High frequency seismic noise at Lajitas, Texas. Bulletin of the Seismological Society of America 74 (5), 2015–2033

Liang, L., & Hale, D. (2010). A stable and fast implementation of natural neighbor interpolation. CWP-657. Ctr. for Wave Phenomena, Colorado School of Mines, Golden.

Longley, P. A., Goodchild, M. F., Maguire, D. J., & Rhind, D. W. Geographic information systems and sciences, 2nd Ed. West Sussex, UK: John Wiley & Sons Ltd.; 2005.

Longuet-Higgins, M. S. (1950). A theory of the origin of microseisms, Philos. Trans. R. Soc. London 243, 1-35.

Lott, F. F., Ritter, J. R., Al-Qaryouti, M., & Corsmeier, U. (2017). On the analysis of wind-induced noise in seismological recordings. Pure and Applied Geophysics, 174(3), 1453-1470.

Lu, G. Y., & Wong, D. W. (2008). An adaptive inverse-distance weighting spatial interpolation technique. Computers & geosciences, 34(9), 1044-1055.

Marzorati, S., Ladina, C., Falcucci, E., Gori, S., Saroli, M., Ameri, G., & Galadini, F. (2011). Site effects "on the rock": the case of Castelvecchio Subequo (L'Aquila, central Italy). Bulletin of Earthquake Engineering, 9(3), 841-868.

Marzorati, S., & Bindi, D. (2006). Ambient noise levels in north central Italy. Geochemistry, Geophysics, Geosystems, 7(9).

Matheron, G. (1971). Universal kriging. In Matheron's Theory of Regionalised Variables (pp. 123-180). Oxford University Press.

McCauley, J. D., & Engel, B. A. (1997). Approximation of noisy bivariate traverse data for precision mapping. Transactions of the ASAE, 40(1), 237-245.

McCreery, C.S., F.K. Duennebier, and G.H. Sutton (1993). Correlation of deep ocean noise (0.4-20 Hz) with wind, and the Holu spectrum - a worldwide constant. J. Acoust. Soc. Am., 93(5), 2639-2648.

McNamara, D. E., & Boaz, R. I. (2019). Visualization of the seismic ambient noise spectrum. Seismic ambient noise, 1-29.

McNamara D, Hutt C, Gee L, Benz HM, Buland R. (2009). A method to establish seismic noise baselines for automated station assessment. Seismol Res Lett. 80 :628–637.

McNamara, D., Buland, R. (2004). Ambient noise levels in the continental United States. Bulletin of the Seismological Society of America 94 (4) 1517-15-27.

Melosantos, A. A., Soriano, K. V. C., Alcones, P. C. M., Pantig, J. U., Bonita, J. D., Narag, I. C., ... & Inoue, H. (2015). Performance of broadband seismic network of the Philippines. Journal of Disaster Research, 10(1), 8-17.

Miche, M. (1944). Mouvements ondulatoires de lamer en profondeur constante ou decroissante, Annales des Ponts et Chaussees 114, 25-78.

Mucciarelli, M., Gallipoli, M. R., Di Giacomo, D., Di Nota, F., & Nino, E. (2005). The influence of wind on measurements of seismic noise. Geophysical Journal International, 161(2), 303-308.

Mueller, T. G., Pierce, F. J., Schabenberger, O., & Warncke, D. D. (2001). Map quality for site-specific fertility management. Soil Science Society of America Journal, 65(5), 1547-1558.

Murdoch, N., B. Kenda, T. Kawamura, A. Spiga, P. Lognonné, D. Mimoun, and W. B. Banerdt (2017). Estimation of the seismic pressure noise on Mars determined from large Eddy simulations and demonstration of pressure decorrelation techniques from the Insight Mission, Space Sci. Rev. 211, nos. 1/4, 457–483.

Nakamura, Y. (1989). A method for dynamic characteristics estimation of subsurface using microtremor on the ground surface. Railway Technical Research Institute, Quarterly Reports, 30(1).

Nakamura, Y. (1996). Real-time information systems for hazards mitigation. Proceedings of the 11th World Conference on Earthquake Engineering, Acapulco, Mexico.

Nakamura, Y., (2000). Clear identification of fundamental idea of Nakamura's technique and its applications. Proceedings of the 12th World Conference on Earthquake Engineering. Auckland, New Zealand.

Nogoshi, M., Igarashi, T., (1971). On the amplitude characteristics of microtremor (part 2). Journal of Seismological Society of Japan 24, 26–40.

Okada, H., (2003). The microtremor survey method. Geophysical Monograph Series, Society of Exploration Geophysicists 12.

Oliver, J. (1962). A worldwide storm of microseisms with periods of about 27 seconds, Bull. Seism. Soc. Am. 52, 507-517.

Oliver, J. and R. Page (1963). Concurrent storms of long and ultra-long period microseisms, Bull. Seism. Soc. Am. 53, 15-26.

Ostrovsky, A. A. and L. N. Rykunov (1982). "Experimental study of ocean bottom seismic noise during passage of a cyclone, Ocean ology 22, 720-722

Peruzzetto, M., Kazantsev, A., Luu, K., Métaxian, J. P., Huguet, F., & Chauris, H. (2018). Broad-band ambient noise characterization by joint use of cross-correlation and MUSIC algorithm. Geophysical Journal International, 215(2), 760-779.

Peterson, J. R. (1993). Observations and modeling of seismic background noise (No. 93-322). US Geological Survey.

Petrosino, S., & De Siena, L. (2021). Fluid migrations and volcanic earthquakes from depolarized ambient noise.

R Development Core Team, (2007). R: A Language and Environment for Statistical Computing. R Foundation for Statistical Computing, Vienna.

Reddy, K. B., Ramana, P. V., & Sumiya, K. (2017, May). Comparative analysis of spatial interpolation methods of different field measurements for cognitive radio. In 2017 2nd IEEE International Conference on Recent Trends in Electronics, Information & Communication Technology (RTEICT) (pp. 2212-2216). IEEE.

Ren L, Glasure Y. (2009). Applicability of the revised mean absolute percentage errors (MAPE) approach to some popular normal and non-normal independent time series. International Advances in Economic Research 15(4):409–420.

Rind, D. and W. Donn (1979). Microseisms at Palisades, 2, Rayleigh wave and Love wave characteristics and the geologic control of propagation, J. Geophys. Res. 84, 5632-5642.

Ripley, B.D. (1981). Spatial Statistics. John Wiley & Sons, New York, 252 pp.

Sambridge, M., J. Braun, and H. McQueen, 1995. Geophysical parameterization and interpolation of irregular data using natural neighbours. Geophys. J. Int., 122, 837–857.

Sampson, R. J. (1978). SURFACE II graphics system: Kansas Geological Survey Series on Spatial Analysis No. 1. University of Kansas, Lawrence, Kansas, 240.

Schloeder, C. A., Zimmerman, N. E., & Jacobs, M. J. (2001). Comparison of methods for interpolating soil properties using limited data. Soil science society of America journal, 65(2), 470-479.

Schmidt, R.O. (1981). A signal subspace approach to multiple emitterlocation and spectral estimation. Ph.D. thesis, Stanford University,California, USA.

Seo, K. (1997). Comparison of measured microtremors with damage distribution. JICA, Research and Development Project on Earthquake Disaster Prevention.

SESAME European project, (2003). Nature of noise wavefield, Final Report WP08,http://sesamefp5.obs.ujfgrenoble.fr/Delivrables/D13.08_finalreport.pdf

Sibson, R. (1981). A brief description of natural neighbour interpolation. In: V. Barnett (Editor), Interpreting Multivariate Data. John Wiley and Sons, Chichester, pp.21-36.

Signoretto M., Suykens J.A.K. (2015). Kernel Methods. In: Kacprzyk J., Pedrycz W. (eds) Springer Handbook of Computational Intelligence. Springer Handbooks. Springer, Berlin, Heidelberg. https://doi.org/10.1007/978-3-662-43505-2_32.

Soliman, M. S. (2013). New seismic noise models obtained using very broadband stations. Pure and Applied Geophysics, 170(11), 1849-1857.

Stutzmann, E., Roult, G., Astiz, L. (2000). GEOSCOPE station noise levels. Bulletin of the Seismological Society of America 90 (3), 690–701.

Sutton, G. H. and N. Barstow (1990). Ocean-bottom ultralow-frequency (ULF) seismo- acoustic ambient noise: 0.002 to 0.4 Hz, J. Acoust. Soc. Am. 87, 2005-2012.

Tape, C., D. Christensen, M. M. Moore-Driskell, J. Sweet, and K. Smith (2017). Southern Alaska Lithosphere and Mantle Observation Network (SALMON): A seismic experiment covering the active arc by road, boat, plane, and helicopter,

Seismol. Res. Lett. 88, 1185–1202.

Tokimatsu K. (1997). Geotechnical site characterization using surface waves. Proceedings of the First International Conference on Earthquake Geotechnical Engineering. 3 1333-1368.

Toksöz, M.N., Lacoss, R.T. (1968). Microseisms: mode structure and sources. Science 159, 872–873.

Umer, M., Kulik, L., & Tanin, E. (2010). Spatial interpolation in wireless sensor networks: localized algorithms for variogram modeling and Kriging. Geoinformatica, 14(1), 101-134.

Vanorio, T., & Kanitpanyacharoen, W. (2015). Rock physics of fibrous rocks akin to Roman concrete explains uplifts at Campi Flegrei Caldera. Science, 349(6248), 617-621.

Vassallo, M., Festa, G., & Bobbio, A. (2012). Seismic ambient noise analysis in southern Italy. Bulletin of the Seismological Society of America, 102(2), 574-586.

Vassallo, M., Cantore, L., Iannaccone, G., & Zollo, A. (2010). Analisi del rumore sismico. Metodi e Tecnologie per l'Early-warning Sismico, 85-115.

Vassallo, M., Bobbio, A., & Iannaccone, G. (2008). A comparison of sea-floor and on-land seismic ambient noise in the Campi Flegrei caldera, southern Italy. Bulletin of the Seismological Society of America, 98(6), 2962-2974

Watson, D. F. (1992). Contouring: A Guide to the Analysis and Display of Spatial Data. Pergamon, Oxford.

Webster, R., Oliver, M. (2001). Geostatistics for Environmental Scientists. John Wiley & Sons, Ltd, Chichester.

Webb, S. C. (2002). Seismic noise on land and on the sea floor. In: Lee, W. H. K., Kanamori, H., Jennings, P. C., and Kisslinger, C. (Eds.) (2002). International Handbook of Earth-quake and Engineering Seismology, Part A, Academic Press, Amsterdam, 305-318.

Webb, S. C., and Crawford, W. C. (1999). Long period seafloor seismology and deformation under ocean waves. Bull. Seismal. Soc. Am., 89(6), 1535-1542.

Wiechert, E. (1904). Verhandlungen der Zweiten Internationalen Seismologischen Konferenz, Gerl. Beitr. Geophys. Erganzungsbd. 2, 41-43.

Withers, M. M., Aster, R. C., Young, Ch. J., and Chael, E. P. (1996). High-frequency analysis of seismic background noise as a function of wind speed and shallow depth, Bull. Seism. Soc. Am., 86, 5, pp.1507-1515.

Wilcock, W. S. D., Webb, S. C., and Bjarnason, I. Th. (1999). The effect of local wind on seismic noise near 1 Hz at the MELT site and on Iceland. Bull. Seismal. Soc. Am., 89(6), 1543-1557.

Wren, A. E. (1975). Contouring and the contour map, a new perspective. Geographical Prospecting 23:1-17.

Wright S. (1921). Correlation and causation. Journal of Agricultural Research XX (7):557–585.

Wu, Y. H., & Hung, M. C. (2016). Comparison of spatial interpolation techniques using visualization and quantitative assessment. Applications of Spatial Statistics, 17-34.

Yamamoto, H. (2000). Estimation of shallow S-wave velocity structures from phase velocities of love- and Rayleigh- waves in microtremors, Proceedings of the 12th World Conference on Earthquake Engineering, Auckland, New Zealand.

Yamanaka H., M. Takemura, H. Ishida and M. Niwa. (1994). Characteristics of long-period microtremors and their applicability in exploration of deep

sedimentary layers. Bulletin of the Seismological Society of America, 84-6, 1831-1841.

Yanovskaya, T. G. (2012). Surface-wave tomography for upper mantle studies: methods and results. Keynote lecture at the 33rd General Assembly of the European Seismological Commission, Moscow,19-24 Aug. 2012.

Youngworth, R. N., Gallagher, B. B., & Stamper, B. L. (2005, August). An overview of power spectral density (PSD) calculations. In Optical Manufacturing and Testing VI (Vol. 5869, p. 58690U). International Society for Optics and Photonics.

Zaccarelli, L., & Bianco, F. (2017). Noise-based seismic monitoring of the Campi Flegrei caldera. Geophysical Research Letters, 44(5), 2237-2244.

Zhang, D. (2017). A coefficient of determination for generalized linear models. The American Statistician, 71(4), 310-316.